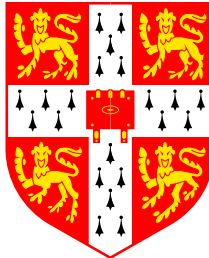


Ab-initio Molecular Dynamics for Metallic Systems

Nicola Marzari
Dottore in Fisica

Pembroke College, University of Cambridge
Theory of Condensed Matter, Cavendish Laboratory



*A dissertation submitted for the
degree of Doctor of Philosophy*

April 1996

Tutto questo avverrà,
te lo prometto.

Madama Butterfly

Preface

This dissertation is submitted for the degree of Doctor of Philosophy at the University of Cambridge. It contains an account of the research carried out between April 1993 and February 1996 in the Theory of Condensed Matter Group at the Cavendish Laboratory, Department of Physics, University of Cambridge, under the supervision of Dr. M. C. Payne. Unless appropriately referenced, the work is original and is not the result of work done in collaboration. No part of this dissertation has been or is currently being submitted for any degree or diploma at this, or any other, University.

Nicola Marzari

Contents

Introduction	11
1 Theory of electronic structure	13
1.1 The Schrödinger equation	14
1.1.1 Variational formulation	17
1.1.2 The Hellmann-Feynman theorem	19
1.2 Density Functional Theory	21
1.2.1 The Hohenberg-Kohn theorems	22
1.2.2 The Levy approach	25
1.2.3 The representability problem	27
1.2.4 Density operators	29
1.2.5 Canonical-ensemble formulation	32
1.3 The Kohn-Sham mapping	34
1.3.1 Fractional occupancies, Janak's theorem	40
1.3.2 Finite-temperature extension	43
2 Methods of electronic structure	47
2.1 The Local Density Approximation	48
2.2 The pseudopotential approximation	51

2.2.1	Basis representation	52
2.2.2	Smoothness and transferability	53
2.2.3	The Kleinman-Bylander representation	57
2.3	Minimizations and dynamics	59
2.3.1	Car-Parrinello molecular dynamics	60
2.3.2	Conjugate-gradient minimization	64
2.3.3	Metallic systems	71
3	Ensemble Density Functional Theory	83
3.1	Ensemble free energy	84
3.2	Minimization strategy	88
3.2.1	Doubly-preconditioned all-bands CG	89
3.2.2	Occupation matrix: an iterative scheme	96
3.3	Applications and comparisons	100
3.3.1	Self-consistency and molecular dynamics	100
3.3.2	Ionic relaxations	107
3.4	Further developments	109
4	Generalized entropy and cold smearing	113
4.1	Generalized free energy	114
4.2	Smeared functionals	118
4.3	Entropy corrections	121
4.3.1	Energy	123
4.3.2	Forces and other derivatives	126
4.4	Cold smearing	130

<i>CONTENTS</i>	3
5 Ensemble-DFT molecular dynamics	143
5.1 Molecular dynamics simulations	144
5.1.1 Technical details	145
5.2 Metal surfaces at finite temperature	150
5.3 Computational LEED	152
5.3.1 Bulk Al	152
5.3.2 Al(110): thermal relaxations	152
5.3.3 Al(110): layer-resolved displacements	153
5.3.4 Al(111)	155
5.4 Sampling the phase space	156
5.4.1 Preroughening, diffusion and liquid layering	156
Conclusions	171
Acknowledgments	173
Bibliography	174

List of Figures

2.1 <i>s</i> -, <i>p</i> - and <i>d</i> - components of a non-local norm-conserving pseudopotential (In), with the all-electron and pseudo-wavefunctions $r\phi(r)$ (solid and dashed, clockwise from top left).	56
2.2 Convergence of the total free energy in a semi-logarithmic scale (base 10). The systems considered are two 1x1 Al(110) slabs, containing respectively 15 and 30 atoms (64 and 128 bands, 4.5 eV of Gaussian smearing), and 32 Å and 52 Å long, both sampled with the $(\frac{1}{4}, \frac{1}{4}, \frac{1}{4})$ Baldereschi point [99]. The iteration count for the longer cell has been halved, for a meaningful comparison.	80
3.1 Ratio between the predicted and the calculated free energy differences in the parabolic fit for the orbital minimization, in the case of a 1x1 15-layer Al(110) slab, 32 Å long	95

3.2	Convergence of the total free energy (in a semi-logarithmic scale) and of the Hellmann-Feynman forces (in the z -direction for the surface atom) in the 15-layer Al(110) slab, as a function of the number of all-bands iterations, for the standard method (ab) and for the case of ensemble-DFT with 2 or 4 iterations in the inner loop (dm_2 and dm_4 respectively)	102
3.3	Convergence of the total free energy (in a semi-logarithmic scale) and of the Hellmann-Feynman forces (in the z -direction for the surface atom) for the 15-layer slab as a function of the number of iterations, for the case of ensemble-DFT fully converged in the inner loop.	104
3.4	Conservation of the constant of motion in a 1 ps molecular dynamics run, for the 15-layer slab. The free energy is shown here together with the constant of motion for a run performed with the standard method and one done with ensemble-DFT. An enlargement for the latter case is also shown.	106
3.5	Total free energy as a function of the number of ionic iterations for the structural relaxations of a 3x3 Al(110) 8-layer slab. . .	109
3.6	Same as the previous figure, in a semi-logarithmic scale. . . .	110
4.1	Density of states for bulk aluminium calculated self-consistently at different (Gaussian) broadenings (the horizontal axes are in eV, the vertical axes in arbitrary units). The total and the occupied (shaded) densities of states are shown.	122

4.2 Total, free and corrected energies for bulk Al as a function of the (Gaussian) broadening. Full sampling convergence even at low temperatures is obtained using a fine (12,12,12) mesh of Monkhorst-Pack points for the 4-atom cubic unit cell.	125
4.3 Structural parameters calculated at 3 eV of smearing and 10 special points in the irreducible wedge of the FCC cell. Al013a converges with 200 eV of cutoff, al013b with 80 eV.	126
4.4 Change in the energy and in the free energy in a displacement \mathbf{d} of one atom in a bulk 4-atom cell, together with the work done in the displacement	127
4.5 Force in the z direction for the surface atom of a 3-layer 1x1 Al(110) slab, as a function of the (Gaussian) broadening and for different meshes of special points in the irreducible wedge of the Brillouin zone.	129
4.6 Broadening function and integrated thermal occupancy for the case of the Gaussian smearing, the first-order Methfessel-Paxton and for the cold smearing introduced here. The occupancies in the latter case are always greater than zero.	136
4.7 Detail of the thermal distributions in correspondence of the two values proposed for a in the broadening function.	137
4.8 Comparison between the cold smearing and the corrected energy, in the model case of α -tin with 12 electrons, as discussed in the text.	138

- 4.9 Convergence of the z -component of the force in the top layer, and of the opposite of the force in the bottom layer, for the 15-atom slab, with these three choices for the smearing function. The inset shows the first 100 iterations for the Gaussian case, with a vertical scale 20 eV/Å wide. 141
- 5.1 Multilayer relaxations for the Al(110) surface, at 0.5 eV of cold smearing. The slab is 1x1 in the plane parallel to the surface. 146
- 5.2 Constant of motion for the 15-layer Al(110) supercell, using the standard method (dashed lines) or ensemble-DFT, either with a set tolerance at every timestep or with a fixed number of iterations. Gaussian smearing is used, except for ensemble-DFT at fixed iterations, where the cold smearing and the inner loop fixed step is used; this constant of motion has been rigidly translated for comparison. The number of iterations in the fixed-number strategy is larger than the average for the fixed-tolerance strategy. The drift for ensemble-DFT is roughly three orders of magnitude smaller. 149
- 5.3 Mean square displacements along the z axis for bulk Al at 300 K and 600 K. Experimental data [159] are represented by the two grey bands; the theoretical data have been obtained averaging the run with a window 1 ps wide. Top left and right are the projections on the xz plane of the orbits in the 8 layers, at 300 K and 600 K respectively. Each orbit is the superposition of 3 atoms along the y axis. 160

5.4 Multilayer relaxations in Al(110) as a function of the temperature. The percentile relaxations are calculated with respect to the lattice parameter appropriate to each temperature. Each run is ~ 3 ps long. Experimental data (3 different shades of grey for each interlayer relaxation) are from Ref. [135] and references therein.	161
5.5 Mean square displacements along the z axis for an Al(110) slab at 300 K. Experimental data for the bulk are shown as a grey band [159]; the theoretical data have been obtained averaging the run with a window 2 ps wide. Top left are the projections on the xz plane of the orbits in the 8 layers of the slab.	162
5.6 Mean square displacements along the z axis for the different layers, as a function of the temperature. “Bulk” refers to the two central layers. Averages are done on the full runs, each ~ 3 ps long.	163
5.7 Mean square displacements for the second layer at different temperatures. The value at a time t represents the average done from t to the end of the run for the square of the displacement around an average position consistently calculated as the average from the time t to the end of the run.	164

5.8	Mean square displacements for the first (dashed) and second layer (solid) at 500 K and with different Brillouin Zone samplings. The value at a time t represents the average done from t to the end of the run for the square of the displacement around an average position consistently calculated as the average from the time t to the end of the run.	165
5.9	Dynamic trajectories for the ions in the Al(111) slab, at 600 K (1 ps of simulation).	166
5.10	Dynamic trajectories for the ions in the Al(110) slab, with the top 5 layers at 600 K and the bottom 3 layers at 300 K; the first adatom/vacancy formation process is highlighted (1 ps of simulation). The xz and the yz projections are shown.	167
5.11	Dynamic trajectories for the ions in the 6 layers + 2 adatoms Al(110) slab; on the right are the first 4 ps at 450 K, on the left all the run with its additional 1 ps at 500 K.	168
5.12	Dynamic trajectories for the ions in the Al(110) slab at 600 K, for a 3 ps simulation. An increased, layered density is clearly noted in proximity of the surfaces.	169

Introduction

In recent years theoretical solid-state physics has dramatically improved the scope and the range of its studies, upgrading from semi-empirical descriptions ultimately based on qualitative models to a thoroughly systematic analysis of quantitative physical properties. Crystalline states are the paradigmatic example of this success, and in particular semiconductors and insulators, due to the achieved ability to characterize much of their properties at both the macroscopic and the microscopic level with an accuracy that is comparable to that of experiments, and that can extend beyond the range of physical quantities for which a real-life experiment is either feasible or cost-effective. This degree of confidence is based on the parameter-free, fundamentally quantum-mechanical description of a system as made of interacting electrons in the field of atomic nuclei (*First-Principles calculations*); the reasons for this success lie in an original reformulation of the many-particle Schrödinger equation (*Density Functional Theory*) coupled with physical insight for the correlation effects of the interacting electrons (*Local Density Approximation*), and to the availability for the scientific community of powerful computers able to deal with the numerical complexity of realistic problems.

The application of these methods and techniques to the case of metallic systems has encountered extensive technical difficulties that have made

progress comparatively slow. This work deals with some of those difficulties, with the goal of bringing ab-initio quantum-mechanical molecular dynamics simulations to the same level of computational cost, efficiency and accuracy that are now obtained for semiconductors and insulators.

The problem is here reviewed from the theoretical and the methodological points of view, with a presentation of the current state of research. The formulation of the electronic structure problem as a Density Functional Theory constrained minimization is examined in detail, both for the zero-temperature case and in its extension to a finite-temperature picture. A novel reformulation is proposed using the language of *Ensemble Density Functional Theory*, and a variational realization for it is developed and implemented. The dramatic improvements that are obtained in the efficiency for the convergence to the electronic ground-state are discussed and explained.

The case for a finite-temperature treatment of the electrons is argued, and its recognized contribution to controlling the statistical errors in the sampling of the Brillouin Zone is highlighted. The systematic errors that a real or fictitious electronic temperature may introduce are also evaluated, together with their known non-self-consistent and self-consistent corrections, and the novel technique of *cold smearing* is introduced.

The methods developed here are applied to the study of the thermal properties of aluminium surfaces¹, to identify the microscopical processes that give rise to the disordering of the (110) surface, gaining evidence for some of the phase transitions that take place at temperatures below the melting point of the bulk system.

¹to the best of our knowledge, first-principles molecular-dynamics simulations for metal surfaces have not been performed before.

Chapter 1

Theory of electronic structure

Introduction

A brief review is given of the problem of finding the ground state for a system of interacting electrons immersed in an external potential. The fundamental law of quantum mechanics—the Schrödinger equation [1]—is introduced, and its equivalence to a variational principle is established. A modern and extremely successful reformulation of the problem—that goes under the name of Density Functional Theory [2]—is presented, and its intrinsic nature as a minimization problem is highlighted. The role of temperature [3] and the introduction of statistical operators to describe mixed states is discussed. Finally, the problem is recast via the Kohn-Sham [4] mapping onto a system of non-interacting electrons in a self-consistent external potential.

1.1 The Schrödinger equation

At the present state of human knowledge, quantum mechanics can be regarded as the fundamental theory of atomic phenomena.

[L. I. Schiff, *Quantum Mechanics*, 1955]

This statement has been supported since the early days that followed the introduction of quantum mechanics by an ever growing evidence for the accuracy of its predictions when compared with experiments. Notwithstanding the existence of many unresolved questions in the formal interpretation of the theory [5], the range of its applications has extended from the description of single isolated atoms to all areas of fundamental and applied physics and chemistry. As a simple example of its extreme accuracy, the gyromagnetic ratio for the electron can be determined in agreement with experiment with a precision greater than one part in a billion. Other disciplines, ranging from materials science to biology, are starting now to benefit from this predictive power and from the development of very powerful electronic structure methods, as described in Chapter 2, that allow for the first time to compute fundamental properties of complex systems from first principles, using quantum mechanics to determine the behaviour of their fundamental constituents, electrons and ions.

In the following we are concerned with the ground-state electronic properties of a finite, isolated system of N interacting electrons in an external potential. The external potential considered is that generated by a configuration of atomic nuclei, assumed for the time being to be fixed point charges. Some of these conditions will be relaxed or modified along the way, namely

by introducing pseudopotentials [6][7] to describe the interactions between the valence electrons and the rest of the system, by allowing for the ions to move adiabatically [8] in the field of the electrons' ground state, and by introducing periodic boundary conditions to reduce or eliminate finite-size errors.

The non-relativistic time-independent Schrödinger equation for the system described is

$$\hat{H}\Psi(\mathbf{r}_1, \dots, \mathbf{r}_N) = E\Psi(\mathbf{r}_1, \dots, \mathbf{r}_N), \quad (1.1)$$

where the Hamiltonian operator¹ \hat{H} is

$$\begin{aligned} \hat{H} &= \hat{T}_e + \hat{V}_{n-e} + \hat{U}_{e-e} + \hat{W}_{n-n} = \\ &= \sum_i \left(-\frac{1}{2} \nabla_i^2 + v(\mathbf{r}_i) \right) + \frac{1}{2} \sum_{i \neq j} \frac{1}{|\mathbf{r}_i - \mathbf{r}_j|} + \hat{W}_{n-n} \end{aligned} \quad (1.2)$$

with

$$v(\mathbf{r}) = - \sum_{\alpha} \frac{Z_{\alpha}}{|\mathbf{r} - \mathbf{R}_{\alpha}|} \quad \text{and} \quad W_{n-n} = \frac{1}{2} \sum_{\alpha\beta} \frac{Z_{\alpha}Z_{\beta}}{R_{\alpha\beta}}. \quad (1.3)$$

The terms in (1.2) are associated, respectively, with the kinetic energy T_e of the electrons, the potential energy V_{n-e} of the electrons in the field of α nuclei of charge Z_{α} , the electrostatic energy U_{e-e} between the electrons, and the electrostatic energy W_{n-n} between the nuclei.

Equation (1.1) is an eigenvalue equation for the N -electron many-body wavefunction $\Psi(\mathbf{r}_1, \dots, \mathbf{r}_N)$ ($\mathbf{r}_1 \dots \mathbf{r}_N$ being the spatial coordinates for the electrons), where \hat{H} is Hermitian; in order for the solutions to be acceptable they must belong to the Hilbert space $\mathcal{L}^2(\mathbb{R}^3) \otimes \dots \otimes \mathcal{L}^2(\mathbb{R}^3)$ of square-integrable functions. The spin coordinates will be ignored (but not the spin=1/2 nature of the electrons), while some relativistic effects—relevant

¹Atomic units are used: $\hbar = m_e = e = 4\pi\epsilon_0 = 1$.

for heavy atoms—can be taken into account *a posteriori* when constructing the pseudopotential. The Fermi-Dirac statistics for the electrons enters the problem as a restriction on the Hilbert space, requiring Ψ to be antisymmetric under the exchange of the coordinates of two electrons. This, translating into the Pauli principle, accounts ultimately for the stability of matter, with the ground state energy bounded below by a constant times the first power of the particle number [9][10].

The solutions to equation (1.1) form a complete set $\{\Psi_n\}$ [11]; once normalized, any two of them that correspond to different eigenvalues are orthogonal, and the set of eigenvectors $\{\Psi_n\}$ is thus always considered fully orthonormal. According to the postulates of quantum mechanics [12], to each observable A there corresponds a Hermitian operator \hat{A} and consequently its complete set of orthonormal eigenfunctions $\{\phi_n\}$ with eigenvalues $\{a_n\}$; the wavefunction of the system can then always be expressed in terms of these eigenfunctions as

$$\Psi = \sum_n c_n \phi_n. \quad (1.4)$$

If we have an ensemble of systems identically prepared, each measurement will yield the eigenvalue a_n with probability $|c_n|^2$. The expectation value of A can thus be expressed, using Dirac notation, as

$$\langle \hat{A} \rangle = \langle \Psi | \hat{A} | \Psi \rangle = \sum_n \sum_{n'} c_{n'}^* c_n \langle \phi_{n'} | \hat{A} | \phi_n \rangle = \sum_n |c_n|^2 a_n, \quad (1.5)$$

where $\langle \Psi | \hat{A} | \Psi \rangle$ stands for $\int \Psi^* \hat{A} \Psi \, d\mathbf{r}_1 \dots d\mathbf{r}_N$.

1.1.1 Variational formulation

Let us consider a time-independent Hamiltonian, as that described in (1.2); for simplicity, we assume that the system is either enclosed in a box of finite size, or that periodic boundary conditions² are applied. Under such conditions, the (non-empty) spectrum of eigenvalues $\{E_n\}$ and eigenfunctions $\{\psi_n\}$ is discrete³ (see Chap. 3 of Ref. [13] for a discussion). For an arbitrary function Ψ in the Hilbert space $\mathcal{L}^2(\mathbb{R}^3) \otimes \dots \otimes \mathcal{L}^2(\mathbb{R}^3)$ that has non-vanishing norm, we define the functional $E[\Psi]$ as

$$E[\Psi] = \frac{\langle \Psi | \hat{H} | \Psi \rangle}{\langle \Psi | \Psi \rangle} \quad (1.6)$$

The following theorem is easily proved:

Variational Principle *The Schrödinger equation $\hat{H}\Psi = E\Psi$ for the Hamiltonian \hat{H} is equivalent to the variational principle $\delta E[\Psi] = 0$.*

Proof: Let us consider a generic unconstrained Ψ ; taking the variation $\delta(E[\Psi]\langle \Psi | \Psi \rangle)$ in (1.6) we have:

$$\delta E[\Psi] \langle \Psi | \Psi \rangle + E[\Psi] \langle \delta \Psi | \Psi \rangle + E[\Psi] \langle \Psi | \delta \Psi \rangle = \langle \delta \Psi | \hat{H} | \Psi \rangle + \langle \Psi | \hat{H} | \delta \Psi \rangle.$$

²In electronic structure calculations it is useful to adopt a looser form of periodic boundary conditions that goes under the names of Born and von Karman: $\Psi(\mathbf{r} + N_i \mathbf{a}_i) = \Psi(\mathbf{r})$, $i = 1, 2, 3$, where \mathbf{a}_i are the primitive vectors of the cell and N_i are the independent primitive cells in each direction. These conditions impose the existence of a discrete, finite number of allowed values for the Bloch wave vector (a good quantum number in a periodic solid) and its corresponding energy. The spacing between different wavevectors goes to zero in the limit $N_i \rightarrow \infty$, recovering thus the continuum limit for the spectrum of a truly infinite periodic crystal.

³The discussion can be generalized to an Hamiltonian with an additional continuum spectrum $\{e_n\}$ such that $\inf\{e_n\} > \min\{E_n\}$.

The following equivalences are established, exploiting the hermiticity of \hat{H} :

$$\delta E[\Psi] = 0 \Leftrightarrow \langle \delta\Psi | \hat{H} - E | \Psi \rangle + \langle \Psi | \hat{H} - E | \delta\Psi \rangle = 0 \Leftrightarrow (\hat{H} - E[\Psi]) | \Psi \rangle = 0$$

QED

The variational principle can be reformulated in order to include automatically the wavefunction normalization, by introducing an undetermined Lagrange multiplier E : the constrained variational problem

$$\delta[\langle \Psi | \hat{H} | \Psi \rangle] = 0 \quad , \quad \langle \Psi | \Psi \rangle = 1$$

is thus transformed in the unconstrained variational problem

$$\delta[\langle \Psi | \hat{H} | \Psi \rangle - E \langle \Psi | \Psi \rangle] = 0. \quad (1.7)$$

The importance of the functional (1.6) is that it provides a variational bound to the ground-state energy of the system; this can be seen by expanding Ψ in the energy eigenvectors $\{\psi_n\}$:

$$\Psi = \sum_n a_n \psi_n \Rightarrow E[\Psi] = \frac{\sum_n |a_n|^2 E_n}{\sum_n |a_n|^2} \Rightarrow E[\Psi] - E_0 = \frac{\sum_n |a_n|^2 (E_n - E_0)}{\sum_n |a_n|^2}$$

where we have indicated with $E_0 = \min\{E_n\}$ the ground-state energy. It is clear from this that a trial Ψ provides an upper bound to the real ground-state energy, and that the value E_0 is reached if and only if $\Psi = \alpha \Psi_0$, $\alpha \in \mathbb{C}$.

The fundamental *minimum principle* thus follows:

$$E[\Psi] \geq E_0 \quad ; \quad \Psi = \alpha \Psi_0 \iff E[\Psi] = E_0 \quad (1.8)$$

The ground-state energy E implicitly defined by the minimization in (1.8) depends only on and is completely identified by the choice of N and v in (1.2);

in this sense, E is said to be a *functional* $E[N, v]$ of the particle number N and of the external potentials v .

This minimum principle has a key importance in practical applications: as an example, it is the basis of the widely used *Rayleigh-Ritz variational method*, where a trial function is constructed that depends on a number of variational parameters, that are determined by the requirement of minimizing the expectation value for the energy. Obviously, the quality of the results depends both on the choice of the trial function and on the dimensionality of the parameter space that is spanned. In addition, if a trial function can be constructed as to be orthogonal to the $n - 1$ lowest eigenfunctions, the Rayleigh-Ritz method provides an upper bound for the n -th eigenvalue. The well-known *Hartree* [14] and *Hartree-Fock* [15] methods correspond to searching the solutions for (1.7) respectively in the subspace of the products of single-particle orbitals and in the subspace of antisymmetrized products of single-particle orbitals (the Slater determinants).

1.1.2 The Hellmann-Feynman theorem

There is an important consequence that can be drawn from equation (1.7): if the Hamiltonian H depends parametrically on some λ , such that $d\hat{H}_\lambda/d\lambda$ is well defined, the following theorem can be demonstrated:

Hellmann-Feynman theorem *Given a Hamiltonian \hat{H}_λ , and a $\Psi(\lambda)$ satisfying the Schrödinger equation $\hat{H}_\lambda\Psi = E_\lambda\Psi$, the following relation holds:*

$$\frac{dE_\lambda}{d\lambda} = \frac{d}{d\lambda}\langle\Psi|\hat{H}_\lambda|\Psi\rangle = \langle\Psi|d\hat{H}_\lambda/d\lambda|\Psi\rangle$$

Proof. It follows from the orthonormality property for the solutions of the

Schrödinger equation, or its equivalent variational formulation (1.7), that:

$$\langle \Psi(\lambda) | \Psi(\lambda) \rangle = 1 \Rightarrow \frac{d}{d\lambda} \langle \Psi | \Psi \rangle = 0 \Rightarrow \langle d\Psi/d\lambda | \Psi \rangle + \langle \Psi | d\Psi/d\lambda \rangle = 0.$$

Using the hermiticity of \hat{H} , it is readily shown that:

$$\begin{aligned} \frac{d}{d\lambda} \langle \Psi | \hat{H}_\lambda | \Psi \rangle &= \langle d\Psi/d\lambda | \hat{H}_\lambda | \Psi \rangle + \langle \Psi | d\hat{H}_\lambda/d\lambda | \Psi \rangle + \langle \Psi | \hat{H}_\lambda | d\Psi/d\lambda \rangle = \\ &= E(\langle d\Psi/d\lambda | \Psi \rangle + \langle \Psi | d\Psi/d\lambda \rangle) + \langle \Psi | d\hat{H}_\lambda/d\lambda | \Psi \rangle = \langle \Psi | d\hat{H}_\lambda/d\lambda | \Psi \rangle \end{aligned}$$

QED

The scope of the theorem is trivially extended to the expectation values of any Hermitian operator \hat{A}_λ dependent on some external parameter λ and for a system prepared in a given eigenstate of \hat{A}_λ .

The original work [16] was concerned with the definition and the calculation of the forces acting on molecular systems: in fact Hamiltonians \hat{H} such as that defined in (1.2) explicitly depend on the nuclear coordinates \mathbf{R}_α , and it is much more convenient to calculate directly the expectation value of $d\hat{H}/d\mathbf{R}_\alpha$ than approximating this derivative with the energy differences⁴. Feynman's original application of the theorem to the Hamiltonian (1.2) leads immediately to the *electrostatic theorem*: the force on a nucleus is given by a completely classical expression, where the potential is obtained by the superposition of the nuclear fields and by the electrostatic potential generated by the electronic charge density $n(\mathbf{r}) = N \int |\Psi(\mathbf{r}_1 \dots \mathbf{r}_N)|^2 d\mathbf{r}_2 \dots d\mathbf{r}_N$:

$$\begin{aligned} \mathbf{F}_\alpha &= -\nabla_\alpha W_{n-n} - \sum_i \int |\Psi(\mathbf{r}_1 \dots \mathbf{r}_N)|^2 \nabla_\alpha v(\mathbf{r}_i) d\mathbf{r}_1 \dots d\mathbf{r}_N = \\ &= -\nabla_\alpha W_{n-n} - \int n(\mathbf{r}) \nabla_\alpha v(\mathbf{r}) d\mathbf{r}. \quad (1.9) \end{aligned}$$

⁴A similar problem for a time-dependent Schrödinger equation had already been addressed by Ehrenfest [17] in 1927; namely he demonstrated a quantum mechanical equivalent $md^2 \langle \Psi | \mathbf{r} | \Psi \rangle / dt^2 = \langle \Psi | -dV/d\mathbf{r} | \Psi \rangle$ for Newton's second law of dynamics.

1.2 Density Functional Theory

The solution to the electronic structure problem has been presented—according to the prescriptions of the Schrödinger equation—as the problem of obtaining the proper ground-state many-body wavefunction $\Psi_v(\mathbf{r}_1, \dots, \mathbf{r}_N)$ for a given external potential v . As such, the ground-state solution has an intrinsically high complexity: while the problem is completely defined by the total numbers of particles N and by the external potential $v(\mathbf{r})$, its solution—uniquely determined by N and $v(\mathbf{r})$, and thus a functional $\Psi \equiv \Psi[N, v(\mathbf{r})]$ —depends on $3N$ coordinates. This makes the direct search for either exact or approximate solutions to the many-body problem a task of rapidly increasing complexity.

Soon after the introduction of the Schrödinger equation there have been attempts to refocus the search on the ground-state charge density $n(\mathbf{r})$, which is the most natural and physical low-complexity quantity in the problem. The first outcome of this effort was the Thomas-Fermi model [18][19]: a functional of the charge density alone was constructed from the basic assumptions of treating the electrons as independent particles, reducing the electron-electron interaction to the Coulomb electrostatic energy, and using a *local density approximation* for the kinetic energy term:

$$T[n] = \int t[n(\mathbf{r})] d\mathbf{r},$$

where $t[n(\mathbf{r})]$ is the kinetic energy density for a system of non-interacting electrons with density n . The functional that is obtained from this hypothesis

$1s^5$

$$E_{TF}[n(\mathbf{r})] = \frac{3}{10}(3\pi^2)^{\frac{2}{3}} \int n^{\frac{5}{3}}(\mathbf{r}) d\mathbf{r} - \int v(\mathbf{r})n(\mathbf{r}) + \frac{1}{2} \int \int \frac{n(\mathbf{r}_1)n(\mathbf{r}_2)}{|\mathbf{r}_1 - \mathbf{r}_2|} d\mathbf{r}_1 d\mathbf{r}_2$$

and the Thomas-Fermi solution is defined as the charge density $n(\mathbf{r})$ that minimizes this functional E_{TF} , with the constraints of being greater than zero and normalized to the total number of electrons N . This approach has been shown to fail in providing even qualitatively correct descriptions of systems more complex than isolated atoms [20], its main limitation coming from the approximate form for the kinetic energy contribution (it should be noted that more sophisticated and accurate choices for the kinetic energy term as a function of the electron density can be made [21]). On a more fundamental basis, the model was introduced when there was no theoretical ground to support the choice of the charge density, rather than the many-body wavefunction, for the search, via the variational principle (1.8), of the electronic ground state.

1.2.1 The Hohenberg-Kohn theorems

The essential role that is played by the charge density in the search for the electronic ground state was pointed out for the first time by Hohenberg and Kohn [2] in their exact reformulation of the problem that now goes under the name of *Density Functional Theory*.

Let us consider a finite, isolated system of N interacting electrons in an external potential $v(\mathbf{r})$, as described in Sec. 1.1, with a Hamiltonian (1.2); the only additional assumption is that the ground-state Ψ be unique, non-degenerate. This latter assumption will be relaxed in 1.2.2. Again, Ψ and

⁵Neglecting for the rest of the chapter contributions from the term W_{n-n} .

$n(\mathbf{r}) = \langle \Psi | \hat{n} | \Psi \rangle$ are perfectly specified (albeit not explicitly) once N and $v(\mathbf{r})$ are formulated, and thus are *functionals* of $[N, v(\mathbf{r})]$. Let now $\mathcal{V}_N(\mathbb{R}^3)$ be the class of all densities that are positive definite, normalized to an integer number N , and such that *there exists* an external potential $v(\mathbf{r})$ for which there is a non-degenerate ground state corresponding to that density; this is the class of v -representable densities, and the following discussion⁶ will be restricted to densities that belong to this class. The first theorem of Hohenberg and Kohn [2] establishes the legitimacy of the charge density as the fundamental variable in the electronic problem.

1st Theorem: the Density as the Basic Variable $\forall n(\mathbf{r}) \in \mathcal{V}_N(\mathbb{R}^3)$ the external potential $v(\mathbf{r})$ is a functional $v(\mathbf{r}) \equiv v(\mathbf{r})[n(\mathbf{r})]$ of the charge density $n(\mathbf{r})$, within an additive constant.

Proof. Let us assume, *ad absurdum*, that there exists a different potential v' with a ground state Ψ' that gives rise to the same charge density $n(\mathbf{r})$. Let E and E' be the respective ground-state energies; taking Ψ' as a trial solution for the Hamiltonian \hat{H} , we have the strict inequality

$$E < \langle \Psi' | \hat{H} | \Psi' \rangle = \langle \Psi' | \hat{H}' | \Psi' \rangle + \langle \Psi' | \hat{H} - \hat{H}' | \Psi' \rangle = E' + \int n(\mathbf{r})[v(\mathbf{r}) - v'(\mathbf{r})]d\mathbf{r}$$

(if $\langle \Psi' | \hat{H} | \Psi' \rangle = E$ then Ψ' would be the ground state for H , in virtue of (1.8), but the two distinct differential equations for \hat{H} and \hat{H}' cannot have the same ground state). Similarly, taking Ψ as a trial solution for \hat{H}' , we have

$$E' < \langle \Psi | \hat{H}' | \Psi \rangle = \langle \Psi | \hat{H} | \Psi \rangle + \langle \Psi | \hat{H}' - \hat{H} | \Psi \rangle = E - \int n(\mathbf{r})[v(\mathbf{r}) - v'(\mathbf{r})]d\mathbf{r}$$

⁶See 1.2.3 for the problem of v - and N -representability of charge densities and density matrices.

Adding together these two inequalities the *absurdum* is obtained:

$$E + E' < E + E'.$$

QED

It is thus demonstrated that the ground-state charge density determines, in principle, the external potential of the Schrödinger equation of which it is solution⁷ and thus, implicitly, all the other electronic ground-state properties of the system. It is then possible to introduce, in the class of v -representable densities $\mathcal{V}_N(\mathbb{R}^3)$, the functional

$$F[n(\mathbf{r})] = \langle \Psi | \hat{T}_e + \hat{U}_{e-e} | \Psi \rangle; \quad (1.10)$$

this is unique and well defined, and, since it does not explicitly depend on the external potential for the electrons, it is a *universal* functional of the charge density. It should be pointed out that no explicit expressions for this functional are known to date, obviously as a by-product of the complexity of the many-body problem that lies at the core of the definition of $F[n(\mathbf{r})]$ [22].

It is now possible to define, for an *arbitrary* external potential $v(\mathbf{r})$ (assumed here to be local), unrelated to the external potential implicitly defined by a density in $\mathcal{V}_N(\mathbb{R}^3)$, the Hohenberg-Kohn *Density Functional* for the energy of the ground state:

$$E_v[n'(\mathbf{r})] = F[n'(\mathbf{r})] + \int v(\mathbf{r}) n'(\mathbf{r}) d\mathbf{r}. \quad (1.11)$$

The second theorem of Hohenberg and Kohn [2] establishes the existence of a variational principle for this functional of the charge density, thus rationalizing the original intuition of Thomas and Fermi.

⁷Precisely, it is an expectation value of the solution, since $n(\mathbf{r})$ determines $v(\mathbf{r})$, which in turn determines the ground state Ψ , and the relation $n(\mathbf{r}) = \langle \Psi | \hat{n} | \Psi \rangle$ holds.

2^{nd} Theorem: the Energy Variational Principle $\forall n'(\mathbf{r}) \in \mathcal{V}_N(\mathbb{R}^3)$, $E_v[n'(\mathbf{r})] = F[n'(\mathbf{r})] + \int v(\mathbf{r})n'(\mathbf{r})d\mathbf{r} \geq E_0$, where E_0 is the ground-state energy for N electrons in the external potential $v(\mathbf{r})$.

Proof. A given $n'(\mathbf{r})$ determines uniquely, via the 1^{st} theorem, its own external potential and ground-state wavefunction Ψ' . If this Ψ' is used as a trial wavefunction for the expectation value of the Hamiltonian with the external potential $v(\mathbf{r})$, the relation $\langle \Psi' | \hat{H} | \Psi' \rangle \equiv \langle \Psi' | \hat{T}_e + \hat{U}_{e-e} | \Psi' \rangle + \langle \Psi' | \hat{v} | \Psi' \rangle = F[n'(\mathbf{r})] + \int v(\mathbf{r})n'(\mathbf{r})d\mathbf{r} = E_v[n'(\mathbf{r})]$ holds. Now, because of the minimum principle 1.8, $E_v[n'(\mathbf{r})] = \langle \Psi' | \hat{H} | \Psi' \rangle \geq E_0$. Since the ground state is non-degenerate, the equality holds only if Ψ' is the ground state for the potential v .

QED

These two theorems show that the problem of solving the Schrödinger equation for the ground state can be exactly recast into the variational problem of minimizing the Hohenberg-Kohn functional (1.11) with respect to the charge density; the complexity of the problem is reduced in principle from having to deal with a function of $3N$ variables to one that depends only on the 3 spatial coordinates.

1.2.2 The Levy approach

A simpler and more direct proof for the Hohenberg-Kohn theorems has been introduced by Levy [23]; this has the advantage of removing the requirement of non-degeneracy for the ground state of the electronic problem, while focusing directly on the minimization procedure in the definition of the func-

tional itself. In addition, the ill-defined problem of the representability of the charge density is greatly simplified (see 1.2.3).

Levy [23][24] introduced a new definition for functionals of the density, based on the concept of *constrained search*. Given an operator \hat{A} and a density $n(\mathbf{r})$, the functional $A[n(\mathbf{r})]$ is defined as the minimum expectation value of A for a constrained search along all the many-body antisymmetric wavefunctions for which $\langle \Psi | \hat{n} | \Psi \rangle = n(\mathbf{r})$:

$$A[n(\mathbf{r})] = \min_{\Psi \rightarrow n} \langle \Psi | \hat{A} | \Psi \rangle \quad (1.12)$$

This definition is meaningful (the set is non-empty) for those densities that do admit a representation derived from a N -body wavefunction; it is the class of N -representable densities, much simpler to characterize than the class of v -representable densities (see 1.2.3). The set is also known to be bounded from below [25]. The Levy proof develops as follows⁸:

Theorem: the Levy proof *The ground-state electron density $n_0(\mathbf{r})$ minimizes the functional $E_v[n(\mathbf{r})] = F[n(\mathbf{r})] + \int v(\mathbf{r})n(\mathbf{r})d\mathbf{r}$, where $F[n(\mathbf{r})]$ is a universal functional of $n(\mathbf{r})$; the minimum value is the ground-state electronic energy E_0 .*

Proof: Let the operator \hat{F} be $\hat{T}_e + \hat{U}_{e-e}$; $F[n(\mathbf{r})]$ is defined uniquely (and it is a universal functional of the charge density alone) via the constrained search $\min_{\Psi \rightarrow n} \langle \Psi | \hat{F} | \Psi \rangle$. For an arbitrary $n(\mathbf{r})$, let Ψ_n be the N -electron wavefunction that yields the charge density $n(\mathbf{r})$ and minimizes $\langle \Psi | \hat{F} | \Psi \rangle$. $E_v[n(\mathbf{r})]$ is $F[n(\mathbf{r})] + \int v(\mathbf{r})n(\mathbf{r})d\mathbf{r}$, and so it follows from the definition of Ψ_n that $E_v[n(\mathbf{r})] = \langle \Psi_n | \hat{F} + \hat{v} | \Psi_n \rangle$; but this is the Hamiltonian in the presence

⁸As a matter of clarity, a subscript is introduced to denote all the quantities that refer to the ground state (Ψ_0, n_0, E_0) .

of the external potential $v(\mathbf{r})$, and so we have, from the minimum principle (1.8), that for every N -representable charge density

$$E_v[n(\mathbf{r})] \geq E_0.$$

Now it remains to be demonstrated what is the value of E_v evaluated on the ground state charge density n_0 . Since the ground-state wavefunction Ψ_0 integrates to the ground-state charge density n_0 , it certainly takes part in the constrained search that defines $F[n_0(\mathbf{r})]$. Thus, $F[n_0(\mathbf{r})] \leq \langle \Psi_0 | \hat{F} | \Psi_0 \rangle$, and so, adding the external potential term on both sides, we have

$$E_v[n_0(\mathbf{r})] \leq E_0,$$

that, together with the previous relation, gives us $E_v[n_0(\mathbf{r})] = E_0$.

QED

It should be mentioned that, although very powerful, this approach misses one of the elegant results of Hohenberg and Kohn, namely that there are no two different external potentials (a part from some additive constant) that give rise to the same ground-state electronic charge density.

1.2.3 The representability problem

The original Hohenberg-Kohn proof takes place in the space of charge densities that are v -representable; again, this means that they are positive definite, normalized to an integer number, and such that there exists an external potential $v(\mathbf{r})$ for which there is a non-degenerate ground state corresponding to that density. In this framework, the Hohenberg-Kohn 1st theorem establishes a one-to-one mapping between a v -representable charge density and

the external potential for which this density is the expectation value of the ground state, and in this space $\mathcal{V}_N(\mathbb{R}^3)$ the universal functional F and the variational principle of the 2nd theorem are formulated. The characterization of the class $\mathcal{V}_N(\mathbb{R}^3)$ is still lacking; v -representability has been demonstrated, in a lattice version of the Schrödinger equation, for all the particle-conserving charge densities that are in the neighbour of a v -representable density [26]. This, together with the more serious necessity to adopt approximations for the universal functional F , has lead to a generalized application of the variational principle for all of its practical implementations. It should be pointed out that simple counter-examples of densities that do not belong to $\mathcal{V}_N(\mathbb{R}^3)$ have been presented [24][27]; e.g. if a Hamiltonian has a ground state with degeneracy greater than 2, the density obtained from a linear average of each ground state is in general not v -representable [24].

The Levy proof overcomes this problem, by requiring the density just to be obtainable from some antisymmetric wavefunction (in addition to being positive definite and normalized to an integer number), in order to allow for a meaningful constrained search. This is the condition of N -representability, a much weaker requirement that is satisfied by any well-behaved charge density. In fact, it has been demonstrated by Gilbert [28] that the only condition required is proper differentiability,

$$\int |\nabla n^{\frac{1}{2}}(\mathbf{r})|^2 d\mathbf{r} \in \mathbb{R},$$

to ensure that the kinetic energy of the auxiliary orbitals used in the construction of an antisymmetric wavefunction from a given $n(\mathbf{r})$ remains finite.

1.2.4 Density operators

Up to now, a quantum state has been described in terms of its N-body wavefunction $\Psi(\mathbf{r}_1, \dots, \mathbf{r}_N)$, with the expectation value for a given observable \hat{A} (Hermitian operator) given by $\langle \hat{A} \rangle = \langle \Psi | \hat{A} | \Psi \rangle$. A more general description can be obtained with the introduction of the *density operator* $\hat{\gamma}_N = |\Psi\rangle\langle\Psi|$, whose representation in the coordinate space is the *density matrix*

$$\Psi^*(\mathbf{r}'_1, \dots, \mathbf{r}'_N)\Psi(\mathbf{r}_1, \dots, \mathbf{r}_N).$$

For a normalized Ψ , $\text{tr}(\hat{\gamma}_N) \equiv \int \Psi^*(\mathbf{r}_1, \dots, \mathbf{r}_N)\Psi(\mathbf{r}_1, \dots, \mathbf{r}_N) d\mathbf{r}_1 \dots d\mathbf{r}_N = 1$; $\hat{\gamma}_N$ is clearly idempotent, and thus it is a projection operator. The expectation values can now be expressed as a trace on this operator; in the coordinate representation and for a normalized Ψ we have

$$\langle \hat{A} \rangle = \text{tr}(\hat{\gamma}_N \hat{A}) = \text{tr}(\hat{A} \hat{\gamma}_N) = \langle \Psi | \hat{A} | \Psi \rangle. \quad (1.13)$$

The description of a system at a finite temperature requires the introduction of an *ensemble density operator*, since then the system is part of a much larger closed system (a heat bath with quasi-infinite thermal capacity) for which a complete Hamiltonian description is unattainable. In this case, the system is said to be in a *mixed state*, where it cannot be characterized by a wavefunction (as opposed to the *pure states* of all the preceding discussion), but only as a mixture over all pure states. The ensemble density operator $\hat{\Gamma}_N$ is thus defined as $\hat{\Gamma}_N = \sum_i w_i |\Psi_i\rangle\langle\Psi_i|$, where the sum is taken over all the available pure states. The w_i are often described as the probabilities of finding the system in the relative pure state, although this is conceptually misleading [29], and the w_i are just a statistical distribution outcome of both the probabilistic interpretation of the wavefunction and of the statistical description

coming for our imperfect knowledge of the full system. This becomes apparent in the statistical generalization of (1.13) for the expectation value of an observable for a mixed state, which is given by

$$\langle \hat{A} \rangle = \text{tr}(\hat{\Gamma}_N \hat{A}) = \text{tr}(\hat{A} \hat{\Gamma}_N) = \sum_i w_i \langle \Psi_i | \hat{A} | \Psi_i \rangle, \quad (1.14)$$

where the cross terms that would arise if the mixed state was actually a superposition of pure states are not included. In contrast to the density operator, the ensemble density operator is no longer idempotent; they are both Hermitian and uniquely defined (as opposed to the wavefunction, that has an arbitrary phase attached). An important relation follows from the definitions and from the time-dependent Schrödinger equation $i\hbar|\dot{\Psi}\rangle = \hat{H}|\Psi\rangle$:

$$\frac{\partial}{\partial t} \hat{\gamma}_N = \left(\frac{\partial}{\partial t} |\Psi\rangle \right) \langle \Psi | + |\Psi\rangle \left(\frac{\partial}{\partial t} \langle \Psi | \right) = \frac{\hat{H}}{i\hbar} |\Psi\rangle \langle \Psi | - |\Psi\rangle \langle \Psi | \frac{\hat{H}}{i\hbar},$$

from which the *Liouville equations* for the density operator and, by the linearity of $\hat{\Gamma}_N = \sum_i w_i |\Psi_i\rangle \langle \Psi_i|$, for the ensemble density operator, are obtained:

$$i\hbar \frac{\partial}{\partial t} \hat{\gamma}_N = [\hat{H}, \hat{\gamma}_N], \quad i\hbar \frac{\partial}{\partial t} \hat{\Gamma}_N = [\hat{H}, \hat{\Gamma}_N]. \quad (1.15)$$

The Hamiltonian and the ensemble density operator commute in the case of a stationary state:

$$[\hat{H}, \hat{\Gamma}_N] = 0, \quad (1.16)$$

and a complete system of eigenvectors for both of them can be found. This is a fundamental relation that will be fully exploited in the development of a practical algorithm (albeit for the slightly different case of non-interacting electrons in a self-consistent potential).

It is possible and useful to define a *reduced density matrix of p^{th} order*, which in the coordinate representation has the following form:

$$\gamma_p(\mathbf{r}'_1 \dots \mathbf{r}'_p; \mathbf{r}_1 \dots \mathbf{r}_p) = \frac{N!}{p! (N-p)!} \int \dots \int \Psi^*(\mathbf{r}'_1 \dots \mathbf{r}'_N) \Psi(\mathbf{r}_1 \dots \mathbf{r}_N) d\mathbf{r}_{p+1} \dots d\mathbf{r}_N.$$

Since the Hamiltonian \hat{H} in (1.2) is a function of one-particle and two-particle terms only, it can be demonstrated that its expectation value can be written as an *explicit functional* of the density matrices of order 1 and 2 [30] (Sec. 2.3), or, since γ_1 descends from γ_2 , just of the density matrix of order 2:

$$\begin{aligned} E &= \text{tr}(\hat{H}\gamma_N) = E[\gamma_1, \gamma_2] = E[\gamma_2] = \\ &= \int [(-\frac{1}{2}\nabla^2 + v(\mathbf{r})] \gamma_1(\mathbf{r}, \mathbf{r}) d\mathbf{r} + \int \int \frac{1}{|\mathbf{r}_1 - \mathbf{r}_2|} \gamma_2(\mathbf{r}_1, \mathbf{r}_2; \mathbf{r}_1, \mathbf{r}_2) d\mathbf{r}_1 d\mathbf{r}_2. \end{aligned} \quad (1.17)$$

It is possible to construct a density-matrix functional theory and demonstrate a variational principle for the functional in (1.17) [31], with the eigenvectors of γ_1 (the natural orbitals) and γ_2 (the natural geminals) as the search variables, and reducing again the complexity of the problem from a $3N$ -dimensional search to a 6-dimensional search. The great obstacle is that γ_1 and γ_2 must be N -representable, thus descending from an appropriate antisymmetric Ψ , and this characterization (especially for γ_2) is still ⁹ unsolved [32]). It is nevertheless interesting to contrast this problem of minimizing an explicit functional in a class of N -representable density matrices that escapes characterization, with the density-functional problem of minimizing a functional that is defined only implicitly in the well-defined simple class of N -representable densities.

⁹Note that γ_2 depends on 4 independent variables, but, because of density-functional theory, is completely characterized by $n(\mathbf{r})$. This means that the set of N -representable density matrices of order 2 has zero Lebesgue measure.

1.2.5 Canonical-ensemble formulation

From the fundamentals of classical statistical mechanics we have that the entropy is

$$S(E, V) \equiv k_B \ln \Omega(E), \quad (1.18)$$

where $\Omega(E)$ is the volume in the phase space occupied by the microcanonical ensemble at energy E . The same definition holds for quantum mechanics, with $\Omega(E)$ computed properly via a sum over all the states of the system:

$$\Omega(E) = \sum_{\{w_i\}} W[\{w_i\}], \quad (1.19)$$

where $W[\{w_i\}]$ is the number of states available for a given set of occupations w_i of the accessible quantum states, and the sum is done on all the possible sets that are compatible with the thermodynamical ensemble. In the statistical description via the ensemble density operator $\hat{\Gamma}_N = \sum_i w_i |\Psi_i\rangle\langle\Psi_i|$, the distribution is over a set of pure states $|\Psi_i\rangle$, with the w_i following the rules of a distribution ($w_i \geq 0$ and $\sum_i w_i = 1$). The entropy can thus be equivalently written as

$$S(E, V) = -k_B \sum_i w_i \ln w_i = -k_B \text{tr}(\hat{\Gamma}_N \ln \hat{\Gamma}_N), \quad (1.20)$$

where the second equality exploits the independence of the value of the trace of an operator from the representation in which it is expressed.

The choice of the ensemble (canonical, in this case) determines the equilibrium ensemble density operator, by requiring that it maximizes the entropy while keeping the constraints on the statistical distribution $\sum_i w_i = 1$ and on the expectation value for the energy $\text{tr}(\Gamma_N \hat{H}) = E$. These conditions lead

to the equilibrium canonical ensemble density operator $\hat{\Gamma}_N^0$ [30] (Sec. 2.7):

$$\hat{\Gamma}_N^0 = \frac{e^{-\beta \hat{H}}}{\text{tr} \left(e^{-\beta \hat{H}} \right)}.$$

Following (1.20) the *Helmholtz free energy* $A = E - TS$ for a given ensemble density operator can be introduced:

$$A[\Gamma_N] \equiv \text{tr} \hat{\Gamma}_N \left(\frac{1}{\beta} \ln \hat{\Gamma}_N + \hat{H} \right). \quad (1.21)$$

Now a variational principle can be demonstrated, that is the exact equivalent of the Rayleigh-Ritz variational principle (1.8) for the case of finite temperature, namely that for every positive definite $\hat{\Gamma}_N$ with unit trace:

$$A[\Gamma_N] \geq A[\Gamma_N^0]. \quad (1.22)$$

where Γ_N^0 is the ground-state ensemble density operator. The proof relies on Gibbs' inequality ($\sum_i w_i (\ln w_i - \ln w_i^0) \geq 0$) and on Jensen's inequality ($\langle \exp(\hat{A}) \rangle \geq \exp(\langle \hat{A} \rangle)$) and can be found in Ref. [33] (Sec. 2.11).

Once the variational principle is formulated, the demonstration of the existence of a finite-temperature, canonical density functional theory follows the steps of Sec. 1.2, either along the original Hohenberg-Kohn proof [3], or in a constrained search formulation. In brief, following the Levy approach, a (canonical ensemble) universal functional of the charge density $n(\mathbf{r})$ can be uniquely defined, via the constrained search on all the density operators that integrate to $n(\mathbf{r})$:

$$F_\beta[n(\mathbf{r})] = \min_{\hat{\Gamma}_N \rightarrow n} \text{tr} \left[\hat{\Gamma}_N \left(\hat{T}_e + \hat{U}_{e-e} + \frac{1}{\beta} \ln \hat{\Gamma}_N \right) \right] \quad (1.23)$$

With this universal functional at hand, the canonical Mermin density functional is written as:

$$A_v[n(\mathbf{r})] = F_\beta[n(\mathbf{r})] + \int v(\mathbf{r}) n(\mathbf{r}) d\mathbf{r}.$$

Now, for a given $n(\mathbf{r})$, a Γ_N that minimizes (1.23) is defined, and a variational principle for the Mermin functional holds (from Eq. 1.22):

$$A_v[n(\mathbf{r})] = A[\Gamma_N] \geq A[\Gamma_N^0]. \quad (1.24)$$

The Mermin functional evaluated on the ground-state charge density $n_0(\mathbf{r})$ involves a search on all the ensemble density operators that integrate to $n_0(\mathbf{r})$, and thus includes the ground state Γ_N^0 ; it follows that $A_v[n_0(\mathbf{r})] \leq A[\Gamma_N^0]$, that, combined with the variational principle for the Mermin functional, gives $A_v[n_0(\mathbf{r})] = A[\Gamma_N^0]$.

1.3 The Kohn-Sham mapping

Density Functional Theory provides the theoretical ground for reformulating the ground-state many-body problem as a variational problem on the charge density; the constrained minimization on the Hohenberg-Kohn density functional for N electrons can be rewritten, introducing the indeterminate multiplier μ , as the variational problem:

$$\delta \left[F[n(\mathbf{r})] + \int v(\mathbf{r})n(\mathbf{r}) \, d\mathbf{r} - \mu \left(\int n(\mathbf{r}) \, d\mathbf{r} - N \right) \right] = 0. \quad (1.25)$$

Formally (1.25) leads to the Euler-Lagrange equation for the charge density¹⁰

$$\frac{\delta F[n(\mathbf{r})]}{\delta n(\mathbf{r})} + v(\mathbf{r}) = \mu. \quad (1.26)$$

¹⁰The derivatives with respect to the charge density are always defined a part an additive constant, since $\int K\delta n(\mathbf{r}) \, d\mathbf{r} = 0$; this can be absorbed into the chemical potential μ . Otherwise, see Sec. 1.3.1, and Refs. [27] and [34] for the characterization of the domain for the variations of the charge density.

The two approaches of minimizing directly the Hohenberg-Kohn density functional (1.11) or solving for the associated differential equation (1.26) are equivalent¹¹, although they might differ in the computational effort associated with their implementation.

With these results in mind, the Thomas-Fermi method can be reinterpreted as a tentative approximation for the unknown universal functional $F[n(\mathbf{r})]$, taken to be the sum of the classical part of the electron-electron interaction plus the kinetic energy of the non-interacting electron gas in the local density approximation. This approach and its subsequent refinements, although very economical, have shown only moderate quantitative agreement with experimental data (see Ref. [37] for a review, and Ref. [21] for recent, more accurate, developments).

A much improved strategy has been developed by Kohn and Sham [4], that successfully readdressed the problem of finding a better approximation to the kinetic energy, albeit at the expense of having to deal with an additional set of auxiliary, orthonormal, orbitals. The kinetic energy is a one-body operator, and as such the expectation value (see Eq. 1.17) can be written in terms of the reduced density matrix of order 1:

$$T = -\frac{1}{2} \int \nabla^2 \gamma_1(\mathbf{r}', \mathbf{r}) \Big|_{\mathbf{r}'=\mathbf{r}} d\mathbf{r} = -\frac{1}{2} \sum_{i=1}^{\infty} w_i \langle \phi_i | \nabla^2 | \phi_i \rangle,$$

where the last equality comes from expressing the density matrix in the representation of its natural orbitals ϕ_i . In general, the natural orbitals are infinite in number. However, if N non-interacting electrons are considered, their ground state antisymmetric wavefunction can be expressed as the Slater

¹¹Note that (1.26) identifies the minimum only if there are no other extremal points; see Ref. [35] for a discussion and [36] for a proof that the *exact* F is indeed a convex functional.

determinant of only N orbitals, which are the lowest eigenstates of the non-interacting Hamiltonian.

The fundamental assumption of Kohn and Sham is to introduce a *reference system of non-interacting electrons in an external potential $v_{KS}(\mathbf{r})$* such that the ground state charge density for this problem is the $n(\mathbf{r})$ that enters the Hohenberg-Kohn functional. This definition is meaningful (at least in its original formulation) if the charge density is non-interacting v -representable, so that there can be a unique definition for the total energy Kohn-Sham functional $T_s[n(\mathbf{r})] + \int v_{KS}(\mathbf{r})n(\mathbf{r}) d\mathbf{r}$, where T_s is now the kinetic energy associated with the new reference system. This technical problem can be overcome, again, by defining the kinetic energy part of the Kohn-Sham functional via a constrained search over all the Slater determinants of order N that integrate to a given charge density $n(\mathbf{r})$:

$$T_s[n(\mathbf{r})] = \min_{\Psi_S \rightarrow n} \langle \Psi_S | \hat{T}_e | \Psi_S \rangle = \min_{\Psi_S \rightarrow n} \left[\sum_{i=1}^N -\frac{1}{2} \int \psi_i^*(\mathbf{r}) \nabla^2 \psi_i(\mathbf{r}) d\mathbf{r} \right].$$

The $T_s[n(\mathbf{r})]$ can then be generalized by extending the search to all the antisymmetric wavefunctions that yield a charge density $n(\mathbf{r})$ (whether it is non-interacting v -representable or not) and it can be demonstrated [25] that this generalized T_s coincides with the original definition for all the densities that are non-interacting v -representable. With this definition at hand, a further decomposition of the universal functional F can take place via the introduction of the classical electrostatic energy term $E_H[n(\mathbf{r})]$:

$$F[n(\mathbf{r})] = T_s[n(\mathbf{r})] + E_H[n(\mathbf{r})] + E_{xc}[n(\mathbf{r})],$$

$$E_H[n(\mathbf{r})] = \frac{1}{2} \int \int \frac{n(\mathbf{r}_1)n(\mathbf{r}_2)}{|\mathbf{r}_1 - \mathbf{r}_2|} d\mathbf{r}_1 d\mathbf{r}_2.$$

This decomposition, where F , T_s and the electrostatic energy are well-defined quantities, acts as an implicit definition for the *exchange-correlation energy* E_{xc} , that collects the contributions from the non-classic electrostatic interaction and from the difference between the true kinetic energy T and the non-interacting one T_s . The real success of the Kohn-Sham reformulation lies ultimately in the fact that E_{xc} , which is the term where all the inescapable complexity of the many-body problem has been finally pushed, is a small fraction of the total energy and, more importantly, that it can be *approximated* surprisingly well. These approximations, discussed in Chap. 2, are at present the strength of Density Functional Theory—in itself a very efficient reformulation for the quantum-mechanical problem—and its limit, in the very good but not exact approximation they provide.

The Euler-Lagrange equation (1.26) is rewritten with the new terminology as

$$\frac{\delta T_s[n(\mathbf{r})]}{\delta n(\mathbf{r})} + v_{KS}(\mathbf{r}) = \mu, \quad (1.27)$$

where the effective potential is

$$v_{KS}(\mathbf{r}) \equiv v(\mathbf{r}) + \int \frac{n(\mathbf{r}')}{|\mathbf{r} - \mathbf{r}'|} d\mathbf{r}' + v_{xc}(\mathbf{r}); \quad v_{xc}(\mathbf{r}) \equiv \frac{\delta E_{xc}[n(\mathbf{r})]}{\delta n(\mathbf{r})}$$

and, again, it is such that the set of non-interacting electrons with kinetic energy T_s in its field have the same ground-state charge density as the interacting electrons in the external potential v . The effective potential is now a function of the charge density itself: the problem has become self-consistent, and the solution for the reference system of non-interacting N-electrons

$$\Psi_S = \frac{1}{\sqrt{N!}} \det[\psi_1, \dots, \psi_N] \quad (1.28)$$

is now bound to produce a charge density that consistently outputs the original input effective potential.

$T_s[n(\mathbf{r})]$ as such is still an unknown functional of the density $n(\mathbf{r})$, but *now* it can be easily (but more expensively) written in terms of the N orbitals ψ_i for the non-interacting electrons, that act as auxiliary variables and properly span the domain of all the N -representable densities (provided that they are continuous and square integrable). The exact kinetic energy for the Kohn-Sham reference system is, straightforwardly:

$$T_s[n(\mathbf{r})] = -\frac{1}{2} \sum_{i=1}^N \langle \psi_i | \nabla^2 | \psi_i \rangle. \quad (1.29)$$

It should be noted that the ψ_i have to be orthonormal (solutions for the non-interacting fermion problem) in order for the kinetic-energy expression (1.29) to be valid.

The variational problem on $n(\mathbf{r})$ is thus finally reformulated in terms of a constrained search on the N ψ_i , where N^2 Lagrange multipliers λ_{ij} are introduced to provide for the orthonormality of the orbitals (and thus for the charge conservation):

$$\delta \left[T_s[n(\mathbf{r})] + \int v_{KS}(\mathbf{r}) n(\mathbf{r}) d\mathbf{r} - \left(\sum_{i,j=1}^N \lambda_{ij} \langle \psi_j | \psi_i \rangle - \mathbb{I} \right) \right] = 0. \quad (1.30)$$

From this a single-particle Schrödinger-like equation is derived:

$$\left[-\frac{1}{2} \nabla^2 + v_{KS} \right] \psi_j = \sum_{i=1}^N \lambda_{ij} \psi_j; \quad (1.31)$$

λ_{ij} is a Hermitian matrix which can be diagonalized via a unitary transformation of the orbitals that leaves the non-interacting N -electron wavefunction (1.28) invariant, and consequently the density and the effective Hamiltonian

$-\frac{1}{2}\nabla^2 + v_{KS}$. From this, the “canonical” Kohn-Sham equations follow¹²:

$$\left[-\frac{1}{2}\nabla^2 + v_H(\mathbf{r}) + v_{xc}(\mathbf{r}) + v_{ext}(\mathbf{r}) \right] \psi_i(\mathbf{r}) = \hat{H}_{KS} \psi_i(\mathbf{r}) = \epsilon_i \psi_i(\mathbf{r}) \quad (1.32)$$

$$v_H(\mathbf{r}) = \int \frac{n(\mathbf{r}')}{|\mathbf{r} - \mathbf{r}'|} d\mathbf{r}', \quad v_{xc}(\mathbf{r}) = \frac{\delta E_{xc}}{\delta n(\mathbf{r})}$$

$$n(\mathbf{r}) = \sum_{i=1}^N |\psi_i(\mathbf{r})|^2.$$

These equations should be iterated to self-consistency, until the minimum for the Kohn-Sham functional is reached; Kohn and Sham proposed taking the lowest N -orbitals to form the determinantal many-body wavefunction, and this choice works consistently for all the charge densities that are non-interacting v -representable (that is, for which T_s can be written in terms of single-particle orbitals).

The Kohn-Sham equations are the Euler-Lagrange equations for the constrained minimization of the Kohn-Sham functional. It should be noted that the search for the ground state can also proceed via the direct minimization of the full functional

$$E[\{\psi_i\}] = \sum_{i=1}^N -\frac{1}{2} \int \psi_i^*(\mathbf{r}) \nabla^2 \psi_i(\mathbf{r}) d\mathbf{r} + E_H[n(\mathbf{r})] +$$

$$+ E_{xc}[n(\mathbf{r})] + \int v_{ext}(\mathbf{r}) n(\mathbf{r}) d\mathbf{r} \quad (1.33)$$

with respect to the N auxiliary orbitals ψ_i , with the proper constraints of orthonormality $\langle \psi_i | \psi_j \rangle = \delta_{ij}$ and charge density conservation. An alternative expression for the total energy can be derived by extracting the *band-energy term* $\sum_i \epsilon_i \equiv \text{tr} (\hat{T}_s + \hat{v}_{KS})$:

$$E[\{\psi_i\}] = \sum_{i=1}^N \epsilon_i - E_H[n(\mathbf{r})] + E_{xc}[n(\mathbf{r})] - \int v_{xc}(\mathbf{r}) n(\mathbf{r}) d\mathbf{r}. \quad (1.34)$$

¹²A subscript is added for clarity to the external potential $v = v_{ext}$.

1.3.1 Fractional occupancies, Janak's theorem

An extension of the previous formalism that includes the case of fractional occupancies has been proposed by Janak [38]. Janak defines a generalized functional of $M(\geq N)$ orbitals $\{\psi_i\}$ and of their occupation numbers $\{f_i\}$; in the language of the constrained search formulation the functional is

$$T_J[n(\mathbf{r})] = \min_{\sum f_i |\psi_i|^2 \rightarrow n} \left[\sum_{i=1}^M f_i \int \psi_i^*(\mathbf{r}) \left(-\frac{1}{2} \nabla^2 \right) \psi_i(\mathbf{r}) d\mathbf{r} \right], \quad (1.35)$$

where the search is performed over all orthonormal orbitals and occupation numbers that yield the density $n(\mathbf{r})$ (hence $\sum_i f_i = N$). The condition $0 \leq f_i \leq 1 \forall i$ assures that the density matrix of order 1 is ensemble N -representable [32], and so it derives from an appropriate Γ_N ; consequently Eq. (1.22) provides the variational principle to develop a density-functional implementation in strict analogy with the Kohn-Sham discussion.

The Janak's functional is formulated:

$$\begin{aligned} E[\{f_i\}, \{\psi_i\}] = & \sum_{i=1}^M f_i \int \psi_i^*(\mathbf{r}) \left(-\frac{1}{2} \nabla^2 \right) \psi_i(\mathbf{r}) d\mathbf{r} + E_H[n(\mathbf{r})] + \\ & + E_{J,xc}[n(\mathbf{r})] + \int v_{ext}(\mathbf{r}) n(\mathbf{r}) d\mathbf{r}, \end{aligned} \quad (1.36)$$

where $E_{J,xc}$ is redefined to take into account the new definition for the non-interacting kinetic energy, and where now the minimization is performed with respect to the $\{\psi_i\}$ and the $\{f_i\}$, instead of the determinantal wave function (1.28) of the Kohn-Sham case. For a fixed set of $\{f_i\}$ the orbitals $\{\psi_i\}$ must satisfy the corresponding Euler-Lagrange equation:

$$\begin{aligned} \frac{\delta}{\delta \psi_i^*} \left\{ E[\{f_i\}, \{\psi_i\}] - \sum_{i=1}^M \lambda'_i (\langle \psi_i | \psi_i \rangle - 1) \right\} = 0, \quad \text{i.e.} \\ \left[-\frac{1}{2} f_i \nabla^2 + f_i \hat{v}_{J,KS} \right] \psi_i = \lambda'_i \psi_i, \end{aligned} \quad (1.37)$$

where now the Lagrange multipliers are diagonal, and the orthogonality comes from the previous differential equation (1.37) (this is due to the choice of the T_J functional as a diagonal sum). These are again Kohn-Sham-like equations, and obviously for $f_i \neq 0$ $\epsilon_i = \lambda'_i/f_i$.

The dependence of the functional E on the occupation numbers can be seen by calculating the unconstrained variation of the energy with respect to one f_i , $\partial E/\partial f_i$, while allowing the orbitals to relax:

$$\begin{aligned} \frac{\partial E}{\partial f_i} &= -\frac{1}{2} \int \psi_i^*(\mathbf{r}) \nabla^2 \psi_i(\mathbf{r}) d\mathbf{r} + \int \frac{\delta(v_H + v_{xc} + v_{ext})}{\delta n(\mathbf{r})} \frac{\delta n(\mathbf{r})}{\delta f_i} d\mathbf{r} = \\ &= -\frac{1}{2} \int \psi_i^*(\mathbf{r}) \nabla^2 \psi_i(\mathbf{r}) d\mathbf{r} + \int v_{J,KS} \psi_i^*(\mathbf{r}) \psi_i(\mathbf{r}) d\mathbf{r} = \epsilon_i \end{aligned} \quad (1.38)$$

The expression above is referred to as *Janak's theorem*. The constrained variation of the energy functional with respect to f_i , that is the unconstrained minimization of $E - \mu N$, gives [39]:

$$\delta[E - \mu N] = \sum_i (\epsilon_i - \mu) \delta f_i, \quad (1.39)$$

which provides a rationale to the choice of $f_i = 0$ or 1 for ϵ_i greater or smaller than μ (so that $\delta[E - \mu N] \geq 0$). It is apparent from Eq. (1.39) that Janak's functional is not variational with respect to the occupation numbers (to a variation in the occupation numbers, precisely), as noted in [39][40].

Finally, it should be mentioned that there are some conceptual problems in the foundations of Eq. 1.38, as noted in Ref. [41], Sec. 9, and more recently in Ref. [34]. The objections arise in considering occupation numbers different from either 0 or 1 in zero-temperature density-functional theory, and in fact there are indications [27][34] that the domain of definition for the functional derivatives with respect to the charge density might not include

charge densities written in terms of fractional occupation numbers. Either on these methodological grounds, or following Janak's analysis, the conclusion is that occupation numbers (with an exception made for orbitals which will eventually be degenerate at the Fermi level) are bound to assume *at self-consistency* a value that is either 0 or 1. Fractional occupation numbers should thus be properly considered only in a statistical sense, as the output of a finite-temperature formulation.

1.3.2 Finite-temperature extension

The extension of density functional theory to the canonical ensemble has been discussed in Sec. 1.2.5, where the variational principle for the canonical Mermin functional $A_v[n(\mathbf{r})]$ has been demonstrated, following from Eq. 1.22. A Kohn-Sham mapping onto single-particle orbitals in a self-consistent potential will be discussed here, first for the case of non-interacting electrons and then for interacting ones.

If the electrons are non-interacting, the allowed states are the solutions of the single-particle equations

$$\left[-\frac{1}{2} \nabla^2 + \hat{v}_{ext} \right] \psi_i = \epsilon_i \psi_i. \quad (1.40)$$

The occupation of each state is determined by the statistics (that is, ultimately, a prescription for counting the states) and by the temperature; the requirement that the entropy $k_B \ln \Omega(E) = \sum_{\{f_i\}} W[\{f_i\}]$ is maximized, together with the Fermi-Dirac statistics, brings in the familiar Fermi-Dirac distribution [42]:

$$f_i = f \left(\frac{\epsilon_i - \mu}{T} \right) = \frac{1}{1 + \exp\left(\frac{\epsilon_i - \mu}{T}\right)}; \quad (1.41)$$

for this distribution the entropy $S = k_B \ln \Omega(E)$ is

$$S = -k_B \sum_i [f_i \ln f_i + (1 - f_i) \ln(1 - f_i)] \quad (1.42)$$

and the expectation value of the kinetic energy operator is:

$$T_s = \sum_i f_i \int \psi_i^*(\mathbf{r}) \left(-\frac{1}{2} \nabla^2 \right) \psi_i(\mathbf{r}) d\mathbf{r} = \sum_i f_i \epsilon_i - \int v_{ext}(\mathbf{r}) n(\mathbf{r}) d\mathbf{r}. \quad (1.43)$$

These expressions can be derived more formally with the help of second-quantization operators (see Ref. [33], Chap. 6).

The Kohn-Sham formulation for a system of interacting electrons (see Refs. [43][41][44]) follows the lines of the zero-temperature case: a reference system of non-interacting electrons is introduced, for which the ground state has the charge density $n(\mathbf{r})$ that enters in the canonical Mermin functional $A_v[n(\mathbf{r})] = F_\beta[n(\mathbf{r})] + \int v_{ext}(\mathbf{r})n(\mathbf{r}) d\mathbf{r}$. An exchange-correlation potential $E_{\beta,xc}[n(\mathbf{r})]$ is then implicitly defined by isolating in $F_\beta[n(\mathbf{r})]$ the non-interacting kinetic energy T and entropy S of the non-interacting system defined in (1.43) and (1.42). The minimization of the Mermin functional, with the constraint of charge normalization, leads to the canonical Mermin-Kohn-Sham equations:

$$\left[-\frac{1}{2}\nabla^2 + v_H(\mathbf{r}) + v_{\beta,xc}(\mathbf{r}) + v_{ext}(\mathbf{r}) \right] \psi_i(\mathbf{r}) = \epsilon_i \psi_i(\mathbf{r}) \quad (1.44)$$

$$v_H(\mathbf{r}) = \int \frac{n(\mathbf{r}')}{|\mathbf{r} - \mathbf{r}'|} d\mathbf{r}', \quad v_{\beta,xc}(\mathbf{r}) = \frac{\delta E_{\beta,xc}}{\delta n(\mathbf{r})}$$

$$\sum_i f_i \left(\frac{\epsilon_i - \mu}{T} \right) = N, \quad n(\mathbf{r}) = \sum_i f_i |\psi_i(\mathbf{r})|^2.$$

These equations are formally similar to the zero-temperature case, although now there is a Lagrange multiplier μ to constrain the sum of the occupations to the total number of electrons N , since the number of states that the finite-temperature brings in jumps from N to ∞ (although for all purposes one can neglect all the states higher than a threshold for which the occupancies are practically zero). Alternatively, one can minimize directly the canonical Mermin functional as a function of the $\{f_i\}$ and $\{\psi_i\}$, with the explicit constraints of charge normalization and orthonormality:

$$A [T ; \{ \psi_i \}, \{ f_i \}] = \sum_i f_i \int \psi_i^*(\mathbf{r}) \left(-\frac{1}{2}\nabla^2 \right) \psi_i(\mathbf{r}) d\mathbf{r} + E_H[n(\mathbf{r})] + E_{\beta,xc}[n(\mathbf{r})] + \int v_{ext}(\mathbf{r})n(\mathbf{r}) d\mathbf{r} + T \left(k_B \sum_i [f_i \ln f_i + (1 - f_i) \ln(1 - f_i)] \right). \quad (1.45)$$

An alternative expression can be obtained introducing the band-energy term:

$$\begin{aligned} A [T ; \{ \psi_i \}, \{ f_i \}] = & \sum_i f_i \epsilon_i - E_H[n(\mathbf{r})] + E_{\beta,xc}[n(\mathbf{r})] + \\ & - \int v_{\beta,xc}(\mathbf{r}) n(\mathbf{r}) \, d\mathbf{r} + T \left(k_B \sum_i [f_i \ln f_i + (1-f_i) \ln(1-f_i)] \right) \end{aligned} \quad (1.46)$$

A different and very interesting approach has been proposed [45] (see also [46]), in which the kinetic-energy is not determined via a Kohn-Sham based orbital representation, but it is propagated a-la Feynman from high temperatures. Starting from the grand-canonical potential for the non-interacting electrons $\Omega = -\frac{1}{\beta} \ln \det [\mathbb{I} + \exp(-\beta(\hat{H} - \mu))]$, where \hat{H} is the single-particle $\hat{T}_e + \hat{v}_{ext}$, a Kohn-Sham decomposition is performed. The minimization of

$$\begin{aligned} A[n(\mathbf{r}); T] = & -\frac{1}{\beta} \ln \det [\mathbb{I} + \exp(-\beta(\hat{H} - \mu))] + \\ & - E_H[n(\mathbf{r})] + E_{\beta,xc}[n(\mathbf{r})] - \int v_{\beta,xc}(\mathbf{r}) n(\mathbf{r}) \, d\mathbf{r} \end{aligned} \quad (1.47)$$

is then reached by iterating to self-consistency with the constraint of charge density normalization; the density matrix is evaluated as a path integral

$$e^{-\beta \hat{H}} = \left(e^{-\beta \hat{H}/P} \right)^P,$$

employing the Trotter decomposition, and with the choice of a real-space propagator for both the external potential *and* the kinetic energy operator. With this real-space formulation, this approach does not suffer from errors in the Brillouin Zone sampling of the kinetic-energy or of the charge density, although it does require a finer representation in real-space. In the present case, the minimization is reached iteratively, and not in a strictly variational fashion. In order to gauge the relative advantages and drawbacks a set of applications to a wider class of systems is needed; the relevant issues are

the relative costs of an orbital-based formulation in comparison to a charge-density one, the cutoff requirements for the chosen representation (e.g. plane waves vs. a real space grid), and the added computational stability that a strictly variational formulation does provide.

Chapter 2

Methods of electronic structure

Introduction

A set of approximations and techniques are introduced that allow an affordable and efficient implementation of the concepts discussed in Chapter 1. First and foremost, the Local Density Approximation [4][47] to the exchange-correlation energy is described. This approximation, or one of its recent refinements [48], brings the conceptualization operated by Density Functional Theory down to an explicit formulation, establishing a limit to its ultimate quantum-mechanical accuracy while making at the same time quantum mechanics practically applicable to an immense variety of systems. The pseudopotential scheme [6][7] is then presented, with its goal of decoupling the small and computationally expensive length scales typical of the core electrons, confined around each nucleus, from those of the interacting gas of the valence electrons, which are responsible for the majority of structural and chemical properties of interest.

These two approximations result in an explicit and manageable form for the total energy of the valence electron gas in the field of the nuclei and their frozen cores; the problem then turns computational, and so a brief description of the most successful methods for the self-consistent minimization of the LDA total-energy functional [49][50] follows. Finally the different problems that arise in dealing with systems that are either metallic or have a vanishing gap are discussed, together with the present state of research in this area.

2.1 The Local Density Approximation

The Kohn-Sham scheme provides an appealing decomposition of the total-energy functional, via its rigorous treatment of the non-interacting kinetic energy term T_s . A local density approximation can then be introduced [4], at variance with the Thomas-Fermi choice of the kinetic energy itself, solely for the remaining unknown *exchange-correlation* functional $E_{xc}[n(\mathbf{r})]$. Kohn and Sham proposed the approximation (universally known as LDA)

$$E_{xc}^{LDA}[n(\mathbf{r})] = \int \epsilon_{xc}(n(\mathbf{r})) n(\mathbf{r}) \, d\mathbf{r}, \quad (2.1)$$

where $\epsilon_{xc}(n) = \epsilon_{xc}(n(\mathbf{r}))$ is the exchange and correlation energy of the homogeneous electron gas of constant density $n = n(\mathbf{r})$. This defines automatically the exchange-correlation potential appearing in the Kohn-Sham equations (1.32) or in the total-energy functional (1.34) as:

$$v_{xc}^{LDA}(\mathbf{r}) = \frac{\delta E_{xc}^{LDA}}{\delta n(\mathbf{r})} = \epsilon_{xc}(n(\mathbf{r})) + \frac{\partial \epsilon_{xc}(n)}{\partial n} n(\mathbf{r}). \quad (2.2)$$

The function $\epsilon_{xc}(n)$ can be decomposed in an exchange part, for which the Dirac [51] result gives

$$\epsilon_x(n) = -\frac{3}{4} \left(\frac{3}{\pi} \right)^{1/3} n^{1/3},$$

and a remaining correlation term $\epsilon_c(n)$, a function solely of n , that can be determined once for all by interpolating between quantum MonteCarlo calculations [47] and the appropriate asymptotic high-density limit [52][39]. The rationale for this approximation is that in the limit of slowly varying density an exchange-correlation contribution $\epsilon_x(n)dn(\mathbf{r})$ can be attributed to each infinitesimal element in \mathbf{r} , and the total exchange-correlation obtained by quadrature [2][4]. The domain of applicability of LDA has been found, unexpectedly, to go much beyond the nearly free-electron gas, and accurate results can be obtained for very inhomogeneous systems (see Ref. [53]). An explanation for this success [54] comes from the analysis of the properties of the *exchange-correlation hole* $n_{xc}(\mathbf{r}, \mathbf{r}')$: the exchange-correlation energy of the interacting system can be reformulated exactly as

$$E_{xc} = \frac{1}{2} \int d\mathbf{r} n(\mathbf{r}) \int d\mathbf{r}' \frac{1}{|\mathbf{r} - \mathbf{r}'|} n_{xc}(\mathbf{r}, \mathbf{r}' - \mathbf{r}), \quad (2.3)$$

where $n_{xc}(\mathbf{r}, \mathbf{r}')$ is defined in terms of the pair-correlation function $g(\mathbf{r}, \mathbf{r}', \lambda)$ for the system described by a density $n(\mathbf{r})$ but interacting via a *reduced* Coulomb interaction $\lambda \hat{U}_{e-e}$

$$n_{xc}(\mathbf{r}, \mathbf{r}' - \mathbf{r}) \equiv n(\mathbf{r}') \int_0^1 [g(\mathbf{r}, \mathbf{r}', \lambda) - 1] d\lambda. \quad (2.4)$$

The exchange-correlation hole describes intuitively the concept of Pauli repulsion, in that an electron at a position \mathbf{r} reduces the probability of finding one in a position \mathbf{r}' , creating a charge depletion around \mathbf{r} . The exchange-

correlation energy can be regarded as the energy resulting from the interaction of an electron and its surrounding exchange-correlation hole. Since $g(\mathbf{r}, \mathbf{r}', \lambda)$ tends to 1 for an increasing separation $|\mathbf{r} - \mathbf{r}'|$, the exchange-correlation hole is essentially associated with the short-range quantum effects of the Coulomb interaction. Given that the latter is isotropic, it can be demonstrated [54] that the exchange correlation energy depends only on the *spherical average* of $n_{xc}(\mathbf{r}, \mathbf{r}')$ for a given \mathbf{r} ; it has been shown in fact [55] that even if the exact and LDA exchange-correlation holes differ significantly, their spherical averages are similar even for very inhomogeneous systems, and this provides the key to understanding the reasons for the success of LDA in a wide and general variety of environments for the electron gas. Finally, the LDA satisfies exactly the sum rule

$$\int n_{xc}^{LDA}(\mathbf{r}, \mathbf{r}' - \mathbf{r}) = \int n_{xc}(\mathbf{r}, \mathbf{r}' - \mathbf{r}) d\mathbf{r}' = -1, \quad (2.5)$$

which explains some of its accuracy; the necessity of enforcing this sum rule is at the origin of some of the difficulties encountered in improving the LDA by means of perturbative expansions (the most recent and successful development being the generalized gradient approximation (GGA) of Perdew and Wang (PW91, Ref. [48])). The LDA will be used in all the applications presented here, which deal with systems where the charge density varies smoothly and which are within the domain of accuracy of the LDA.

2.2 The pseudopotential approximation

The pseudopotential approximation¹ provides a rational way to isolate the fundamental role played by the valence electrons in the electronic-structure problem. In a mean-field picture, the valence electrons can be thought of as the loosely bound orbitals which are most strongly modified on formation of the chemical bonds in a molecule or the bands in a solid. The length-scales of these orbitals (and energies, since the Schrödinger equation mixes the two via the Laplacian) are those characteristic of inter-atomic separations and chemical bond energies. In contrast, inner electrons are tightly bound around each atomic nucleus and are largely unperturbed by the environment surrounding their atom. In a Hartree-Fock or Kohn-Sham mean-field picture, the higher orbitals must have features on the inner core length-scales via the orthogonality constraint to the lower orbitals. Nevertheless, it can be argued that the atomic problem can be projected for the valence electrons into an effective energy-dependent Hamiltonian, where the nuclear attraction is largely screened by a repulsive term that mimics the effects of the orthogonality constraint; this is the rationale behind the *cancellation theorem* [6]. The resulting potential is commonly referred to as a *pseudopotential* and it is much weaker and smoother than the original Coulombic potential. This weak potential brings in a picture for the electron-ion interaction in solids of a inhomogeneous electron gas weakly perturbed by an array of effective pseudopotentials [7].

¹See Refs. [56] and [57] for some recent and comprehensive reviews.

2.2.1 Basis representation

The pseudopotential approach allows for a representation of the quantities of interest —the charge density and its decomposition into the Kohn-Sham orbitals—that is as general and as economical as possible, since the electronic structure problem can then be solved on a discrete grid in real space where the accuracy on the spacing needs to be only that necessary to follow the oscillations of the pseudo-orbitals and the motion of the pseudo-ions. Methods that operate exclusively in real-space are being introduced nowadays, based either on regular grids [58], or on the variable metrics provided by adaptive coordinates [59], or based on multi-grid techniques [60].

In what follows we will adopt what is presently the method of choice for the description of periodic solids, introducing periodic-boundary conditions [61] that eliminate or reduce the finite size errors in the description of perfect bulk crystals or systems with some degree of periodicity². The induced periodicity in the external potential makes the Hamiltonian operator commute with the set of translation operators identified by the periodic boundary conditions [62]; the set of common eigenstates for these operators is (*Floquet’s*, or *Bloch’s theorem*):

$$\psi_{\hat{H}}(\mathbf{r}) = \psi_{n\mathbf{k}}(\mathbf{r}) = e^{i\mathbf{k}\cdot\mathbf{r}} u_{n\mathbf{k}}(\mathbf{r}), \quad (2.6)$$

where \mathbf{k} is the quasi-momentum and $u_{n\mathbf{k}}(\mathbf{r})$ has the periodicity of the unit cell. The infinite wavefunctions of an extended system become represented, with these periodic boundary conditions, by a finite number of wavefunctions for each quasi-momentum \mathbf{k} , spanning the infinite set of points \mathbf{k} inside the

²E.g. surfaces, that can be described by periodically repeated thick slabs in the direction perpendicular to the surface, while keeping the perfect periodicity parallel to it.

Brillouin Zone. The periodicity of $u_{n\mathbf{k}}(\mathbf{r})$ is exploited when representing the wavefunction with the *discrete* basis of plane waves (that are an orthogonal and complete set):

$$\langle \mathbf{r} | \mathbf{k} + \mathbf{G} \rangle = \frac{1}{\sqrt{V}} e^{i(\mathbf{k} + \mathbf{G}) \cdot \mathbf{r}},$$

where V is the volume of the unit cell; additionally, a metric for the completeness can be naturally introduced by selecting the *finite set* of plane waves for which $|\mathbf{k} + \mathbf{G}|^2 \leq E_{cutoff}$. The expectation value for the kinetic energy of a wavefunction represented on a basis of plane waves is calculated efficiently in reciprocal space:

$$\psi_{n\mathbf{k}}(\mathbf{r}) = \sum_{\mathbf{G}} c_{n\mathbf{k},\mathbf{G}} e^{i(\mathbf{k} + \mathbf{G}) \cdot \mathbf{r}} \Rightarrow \langle \psi_{n\mathbf{k}}(\mathbf{r}) | -\nabla^2 | \psi_{n\mathbf{k}}(\mathbf{r}) \rangle = \sum_{\mathbf{G}} c_{n\mathbf{k},\mathbf{G}}^2 |\mathbf{k} + \mathbf{G}|^2,$$

while the action of the (local) pseudopotential is expressed in real space; in other words the kinetic-energy operator is diagonal in reciprocal space, and the external potential is diagonal in real space. It is computationally more convenient to calculate these expectation values in the representation for which they are diagonal, switching back and forth from one representation (the Fourier coefficients $c_{n\mathbf{k},\mathbf{G}}$) to the other (the wavefunction $\psi_{n\mathbf{k}}(\mathbf{r})$ on a grid in real space), since efficient algorithms are available (the so-called Fast Fourier Transforms, see Chapter 12 of Ref. [63]) whose cost is roughly proportional to the number N of elements in the mesh to be transformed (more precisely it is $\mathcal{O}(N \ln N)$).

2.2.2 Smoothness and transferability

Simple and fairly accurate models of pseudopotentials were developed initially by choosing some simple analytical form (either in real space, like in

the “empty-core” potential [64], or for its Fourier components, as in the “Empirical Pseudopotential Method” [65]), and then adjusting the parameters in order to fit the atomic energy levels or the band structures. Whilst providing considerable insight for the theory of the electronic structure of solids, these pseudopotentials do not provide the fundamental requirement of *transferability*, in that their ad-hoc fitting procedure does not guarantee a faithful representation outside the configuration space in which the fitting has been performed, and so little success is expected when using these pseudopotential in widely different chemical environments. This generally precludes the ability to perform truly first-principles calculations, that require to determine material properties without the need of any experimental input, and in particular without the need of adopting procedures that are tuned in advance to the specific problem addressed. To improve this accuracy, and given the angular symmetry of the atomic orbitals and the independent orthogonality constraints that they generate, it is natural to develop a scattering approach [7] in which the pseudopotential acts differently on each angular-momentum component of the scattering wavefunction; the pseudopotentials is thus decomposed onto a sum of projections over different angular momenta, and becomes a *non-local* (or semi-local, more accurately in this case) operator

$$V_{ps}(\mathbf{r}, \mathbf{r}') = V^{loc}(r) \delta(\mathbf{r} - \mathbf{r}') + \sum_l V_l^{non-loc}(r) \delta(r - r') P_l(\hat{\mathbf{r}}, \hat{\mathbf{r}}').$$

In addition to this, the modern theory of pseudopotentials builds around the key issue of transferability, constructing a pseudopotential that scatters the incoming wavefunction as closely as possible to the original potential over a wide range of energies. A systematic and successful procedure for the development of accurate and transferable pseudopotentials has been developed [66]

[67], where the added constraint of *norm-conservation* is introduced in order to preserve transferability. In summary, the requirements in constructing the pseudopotential are:

- the lowest eigenvalues for $T + V_{ps}$ must equal the valence all-electron eigenvalues.
- the pseudo-wavefunctions ϕ_l should be nodeless, and they and their first derivatives must be differentiable.
- the pseudo-wavefunctions ϕ_l must be identical with the all-electron wavefunctions beyond a chosen core radius.

or equivalently (norm-conservation)

- the total integrated pseudo-charge density from a given ϕ_l and the corresponding all-electron charge density are identical inside the core radius.

The norm-conservation requirement ensures that the logarithmic derivative of ϕ_l (related to the phase shifts in the scattering) has the same behaviour—up to the first order in changes in energy—as in the all-electron case. Thus the pseudopotential is constructed from the beginning with an intrinsic degree of transferability. An example of a non-local norm-conserving pseudopotential, together with its pseudo-wavefunctions, is given in Fig. 2.1.

The original choice [67] for the pseudopotentials’ core radii along the periodic table was conservatively small, thus aiding transferability at the cost of smoothness and computational effort. Several groups have proposed modified schemes for generating pseudopotentials aimed at reducing the number of

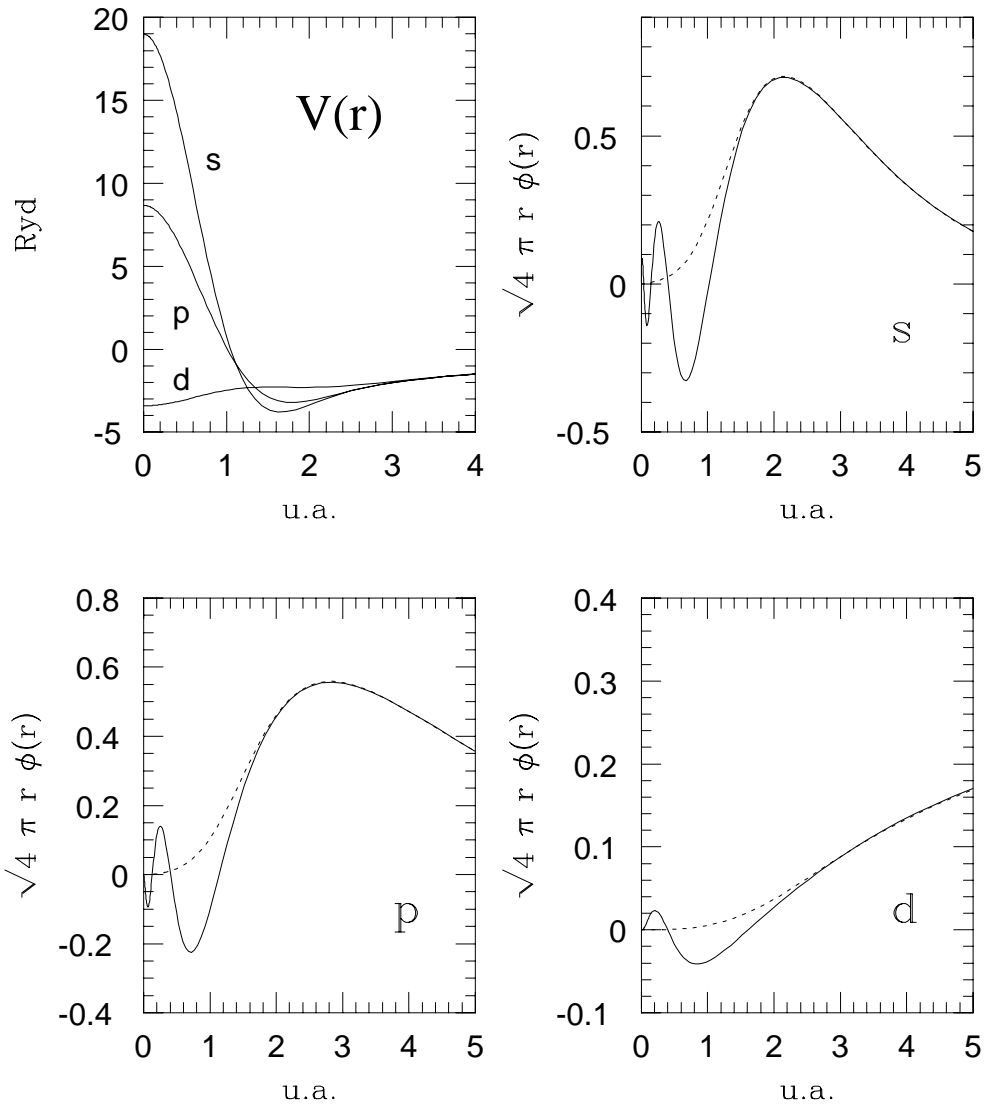


Figure 2.1: s -, p - and d - components of a non-local norm-conserving pseudopotential (In), with the all-electron and pseudo-wavefunctions $r\phi(r)$ (solid and dashed, clockwise from top left).

plane waves required to describe properly the electron-ion interaction, either focusing on producing improved smoother wave-functions in the pseudizing process [68] [69] [70] [71] or smoother potentials [72]. In particular, a formulation has been proposed (the *ultrasoft pseudopotential formulation* [73]) that partially releases the constraint of norm-conservation while it imposes at the same time the matching of the scattering properties on a broader range of energies. This allows for improved transferability *and* much increased smoothness, at the price of introducing a mechanism of *charge augmentations* to restore norm-conservation and hence the proper balance of valence charge density in the core region. In all the applications presented here an optimized pseudopotential for Al (courtesy of M.H. Lee, Ref. [71]) has been used, which was generated along the lines of Refs. [69] [70] [71], with the aim of reducing the residual kinetic-energy of the pseudo-wavefunction beyond a given cutoff in reciprocal space in order to improve smoothness:

$$\Delta E_{kin} = \sum_{i, \mathbf{G}_i > \mathbf{q}_c} \mathbf{G}_i^2 |\phi_l(\mathbf{G}_i)|^2.$$

2.2.3 The Kleinman-Bylander representation

The introduction of non-local or semi-local pseudopotentials makes the plane-wave representation of the Hamiltonian much more expensive to calculate. The kinetic-energy operator $\langle \mathbf{G}_i | \hat{T}_e | \mathbf{G}_j \rangle$ is diagonal in reciprocal space, and thus requires a number of operations proportional to the number of plane waves; the local potential, diagonal in real space, is expressed in reciprocal space via a Fast Fourier Transform, and it depends on \mathbf{G}_i and \mathbf{G}_j only as $(\mathbf{G}_i - \mathbf{G}_j)$ (this also makes the cutoff for the representation of the local pseudopotential twice as large as that necessary for the wavefunctions). The

non-local pseudopotential, on the other hand, is a non-trivial dense matrix in \mathbf{G}_i and \mathbf{G}_j , and computing this expectation value requires a number of operations which is proportional to the *square* of the number of plane waves. A shortcut around this problem is offered by rewriting the pseudopotential in the Kleinman-Bylander representation [74], making it fully non-local but at the same time separable in \mathbf{G}_i and \mathbf{G}_j , and thus making the workload just proportional to the number of plane waves. If $\phi_{lm}(\mathbf{r}) = \chi_l(r)Y_{lm}(\hat{\mathbf{r}})$ is an eigenfunction of the atomic pseudo-Hamiltonian, the Kleinman-Bylander representation is defined by:

$$V_{KB}(\mathbf{r}, \mathbf{r}') = V_{KB}^{loc}(r) \delta(\mathbf{r} - \mathbf{r}') + \sum_{lm} \frac{|V_l^{non-loc} \phi_{lm}\rangle \langle \phi_{lm} V_l^{non-loc}|}{\langle \phi_{lm} | V_l^{non-loc} | \phi_{lm} \rangle}.$$

This representation of the potential is different from the original semi-local one, but it can be seen that it acts identically on the reference states $|\phi_{lm}\rangle$, and thus it is conceptually equally well-justified and it is expected to maintain the same degree of smoothness and transferability of the original representation. The fully non-local formulation allows for a completely separable representation in reciprocal space, where the non-local component is given by:

$$V_{KB}^{non-loc}(\mathbf{G}, \mathbf{G}') = \sum_l F_l(\mathbf{G}) F_l^*(\mathbf{G}')$$

and can be computed with a cost that is directly proportional to the number of plane waves. A further improvement towards a more economical representation of the non-local effects of the pseudopotential is obtained by taking advantage of the localization of $V_l^{non-loc}$ in real-space [75], significantly reducing the cost in the limit of very large systems, thanks to the improved scalability.

2.3 Minimizations and dynamics for electrons and ions

The approximations previously described provide an explicit functional form for the exchange-correlation functional of the Kohn-Sham formulation, and an accurate and affordable—at some computational price—form for the interaction between electrons and ions, that acts as external potential for the electron gas. This external potential is fully determined once the nature and coordinates of the pseudo-ions $\{\mathbf{R}_I\}$ are specified; the ground state is then obtained by minimizing the total energy functional (1.33) to self-consistency with respect to the set of orbitals $\{\psi_i\}$. We can consider the total energy of the ground-state as a parametric function of the ionic coordinates $\{\mathbf{R}_I\}$, or in other words as the adiabatic Potential Energy Surface (PES)

$$\mathcal{V}(\mathbf{R}_1, \dots, \mathbf{R}_N) = \min_{\{\psi_i\}} E[\{\psi_i\}; \{\mathbf{R}_I\}].$$

In addition to determining the electronic ground-state properties for a given ionic configuration, it might be important to be able to perform *structural relaxations*, thus determining the local or the global minimum of $\mathcal{V}(\{\mathbf{R}_I\})$ as a function of $\{\mathbf{R}_I\}$, or to perform *molecular dynamics* simulations, where the ions move according to the Newton's equation of motion in the potential field (the PES) determined by the instantaneous electronic ground-state [76].

The total energy depends non-linearly on the orbitals $\{\psi_i\}$, themselves constrained to be orthonormal and bound by the self-consistency requirement to reproduce at the ground state the charge-density dependent Hamiltonian for which they are solutions. In addition, the orbitals have to be represented in a basis of plane waves, and this involves a number of coefficients of the

order of few tens to several hundreds for every atom contained in the unit cell (per “atomic volume”, more appropriately). These requirements result in a problem that is computationally very intensive, and a long and focused effort of the scientific community has been geared to the development of efficient algorithms and techniques tuned to the available resources.

A brief description is given here of the more recent and successful approaches, and on how they can be applied to perform electronic-structure calculations and first-principles structural relaxations or molecular dynamics.

2.3.1 Car-Parrinello molecular dynamics

Car and Parrinello³ [49] proposed to apply the idea of an *extended Lagrangian formulation* [80] [81] to the domain of quantum mechanics: the classical Lagrangian for a system of ions in the potential $\mathcal{V}(\{\mathbf{R}_I\})$,

$$\mathcal{L} = \frac{1}{2} \sum_I M_I \dot{R}_I^2 - \mathcal{V}(\{\mathbf{R}_I\}),$$

is substituted with an effective Lagrangian in which the *electronic degrees of freedom* have been introduced in the form of *classical dynamical variables*, characterized by an appropriate fictitious mass and kinetic energy, and where the potential energy surface is defined in all generality as $E = E[\{\psi_i\}; \{\mathbf{R}_I\}]$. Following these assumptions the Car-Parrinello Lagrangian takes the form:

$$\mathcal{L} = \sum_i \frac{1}{2} \mu \int |\dot{\psi}_i(\mathbf{r})|^2 d\mathbf{r} + \frac{1}{2} \sum_I M_I \dot{R}_I^2 - E[\{\psi_i\}; \{\mathbf{R}_I\}], \quad (2.7)$$

³See Refs. [77] and [78] for comprehensive reviews of the molecular dynamics method, and Ref. [79] for a discussion of the computational efficiency in systems *with a gap*.

with the orbitals subject to the holonomic constraints of orthonormality:

$$\int \psi_i^*(\mathbf{r}, t)\psi_j(\mathbf{r}, t) d\mathbf{r} = \delta_{ij}.$$

The first term in (2.7) is the fictitious kinetic energy associated with the classical motion of the orbitals (more precisely, of the coefficients of their plane-wave representation), that are given a fictitious mass μ whose role is to tune the dynamics of these orbitals with respect to the dynamics of the ionic masses M_I (μ can also vary from orbital to orbital; for the case of fixed ions it can be simply renormalized into the integration time-step). The Euler-Lagrange equations of motion determined by the effective Lagrangian (2.7) are:

$$\mu\ddot{\psi}_i = -\frac{\delta E}{\delta\psi_i^*} + \sum_j \Lambda_{ij}\psi_j \quad (2.8)$$

$$M_I\ddot{\mathbf{R}}_I = -\frac{\partial E}{\partial \mathbf{R}_I}, \quad (2.9)$$

where the Lagrangian multipliers Λ_{ij} have been introduced explicitly to impose the holonomic constraint of orthonormality to the orbitals. It should be underlined that the functional derivative $\frac{\delta E}{\delta\psi_i^*}$ is $\hat{H}_{KS}\psi_i$, where \hat{H}_{KS} is the single-particle Kohn-Sham operator defined in (1.32). Neither Eq. (2.8) nor, in particular, Eq. (2.9), are immediately associated with some real trajectories of the physical system. The role of the present formulation is, at first, to introduce the idea of *simulated annealing* [82] as a practical method to determine the ground state. A procedure can be devised by which some kinetic energy is initially given to the system (either to the electronic degrees of freedom or also to the ions) and then the dynamical evolution in the configuration space is followed according to the Lagrangian dynamics, while the temperature gets slowly decreased towards zero. In the absence

of metastable states that can trap the system⁴ the equilibrium will be finally reached when the temperature has dropped to zero, so that also the fictitious classical kinetic energy of the orbitals and the ions are zero, and the relations $\ddot{\psi}_i = 0$ and $\ddot{\mathbf{R}}_I = 0$ hold. It is readily seen from Eqs. (2.8) and (2.9) that the first condition implies that the orbitals at this point satisfy the self-consistent Kohn-Sham equations (1.32) (a part from a unitary transformation that leaves the Hamiltonian invariant) and consequently the derivatives $\frac{\partial E}{\partial \mathbf{R}_I} = \frac{\partial \mathcal{V}}{\partial \mathbf{R}_I}$ are the true Hellmann-Feynman forces; the second condition implies that the system has reached either a local or possibly a global minimum of the potential energy surface $\mathcal{V}(\{\mathbf{R}_I\})$.

One of the significant improvements that such a formalism brings in [83] is that it does not require to ever store the full Hamiltonian matrix, which is very large in a plane-wave based formulation, since it can take full advantage of the existence of (different) diagonal representations for the kinetic energy and the pseudopotential, switching back and forth from real to reciprocal space with Fast Fourier Transforms. For this reason and since only the lowest eigenstates are needed, the evolution towards the ground state (requiring the repeated application of the operator \hat{H}_{KS} to all the wavefunctions) has an associated cost that is much lower than an iterative sequence of full diagonalizations of the Hamiltonian.

This same Car-Parrinello Lagrangian can be subtly exploited to perform some realistic molecular dynamics: if the mass associated with the electronic

⁴This is not a problem for the annealing at fixed ions, although if the ions are simultaneously allowed to relax it can be very easy to get trapped into a local ionic minimum. The procedure itself is meant to reach eventually the *global* minimum, but it requires an asymptotically slow decrease of the temperature that is not practically affordable.

motion is chosen to be much smaller than that of the ions, for appropriate initial conditions the system will be characterized by a metastable separation between a subsystem of fast oscillators (the orbitals) that have only a tiny fraction of the total (ionic and electronic) kinetic energy associated with them, and a subsystem of slow and massive ions that act adiabatically on the electrons as a driving potential. The equations of motion (2.8) favour those natural oscillations of the orbitals that are coherent with the instantaneous ionic motion; the higher frequencies and smaller fictitious mass(es) of the electronic variables assure that, in an average sense, the orbitals will keep redistributing in order to be always close to the real ground-state, parametrically evolving as a function of the ionic coordinates, and with a tolerance in the thickness of their Born-Oppenheimer confinement that is essentially determined by the fictitious electronic kinetic energy. The trade-off in the simulations is between having smaller electronic masses, thus keeping the system closer to the Born-Oppenheimer minimum and characterized by more responsive electronic degrees of freedom, and the necessity of keeping the time-step for the expensive integration of the equations of motion as large as possible, in order to simulate the dynamics for a time adequate to the atomic scales (typically from a fraction of a picosecond up to several picoseconds). Although the forces that drive the ionic dynamics are never the exact Hellmann-Feynman forces, the adiabatic separation assures that, in an average sense, their trajectory will be close to the exact one, the more so the smaller the electronic mass (and the time step) associated with the quasi-equilibrium electron dynamics.

It should be pointed out [84] that the eigen-frequencies of the oscillations

for the electronic degrees of freedom are, at fixed ions:

$$\omega_{ij} = \left(\frac{2(\epsilon_j - \epsilon_i)}{\mu} \right)^{\frac{1}{2}},$$

where ϵ_j is a Kohn-Sham eigenvalue for a higher unoccupied state and ϵ_i is an eigenvalue for an occupied state. Thus, the lowest frequency that can appear in the electronic motion is of the order of $\omega_{min} = (2E_{gap}/\mu)^{1/2}$; for a semiconductor or insulator, with a suitable choice of μ this critical frequency can be higher than the typical frequencies of the ionic motion, and thus the condition of adiabatic separation can be satisfied for all the duration of a typical simulation (this technical detail depends on the size of the gap, and on the condition that the gap is not reduced following disordering or reconstruction). For very long simulation times, the electrons can be periodically quenched back to the Born-Oppenheimer ground-state [85], although this procedure destroys the proper evolution of the holonomic constraints [84], that requires a coherent evolution in the subspace of occupied orbitals (the total energy is invariant with respect to a unitary transformation in this subspace, but the fictitious kinetic energy is not, unless the unitary transformation is time-independent). In the case of a metal, the gap tends to zero in the limit of the periodic unit cell going to infinity (or the sampling of the Brillouin-zone becoming increasingly fine), and the metastability of the adiabatic separation breaks down immediately.

2.3.2 Conjugate-gradient minimization

A straightforward and very efficient approach can be taken by reconsidering the original problem of the functional minimization for the total energy

functional

$$\begin{aligned} E[\{\psi_i\}; \{\mathbf{R}_I\}] = & \sum_{i=1}^N -\frac{1}{2} \int \psi_i^*(\mathbf{r}) \nabla^2 \psi_i(\mathbf{r}) d\mathbf{r} + E_H[n(\mathbf{r})] + \\ & + E_{xc}[n(\mathbf{r})] + \int v_{ext}(\mathbf{r}; \mathbf{R}_1, \dots, \mathbf{R}_N) n(\mathbf{r}) d\mathbf{r} \quad (2.10) \end{aligned}$$

and treating it as a complex problem of non-linear constrained optimization, either in the electronic variables alone, or together with the ionic degrees of freedom. The electronic problem will be discussed first, i.e. the problem of minimizing the total energy as a function of the coefficients of the plane waves on which the orbitals are represented. For this case, the total energy functional possesses a single, well-defined minimum, but it has a very large number of degrees of freedom and a fairly complex set of non-linear constraints.

There are two well-established analytical methods that exploit optimally the knowledge of the function to be minimized and of its first derivatives to map out improved directions towards the multi-dimensional minimum: these are respectively the *conjugate-gradient methods* (CG, either in the Fletcher-Reeves or Polak-Ribiere formulation) and the *variable-metric methods* (often found in the BFGS formulation of Broyden-Fletcher-Goldfarb-Shanno) [63]. Both use the knowledge of the multi-dimensional function and—if available—of its first derivatives to iteratively produce more efficient multi-dimensional search directions; they share the concept that it is the information on the second-derivatives, in the neighborhood of a multi-dimensional minimum, the obvious fundamental quantity that locates the position of the minimum with respect to the points that have already been sampled. The BFGS minimization operates by explicitly accumulating an estimate of the inverse Hessian matrix, while the CG method takes the indirect approach of reducing the di-

mensionality of the search space at every iteration. The conjugate-gradient algorithm needs only a storage proportional to the number of dimensions in the full search space (i.e. the number of plane waves), while variable-metrics methods require a storage proportional to the square of the number of dimensions, and for this very reason have to be ruled out from the beginning in the context of plane-wave electronic structure calculations. In addition, there is no clear computational advantage for either method that can be generally foreseen in advance, both relying for their efficiency on the information that is, directly or indirectly, gained on the curvature of the function that is being minimized.

The ideas beneath the conjugate-gradient algorithm can be exemplified⁵ considering the problem of minimizing in the N dimensions a symmetric positive-definite function $F = \frac{1}{2}\mathbf{x} \cdot G \cdot \mathbf{x}$, where G is the gradient operator such that the gradient at \mathbf{x} is $\mathbf{g} = -G\mathbf{x}$. Starting from a generic point \mathbf{x}^1 , the best initial direction is the steepest-descent direction $\mathbf{d}^1 = \mathbf{g}^1 = -G\mathbf{x}^1$; a minimization along this multidimensional line yields $\mathbf{x}^2 = \mathbf{x}^1 + b^1\mathbf{d}^1$, where b^1 , being the minimum of F along \mathbf{d}^1 , is such that

$$\frac{dF}{db^1} = (\mathbf{x}^1 + b^1\mathbf{d}^1) \cdot G \cdot \mathbf{d}^1 = 0.$$

The straightforward application of the steepest-descent method would call now for a subsequent minimization from \mathbf{x}^2 along the direction of steepest-descent $\mathbf{d}^2 = \mathbf{g}^2 = -G\mathbf{x}^2$. This would lead to a new point along \mathbf{d}^2 , $\mathbf{x}^3 = \mathbf{x}^2 + b^2\mathbf{d}^2$, such that, as above,

$$\frac{dF}{db^2} = (\mathbf{x}^1 + b^1\mathbf{d}^1 + b^2\mathbf{d}^2) \cdot G \cdot \mathbf{d}^2 = 0.$$

⁵For this, and for an in-depth review of the total-energy pseudopotential method and its implementation as a direct minimization problem, see Ref. [50].

At this point, the problem can be reexamined; in fact, given *both* the optimal search directions \mathbf{d}^1 and \mathbf{d}^2 , the minimization problem can be regarded as a global two-dimensional problem in the space of \mathbf{d}^1 and \mathbf{d}^2 . The optimal b^1 and b^2 are those that satisfy the two coupled equations:

$$\begin{aligned}\frac{dF}{db^1} \Big|_{\mathbf{x}^3} &= (\mathbf{x}^1 + b^1 \mathbf{d}^1 + b^2 \mathbf{d}^2) \cdot G \cdot \mathbf{d}^1 = 0 \\ \frac{dF}{db^2} \Big|_{\mathbf{x}^3} &= (\mathbf{x}^1 + b^1 \mathbf{d}^1 + b^2 \mathbf{d}^2) \cdot G \cdot \mathbf{d}^2 = 0.\end{aligned}$$

These equations are clearly valid if the directions \mathbf{d}^1 and \mathbf{d}^2 are *conjugate* to each other, that is if $\mathbf{d}^1 \cdot G \cdot \mathbf{d}^2 = \mathbf{d}^2 \cdot G \cdot \mathbf{d}^1 = 0$.

This requirement can be iteratively extended [86], and it defines a sequence of search directions, starting from the initial steepest-descent one, that do identify analytically the minimum of a N -dimensional quadratic function in exactly N iterations; the search directions are given by:

$$\mathbf{d}^i = \mathbf{g}^i + \gamma^i \mathbf{d}^{i-1}, \quad (2.11)$$

where the mixing factor between the current gradient and the previous search direction, outcome of all the previous history of the minimization, is

$$\gamma^i = \frac{\mathbf{d}^i \cdot \mathbf{d}^i}{\mathbf{d}^{i-1} \cdot \mathbf{d}^{i-1}}, \quad \gamma^1 = 0. \quad (2.12)$$

The method operates by mapping out from the minimization process all the explored degrees of freedom, effectively reducing the dimensionality of the search space at every iteration. A clear example comes from visualizing a 2-dimensional paraboloid whose principal axes have very different eigenvalues; a steepest-descent strategy, starting from a generic point, would proceed via an infinite series of damped searches approaching asymptotically

the minimum (each steepest-descent direction is bound to be orthogonal to the previous one), while the conjugate-gradient algorithm reaches the minimum in two iterations, by choosing the optimal steps and directions in the combined subspace. Finally, it should be noted that, if the principal axes of the quadratic form are all equal (i.e. the eigenvalues are all identical), the descent direction is always directed towards the minimum, and one iteration is all what is needed, independently from the dimensionality, to conclude the minimization process. This illustrates the key idea of *preconditioning*, that consists of adapting the metrics of the space in which the search directions are chosen in order to make all the eigenvalues be as similar as possible (or, in other words, to make the quadratic form look as spherical as possible).

The conjugate-gradient/steepest descent method has been introduced in the context of the electronic structure of solids both as an indirect minimization technique [87] and as a direct one [88] [44]. The former implementation considers the minimization problem, similarly to the molecular dynamics approach, as a propagation in (imaginary) time, where an initial arbitrary trial state gets projected more and more accurately to the ground state by a repeated application of the operator \hat{H}_{KS} . In this, it suffers inevitably from an intrinsic instability with the growth of the system size, originating from the small wavenumber terms that appear in the denominator of the Hartree energy, and that can be controlled only by reducing a priori the time step of the fictitious evolution. The latter approach operates differently, in introducing the concept of direct minimization by taking into account the *response* of the system when a line search is performed, and choosing a variable step that minimizes the actual value of the total energy along the search direction. This

has the net effect of making the process strictly variational and very stable, in addition to greatly improving the efficiency of the minimization. This approach has been extensively developed [50] [89] [90] and successfully applied to a wide variety of semiconducting and insulating systems [91] [92] [93] [94] [95] [96] [97]. In its original formulation [88] [50] the optimization strategy was broken down into a *band-by-band* updating strategy, in order to minimize the memory requirements for the working arrays containing the gradients, the conjugate directions, and the current wavefunctions. The strategy adopted here and in the following will be an *all-bands* approach [44], that offers a much improved performance, especially in the case of metallic systems (since the cross-terms between the bands are considered in the response), together with a simpler theoretical formulation, albeit at the cost of a significant increase in the dynamic memory requirements. Given that it is currently possible to fit on a common workstation systems whose size is of the order of one hundred atoms, provided they do not need hard pseudopotentials, and given the trend of large-scale electronic structure computations towards distributed memory machines, the overhead costs associated with an all-bands scheme can be considered to be paid off by its increased performance (by at least a factor of 2 or 3, although it can be much more than that for “difficult” systems, like the very elongated cells discussed below). As an aside it should be noted that a single conjugate-gradient iteration on all the orbitals, in a band-by-band scheme, requires a much larger computational effort than one iteration in an all-bands scheme (due to the requirements of orthogonality and preconditioning along every band-by-band search), and so iteration counts are not immediately meaningful for a performance comparison. The technical details

of the implementation, specifically in a metallic system, will be sketched in the following Section and in Chapter 3, where the ionic relaxations are also discussed. As a conclusion to the points presented here, the more relevant features of conjugate-gradient methods are outlined in the following, focusing the perspective on applying the technique to large-scale or traditionally difficult cases (metallic systems being paradigmatically difficult), or to dynamical simulation, especially where the nature of the system changes during the simulation.

Conjugate-gradient direct minimization: an outline

- it is an iterative procedure driven by the functional derivatives (gradients) of the total energy $\frac{\delta E}{\delta \psi_i} = \hat{H}_{KS}\psi_i$, and so it shares with the Car-Parrinello method the advantages in evaluating and storing the Kohn-Sham Hamiltonian
- in the limit of a proper preconditioning formulation, it is heuristically known to converge very fast even with respect to the theoretical asymptotic behaviour [98]
- it is robust and stable, ultimately based on the directions of (steepest, conjugate) descent, and it is naturally implemented in a strictly variational fashion
- it allows the direct minimization of the self-consistent functional, invariably with just a single interpolation along the line of descent, and thus it employs the optimal (imaginary time) step at every iteration

2.3.3 Metallic systems

Severe technical difficulties arise in the treatment of metallic systems, both in static self-consistent calculations and in molecular dynamics simulations. To begin with, static calculations show a dramatic decrease of the sampling accuracy in the Brillouin Zone.

Brillouin-Zone sampling In periodic boundary conditions the translational symmetry of the external potential leads to a representation for the wavefunctions in the form of Bloch states (2.6); the sum on all the infinite states of the system (or quasi-infinite, with the Born-von Karman conditions for the wavefunctions) thus becomes an integral over the first Brillouin Zone (or a sum, done on the discrete fine mesh of wavevectors allowed by the Born-von Karman conditions), where for each wavevector there corresponds only a finite and small number of states (for a spin-degenerate calculation in an insulator, there are $\frac{N_e}{2}$ states occupied at each wavevector, with N_e the number of electrons in the unit cell). The kinetic energy, the band energy term and the charge density in (1.33), (1.34) are all defined via a full integration on the first Brillouin Zone; e.g. the charge density is

$$n(\mathbf{r}) = \frac{1}{V} \int_{BZ} \left\{ \sum_i f(\epsilon_{i\mathbf{k}}) |\psi_{i\mathbf{k}}(\mathbf{r})|^2 \right\} d\mathbf{k}, \quad (2.13)$$

where $f(\epsilon_{i\mathbf{k}}) = 2$ (if the system is spin degenerate) for the lowest $\frac{N_e}{2}$ states at each \mathbf{k} , 0 otherwise.

It was first recognized by Baldereschi [99] that the integrations over the Brillouin Zone could be performed to a very high accuracy by using just a single *special k-point*, carefully chosen according to the point group symmetry of the unit cell lattice. This analysis has been subsequently generalized

to identify a set of prescriptions for choosing relatively coarse meshes that can provide excellent accuracy in estimating the exact integrals [100] [101] [102]; the existence of symmetry operators that commute with the Hamiltonian can be further exploited via the simple relations that are satisfied by the common eigenstates at different but symmetry related \mathbf{k} -points, and effectively reducing the problem to an integration over the *irreducible wedge* of the Brillouin Zone (e.g. the time-reversal symmetry brings the relation $\psi_{\mathbf{k}}(\mathbf{r}) = \psi_{-\mathbf{k}}^*(\mathbf{r})$, straightforwardly halving the number of \mathbf{k} -points that are needed). The success of these integration techniques is analogous in nature to that of the well-known Gaussian quadrature, in that they rely on integrating accurately the lowest harmonics of the representation of the integrand, which in this case is naturally expanded as a series on the symmetrized lattice stars.

This accuracy degenerates immediately if the function to be integrated is discontinuous. This is precisely what happens in a metal, where only the states inside the Fermi surface contribute to the integrals, and the occupations drop to zero when the Fermi surface is crossed. A partial solution to this problem has been obtained by introducing a smearing technique [103] [104]: the exact density of states $n(\epsilon)$ (not to be confused with the charge density $n(\mathbf{r})$),

$$n(\epsilon) = \sum_{i\mathbf{k}} \delta(\epsilon - \epsilon_{i\mathbf{k}}), \quad (2.14)$$

is substituted with a smoother, smeared density of states

$$n(\epsilon) = \sum_{i\mathbf{k}} \frac{1}{\sigma} \tilde{\delta}\left(\frac{\epsilon - \epsilon_{i\mathbf{k}}}{\sigma}\right), \quad (2.15)$$

where the $\tilde{\delta}$ function is some broadened approximation to the original Dirac's delta (e.g. a Gaussian). The immediate effect of this broadening is to remove

the sharp discontinuity around the Fermi energy, and to *greatly* improve the sampling accuracy. This approach will be rationalized in the discussion of Chapter 4, with a careful examination of the sampling errors that the approach can cure and the systematic errors that are eventually introduced, and how they can be corrected for; for the time being it should be stressed that it is absolutely equivalent to introducing a (real or fictitious) temperature for the electronic degrees of freedom of the system.

Finite temperature formulation A finite temperature formulation in which the system is characterized by a total free energy functional, as in (1.45), (1.46), comes initially from this necessity of improving the sampling accuracy in the Brillouin Zone; the approach is actually very successful, because it offers at the same time a vastly improved sampling precision and it allows an a-posteriori rationalization of the smearing scheme that can help in correcting the systematic errors that arise from the introduction of a broadened density of states (see Chapter 4 for a discussion). Additionally, a finite temperature formulation helps in controlling the discontinuities in the energy derivatives that would be introduced by level-crossing events, i.e. by the sudden occupation or emptying of states whose energies cross the Fermi level during the iterative process towards self-consistency. Finally, a canonical formulation provides a natural way to include in the minimization process fractional occupancies and subspace rotations: in a metal, at variance with the case of a semiconductor, the charge density (2.13) and consequently the self-consistent Hamiltonian are no longer invariant with respect to unitary transformations of the occupied orbitals, which thus enter the problem and have to be considered as additional non-linear degrees of freedom.

Molecular dynamics The objective of performing stable molecular dynamics simulations in a metallic system raises additional difficulties. Unless the system size is tuned to be small enough to allow for the appearance of a *pseudo-gap* in the system [105], there is otherwise a significant overlap between the typical ionic frequencies and the electronic excitations. This breaks the adiabatic separation that is needed to perform a Car-Parrinello simulation, *even more* so if fractional occupancies and subspace rotations are introduced in the problem [106]. Ad-hoc procedures can be devised to work around this problem, e.g. by repeatedly quenching the system to the ground state [107] while coupling the ions with a Nosé thermostat [108] (provided that the system is quasi-semiconducting in character), or by forcibly coupling a second Nosé thermostat to the electronic system [109] [110], at the price of introducing in the process velocity-dependent forces in the electronic equations of motion. In both cases the treatment of the electronic degrees of freedom remains somewhat unsatisfactory [77] or restrictive.

Additionally, the treatment of the occupation numbers and subspace rotations has to be considered as an essential part in the development of an optimal minimization strategy [44] [111] [112] [113], since the non-linear constraints on these degrees of freedom, together with their intrinsic non-local character⁶, makes the control of the convergence for the energy extremely demanding even in the limit of moderate cell-sizes [114] [106][115]. This problem is even more severe in the convergence of the Hellmann-Feynman forces, whose errors are first-order in the distance between the true ground state and the trial solution, as opposed to the total (free) energy, that has

⁶A small modification of an occupation, or a subspace rotation, amounts to a non-local displacement of charge density all over the unit cell

an error that is of second-order.

Finally it should be noted that the Hellmann-Feynman theorem implies that the forces calculated in a simulation are the true derivatives of the total free energy (that is the smeared energy functional); this explains the observation of an improved conservation of the constant of motion [116] when free energies and Hellmann-Feynman forces are considered. It should be noted from now on that, unless the temperature is introduced in order to properly consider a finite-temperature Fermi-Dirac electron gas and its relative isothermal dynamics⁷, a systematic error arises in adopting the free energies and forces as an approximation to the zero-temperature (zero-smearing) limit. The errors on the energies can be corrected very easily a-posteriori [44] [117]: this allows for the choice of larger smearing widths for a given tolerance in the systematic errors, in turn allowing for accurate sampling of the Brillouin Zone with coarser grids, or for an improved accuracy at a given smearing. In order to perform consistent dynamics, the systematic smearing errors on the forces should also be corrected (this problem will be discussed, together with the solution that is here introduced, in Chapter 4; some of the relevant concepts can be found in Refs. [44] [117] [118] [119]).

The sampling technique of special \mathbf{k} -points, together with the smearing of the density of states, provides also the relevant advantage of producing consistent free energies and forces, in contrast to the improved tetrahedron methods [120], and of requiring only one single special \mathbf{k} -point in the limit of large unit cells (this will be the case for most of the results presented here).

⁷E.g. to characterize the electric conductivity of systems with small gaps, or to study processes in which the electron gas is at a much high temperature than the ionic lattice, like in laser irradiation.

Variational free energy minimization The goal of performing molecular dynamics simulations requires the development of a minimization algorithm that is both very efficient (in order to control the convergence of the Hellmann-Feynman forces, in the presence of the additional degrees of freedom of the fractional occupancies and subspace rotations) and very robust and stable (to converge to the minimum against all the ill-conditioned features of the problem). These requirements call for a minimization strategy realized by a *strictly variational conjugate-gradient method*, that is an algorithm that can ideally provide both the efficiency and, especially, the robustness that is necessary.

Its formulation requires the identification of the proper variational functional that has to be minimized, and that is the *electronic free energy* [either in a Fermi-Dirac or in a *generalized entropy* formulation (see Chapter 4), the latter being equivalent to a smeared total energy formulation [103] [119]], and the proper consideration of the dependence of the total free energy on the fractional occupancies and subspace rotations. The occupancies, in particular, can be considered either as independent variables, with all the instability coming from their non-local connection to the charge density in the unit cell, or as dependent variables, where they introduce in principle a very complicated dependence of the free energy as a function of the wavefunctions (that determine the expectation values $\langle \psi_i | \hat{H} | \psi_i \rangle$ upon which the occupancies are calculated).

The total free energy at a finite temperature T is given by (1.45); it is useful to regroup the kinetic-energy term and the non-local pseudopotential in order to highlight the dependence of the various terms on the wavefunctions

or just on the charge density:

$$A [T ; \{\psi_i\}, \{f_i\}] = \sum_i f_i \langle \psi_i | \hat{T}_e + \hat{V}_{nl} | \psi_i \rangle + E_{\text{Hxc}}[n] - TS[\{f_i\}] \quad (2.16)$$

$$n(\mathbf{r}) = \sum_i f_i \psi_i^*(\mathbf{r}) \psi_i(\mathbf{r})$$

where S is either the Fermi-Dirac entropy or one of its generalizations, and where the constraints of normalization of the orbitals and charge conservation for the occupancies have also to be imposed (the latter introduces a chemical potential μ in the problem). These two constraints can be introduced via the respective Lagrange multipliers, as in (1.37), adding to (2.16) the terms

$$\begin{aligned} \sum f_i \epsilon_i (\langle \psi_i | \psi_i \rangle - 1) \quad &\text{and} \\ \mu(N - \sum f_i). \end{aligned}$$

Assuming that both the wavefunctions and the occupations are independent constrained variables, the steepest descent directions that lead to the minimization of the total free energy functional are given by:

$$\left\{ \begin{array}{l} -\frac{\delta A}{\delta \psi_i^*} \quad \left(\Rightarrow \hat{H} \psi_i = \epsilon_i \psi_i \right) \\ -\frac{\partial A}{\partial f_i} \quad \left(\Rightarrow \langle \psi_i | H | \psi_i \rangle - \mu = T \frac{\partial S}{\partial f_i} \right) \\ \text{subspace rotations} \end{array} \right. \quad (2.17)$$

where the additional operation of subspace rotation has to be added separately, since the search directions are projected out of the occupied subspace to conserve orthonormality (to first-order). It should be noted that at self-consistency, when all the first derivatives are zero, the first equation implies

that the orbitals satisfy the Mermin-Kohn-Sham equations (1.44), while the equilibrium distribution for the occupations is given by the second equation, and it is a Fermi-Dirac distribution (1.43) if the canonical form for the single-particle entropy (1.42) has been employed.

The equations in (2.17) define a multi-dimensional search direction, and a variational minimization strategy can be practically implemented following the prescriptions of Ref. [44] (see also Ref. [121]). In particular, the search on the wavefunctions is naturally decomposed into a search in the orthogonal and in the parallel subspaces (the latter being defined as the space spanned by the orbitals that have non-zero occupancies, and which are just a fraction of the total number of plane waves). The search in the orthogonal subspace is performed via a conjugate-gradient algorithm, while the search in the parallel subspace takes place via a subspace rotation. The rotation matrix can be defined with the help of perturbation theory, and constructed in order to always satisfy the constraint of lowering the total free energy [44]: if a transformation in the parallel subspace is defined by

$$\psi_i \Rightarrow \psi_i + \sum_j W_{ij} \psi_j,$$

the requirement of preserving orthonormality up to linear order in the rotation requires to W_{ij} to be anti-hermitian. Perturbation theory provides an explicit expression for W_{ij} ($W_{ii} = 0$ from the requirement of being anti-hermitian)

$$W_{ij} = \frac{\langle \psi_i | \hat{H} | \psi_j \rangle}{\langle \psi_i | \hat{H} | \psi_i \rangle - \langle \psi_j | \hat{H} | \psi_j \rangle}, \quad (2.18)$$

and from this the actual rotation matrix is defined by $\zeta_{ij} W_{ij}$, where ζ_{ij} acts as a cutoff if the elements in (2.18) are too large (that is to say, if the mixing between states is too big and perturbation theory does not apply), and is set

to zero if a reverse ordering is found (i.e. if two states have occupations and expectation values in reverse order). This latter condition forces the subspace rotation to be a proper minimization step, in the limit of small rotations.

This formulation, properly implemented, allows for a very robust, if not optimal, minimization strategy; as an example, the convergence of the total free energy for two very long metallic slabs is shown in Fig. 2.2. The case presented here is a paradigmatically difficult one, since the cells are very elongated, and the so-called *sloshing instabilities* can take over if the minimization procedure is not strictly variational. As it can be seen, the fundamental requirement of robustness, that comes from the variational formulation, is fully satisfied. It should be noted that an unrealistic (Gaussian) smearing of 4.5 eV has been adopted, to assure full sampling convergence with just one special point, but especially to underline the role played by a proper treatment of the temperature.

This scheme, called here the *standard scheme*, is thus composed of a sequence of variational steps in the wavefunctions, in the occupancies and in the subspace rotations. The order of these operations, as well as performing some or all of them simultaneously, is a matter of choice; it should be noted that an all-bands conjugate-gradient scheme is much more efficient than a band-by-band scheme, for difficult metallic systems, due to the interdependence of the bands. For the same reason it can be useful to perform the updating in more than one subspace at the same time (usually updating the orthogonal subspace and the occupations together), although sometimes a mixing factor between the different subspaces has to be empirically introduced. Such formulation of the standard scheme can be applied successfully

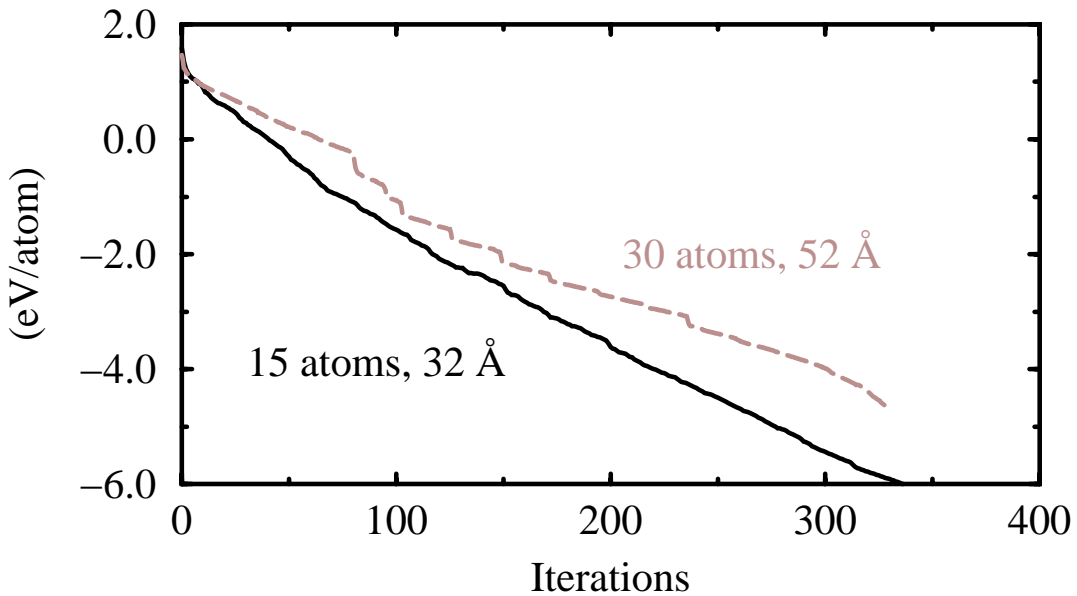


Figure 2.2: Convergence of the total free energy in a semi-logarithmic scale (base 10). The systems considered are two 1x1 Al(110) slabs, containing respectively 15 and 30 atoms (64 and 128 bands, 4.5 eV of Gaussian smearing), and 32 Å and 52 Å long, both sampled with the $(\frac{1}{4}, \frac{1}{4}, \frac{1}{4})$ Baldereschi point [99]. The iteration count for the longer cell has been halved, for a meaningful comparison.

to molecular dynamics simulations, especially if the systems considered are bulk or liquid metals, or if they have a mixed metallic/covalent behaviour [122] [123] [124] [125], so that either the charge density is relatively constant over the unit cell (this is not the case for metallic surfaces, represented as a slab in periodic boundary conditions) or it is more bound in the localized

covalent bonds. It should be pointed out that the formulation presented here suffers from overall poor convergence of the Hellmann-Feynman forces, which severely hampers the ability to perform efficient simulations in very large cells; additionally, the ionic forces used are the derivative of the free energy, and thus are not corrected against the systematic errors that come from a finite-temperature/smeared formulation.

Chapter 3

Ensemble Density Functional Theory

Introduction

A novel reformulation of the electronic structure problem at finite temperature is introduced here¹. A free energy functional is defined that is invariant with respect to unitary transformations in its representation (e.g. the basis of occupied orbitals). This formulation allows for a meaningful definition of a projected functional G , dependent only on the orbitals, for which the one-particle statistical operator commutes with the (non-self-consistent) Hamiltonian. The minimization to self-consistency is performed on this functional G , that *does not* depend explicitly on the occupations and on the rotations of the orthonormal orbitals, with a doubly-preconditioned all-bands conjugate-gradient method. A simple iterative and variational procedure is devised,

¹Work done also in collaboration with D. Vanderbilt.

that at every iteration ensures that the statistical operator commutes with the current orbital representation of the Hamiltonian, establishing a natural dynamics for the evolution of the occupations and the rotations of the orbitals in the free energy functional.

The method is shown to dramatically increase the rate of convergence to the ground state, particularly so for the case of the Hellmann-Feynman forces, leading to a greatly improved methodology for performing structural relaxations and molecular dynamics.

3.1 Ensemble free energy

The implementation of the Mermin-Kohn-Sham formulation for finite-temperature density functional theory that has been discussed in the preceding Chapter has required choosing an ad-hoc procedure for the updating of the orbitals in the occupied subspace. In addition, the evolution of the occupancies themselves was driven by the rescaled diagonal elements of the Hamiltonian ($\frac{\langle \psi_i | \hat{H} | \psi_i \rangle - \mu}{T}$), and although this choice, originating from the usual Janak's expression for the non-interacting kinetic energy, is perfectly valid, it neglects the existence of large non-diagonal terms in the Hamiltonian away from self-consistency, relying on the rotation dynamics to evolve these contributions towards the diagonal representation.

On the other hand, canonical ensemble density functional theory is expressed in the language of statistical mechanics, i.e. in terms of operators and traces, and the Helmholtz free energy defined in (1.21) is expressed as a

trace on the many-body density operator Γ_N :

$$A[\Gamma_N] \equiv \text{tr } \hat{\Gamma}_N \left(\frac{1}{\beta} \ln \hat{\Gamma}_N + \hat{H} \right). \quad (3.1)$$

Prompted by this analogy, a description in terms of traces is developed in the following. First, a generalized occupation matrix $\mathbf{f} = f_{ij}$ is introduced [126], that is the representation of the effective Mermin-Kohn-Sham one-electron statistical operator in the basis of the orbitals $\{\psi_i\}$. In terms of this occupation matrix f_{ij} , a *representation-invariant* free energy functional is formulated, similar to (2.16), that is written with complete generality as:

$$A[T; \{\psi_i\}, \{f_{ij}\}] = \sum_{ij} f_{ji} \langle \psi_i | \hat{T}_e + \hat{V}_{nl} | \psi_j \rangle + E_{\text{Hxc}}[n] - TS[\{f_{ij}\}], \quad (3.2)$$

where, as usual, there are the added constraints that the $\{\psi_i\}$ should be normalized *and* orthogonal, and that the trace of \mathbf{f} should be equal to the number N of electrons (its eigenvalues should also be bounded between 0 and 1). Similarly, the charge density $n(\mathbf{r})$ is written as a trace:

$$n(\mathbf{r}) = \sum_{ij} f_{ji} \psi_i^*(\mathbf{r}) \psi_j(\mathbf{r}). \quad (3.3)$$

Now, all the terms in (3.2) and the charge density (3.3) are invariant under a unitary transformation \mathbf{U} of the basis $\{\psi_i\}$; this can be understood intuitively by considering the invariance of the trace of an operator or a product of operators under a unitary transformation of the basis in which they are represented. It can also be proved explicitly, e.g. by calculating the charge density n' in a new rotated representation, where the occupation matrix is $\mathbf{f} \rightarrow \mathbf{f}' = \mathbf{U} \mathbf{f} \mathbf{U}^\dagger$ and the orbitals are $|\psi_j\rangle \rightarrow |\psi_j'\rangle = |\psi_j\rangle \mathbf{U}^\dagger = \sum_m U_{jm}^* \psi_m$. It should be noted that $S[\{f_{ij}\}]$ is defined as an operator relation, and thus \mathbf{f} has to be diagonalized in order to evaluate the trace of S ; for the case of the

Fermi-Dirac distribution, the entropy is $S = -k_B \sum_i [f_i \ln f_i + (1 - f_i) \ln(1 - f_i)]$, where the sum is done on the eigenvalues of \mathbf{f} .

The introduction of a representation-invariant functional has several consequences:

- it allows for a meaningful definition of the *rotation-invariant projected functional* G , defined as

$$G [T ; \{\psi_i\}] = \min_{\{f_{ij}\}} A [T ; \{\psi_i\}, \{f_{ij}\}], \quad (3.4)$$

that is a well-defined functional of the *orbitals only*;

- it represents coherently occupations and rotations as *part of the same problem*, namely of finding the equilibrium \mathbf{f} that commutes with the self-consistent Hamiltonian, leading to the development of a much more effective algorithm;
- it shifts the expensive and inefficient evolution for the orbital rotations (followed by the conjugate-directions rotations) to the matrix \mathbf{f} , greatly improving the coherence in the minimization of G in the orbital subspace, since an actual rotation can now be realized by changing the relative “phase” of one matrix with respect to the other.

The minimization strategy breaks down naturally in a nested algorithm, in which the functional G is brought to self-consistency with a minimization with respect to the $\{\psi_i\}$, where after every iteration on the $\{\psi_i\}$ the f_{ij} are updated to minimize A . In other words, the f_{ij} are projected onto the G surface, where \mathbf{f} commutes with the non-self-consistent Hamiltonian defined in the phase-space of G .

In this sense, the f_{ij} are dependent (hidden) variables in the evolution of G , but, as a by-product of the minimization operation in (3.4), the functional derivatives do not introduce any additional terms to take account of the variation of f_{ij} , $\frac{\delta f_{ij}}{\delta \psi_k^*}$ (practically impossible to calculate), since all these terms are zero because of the minimum condition. In fact, this simple relation for the functional derivatives holds:

$$\frac{\delta G}{\delta \psi_i^*(\mathbf{r})} = \frac{\partial A}{\partial \psi_i^*(\mathbf{r})}. \quad (3.5)$$

The relation between \mathbf{f} and \hat{H} in the stationary Liouville equation ($[\mathbf{f}, \hat{H}] = 0$) that is satisfied by every point on the G surface can be made apparent from the definition (3.4) of G as a minimum with respect to the f_{ij} in the free energy A (3.2). Introducing the notation

$$h_{ij} = \langle \psi_i | \hat{T}_e + \hat{V}_{nl} | \psi_j \rangle ,$$

$$V_{ij}^{[n]} = \langle \psi_i | V_{\text{Hxc}}^{[n]} | \psi_j \rangle ,$$

for the matrix elements of the Hamiltonian that depend either on the orbitals or just on the charge density, and introducing a Lagrange multiplier μ via the additional term $\mu (\text{tr } \hat{\mathbf{f}} - N)$, the minimum condition is rewritten as:

$$\begin{aligned} \frac{\delta A}{\delta f_{ji}} &= h_{ij} + \frac{\delta E_{\text{Hxc}}}{\delta f_{ji}} - T \frac{\delta S}{\delta f_{ji}} - \mu \delta_{ij} \\ &= h_{ij} + \int d\mathbf{r} \frac{\delta E_{\text{Hxc}}}{\delta n(\mathbf{r})} \frac{\delta n(\mathbf{r})}{\delta f_{ji}} - T [s'(\mathbf{f})]_{ij} - \mu \delta_{ij} \\ &= h_{ij} + V_{ij}^{[n]} - T [s'(\mathbf{f})]_{ij} - \mu \delta_{ij} = 0 . \end{aligned} \quad (3.6)$$

The notation $[s'(\mathbf{f})]_{ij}$ has been used for $d \text{tr } s(\mathbf{f}) / df_{ji}$; in the case of a Fermi-Dirac entropy the derivative can be written in terms of the occupation numbers, $s'(f) = \ln[f/(1-f)]$, and it can be explicitly calculated diagonalizing

f. The equilibrium condition in (3.6) that defines the functional G is thus rewritten as:

$$\mu \delta_{ij} = h_{ij} + V_{ij}^{[n]} - T [s'(\mathbf{f})]_{ij} ; \quad (3.7)$$

this relation implies that the matrix \mathbf{f} and the Hamiltonian $\mathbf{h} + \mathbf{V}^{[n]}$ can be diagonalized by the same unitary rotation (at fixed orbitals) and thus are “commuting” operators. It should be noted that the relation (3.7) does not mean that $\mathbf{h} + \mathbf{V}^{[n]}$ and \mathbf{f} are diagonal matrices, but just that they can be diagonalized together, since a unitary transformation of δ_{ij} would still be the identity, and so the transformation that diagonalizes $\mathbf{h} + \mathbf{V}^{[n]}$ diagonalizes also \mathbf{f} , and viceversa. Obviously, if the orbitals are updated, the relation does not hold any more, unless self-consistency has been reached.

3.2 Minimization strategy

The minimization algorithm takes naturally the form of a two-loop nested update. In the inner loop the orbitals $\{\psi_i\}$ are kept fixed, and the matrix f_{ij} is updated projecting it onto the surface G via the minimization on the f_{ij} in the free energy A . When this local minimum is reached, the Liouville equilibrium condition $[\mathbf{f}, \hat{H}] = 0$ holds, and the Hamiltonian, although still non self-consistent with respect to an updating of the orbitals, is “self-consistent” with respect to the occupancies, since the minimization will be performed taking consistently into account the variations in the charge density and in $E_{\text{Hxc}}[n]$ that follow a f_{ij} update. It should be mentioned that a sufficient accuracy in this inner loop is reached after just one or two iterations, when the procedure that will be described below is employed. Additionally, this loop is faster than the orbital updating loop, mainly because it does not need

to operate on the representation of the kinetic-energy or of the non-local part of the electron-ion interaction.

This implies that the most expensive part of the calculation is still the orbital updating, although both loops share the same asymptotic scaling, and their computational cost is proportional to the square of the number of orbitals times the number of plane waves in the limit of large systems.

The outer loop on the wavefunctions is required to bring the functional G to self-consistency. Since the functional itself does not depend any more (at least to first-order, i.e. in the functional derivatives) on the occupations and rotations, the methods of electronic structure that were developed for the cases of semiconductors/insulators, and that were described in the previous chapter, should be applicable. It should be noted that the rotation-invariance shared with the case of semiconductors and insulators implies that the slow frequencies of the subspace rotations, that were intrinsic in a standard finite-temperature formulation, have now been compressed to zero² as a consequence of the minimization of the f_{ij} .

3.2.1 Doubly-preconditioned all-bands CG

The direct minimization of G with a conjugate-gradient algorithm appears as the method of choice for this problem, providing the efficiency and the stability required. A key feature to be considered is that the functional G has

²It can be envisaged that this could also solve some of the problems that the Car-Parrinello formulation displays in the case of metallic systems [106]; in addition, it would be interesting to analyze the propagation of the holonomic constraints of orthonormality in this formulation, eventually with an appropriately invariant fictitious kinetic energy and under initial conditions of zero velocity for the rotations.

now a much broader spectrum of eigenvalues for its principal axes, than what would be expected. In fact, the dispersion of the spectrum has gone from spanning the set of $\{\epsilon_i\}$, as was the case for semiconductors/insulators, to the set of $\{f_i \epsilon_i\}$ (in the diagonal representation), where a significant fraction of the set extends to values very close to zero. This implies that the evolution of the higher bands does become very slow, down to zero velocity in the limit of almost empty states. Under these conditions the ratio of convergence for the total free energy becomes unacceptably low, even if the charge density is almost converged to tolerance.

The solution to this problem resorts to the help of preconditioning, that, as discussed before, relies on changing the metric of the space in which the gradients are calculated in order to have the functional resemble as closely as possible a spherical minimum.

Occupancy preconditioning The objective here is first to choose a set of scaled variables for which the functional has a more compressed spectrum, then to calculate the search directions in this new metric, and finally to transform them back in the original representation, establishing the relation that they hold with the original search directions. This procedure is shown here explicitly: let us group in a subscript i the indexes $n, \mathbf{k}, \mathbf{G}$ of the band, the Bloch state, and the plane wave respectively, so that $c_i = c_{n\mathbf{k},\mathbf{G}}$. If a set of scaled variables $\tilde{c}_i = \alpha_i c_i$ is defined, in the metric that will be denoted by a tilde, the gradients, the search directions and the mixing factors for the unscaled and scaled variables at an iteration k are:

$$\mathbf{g}_i^k = -\frac{\partial A}{\partial c_i} \quad ; \quad \mathbf{d}_i^k = \mathbf{g}_i^k + \gamma^k \mathbf{d}_i^{k-1} \quad ; \quad \gamma^k = \frac{\mathbf{g}_i^k \cdot \mathbf{g}_i^k}{\mathbf{g}_i^{k-1} \cdot \mathbf{g}_i^{k-1}} \quad ,$$

$$\tilde{\mathbf{g}}_i^k = -\frac{\partial A}{\partial \tilde{c}_i} \quad ; \quad \tilde{\mathbf{d}}_i^k = \tilde{\mathbf{g}}_i^k + \tilde{\gamma}^k \tilde{\mathbf{d}}_i^{k-1} \quad ; \quad \tilde{\gamma}^k = \frac{\tilde{\mathbf{g}}_i^k \cdot \tilde{\mathbf{g}}_i^k}{\tilde{\mathbf{g}}_i^{k-1} \cdot \tilde{\mathbf{g}}_i^{k-1}} \quad ,$$

(this is expressed in the same notation of (2.11), (2.12), with the iteration superscript referred here as k). The update along the search directions for the scaled variables in their own metric is:

$$\tilde{c}_i^{k+1} = \tilde{c}_i^k + \lambda \tilde{\mathbf{d}}_i^k \quad ;$$

this algorithm is identically rewritten in terms of the unscaled variables as

$$\alpha_i c_i^{k+1} = \alpha_i c_i^k + \lambda \tilde{\mathbf{d}}_i^k \Rightarrow c_i^{k+1} = c_i^k + \lambda \frac{1}{\alpha_i} \tilde{\mathbf{d}}_i^k .$$

The last equality defines $\frac{1}{\alpha_i} \tilde{\mathbf{d}}_i^k$ as the set of preconditioned search directions for the unscaled variables chosen in order to reproduce the search performed by the scaled variables in their own space. These preconditioned directions \mathbf{D}_i^k are thus defined as:

$$\mathbf{D}_i^k = \frac{1}{\alpha_i} \tilde{\mathbf{d}}_i^k = \frac{1}{\alpha_i} \tilde{\mathbf{g}}_i^k + \tilde{\gamma}^k \frac{1}{\alpha_i} \tilde{\mathbf{d}}_i^{k-1} = \frac{1}{\alpha_i^2} \mathbf{g}_i^k + \tilde{\gamma}^k \mathbf{D}_i^{k-1} .$$

The previous relation shows that the gradients to be used for the preconditioned search are $\mathbf{G}_i^k = \frac{1}{\alpha_i^2} \mathbf{g}_i^k$, to be used also to form the conjugate directions, but with a slightly different mixing factor

$$\tilde{\gamma}^k = \frac{\tilde{\mathbf{g}}_i^k \cdot \tilde{\mathbf{g}}_i^k}{\tilde{\mathbf{g}}_i^{k-1} \cdot \tilde{\mathbf{g}}_i^{k-1}} = \frac{\mathbf{G}_i^k \cdot \mathbf{g}_i^k}{\mathbf{G}_i^{k-1} \cdot \mathbf{g}_i^{k-1}} .$$

It is observed that some degree of overcorrection in the mixing factor does not interfere with the minimization process; this leads to a simplified algorithm, in which the preconditioned gradients are defined once for all as $\mathbf{G}_i^k = \frac{1}{\alpha_i^2} \mathbf{g}_i^k$, and then all the standard formalism for the conjugate-gradient applies, with search directions and mixing factors expressed in the usual way, but with

respect to the \mathbf{G}_i^k :

$$\mathbf{D}_i^k = \mathbf{G}_i^k + \Gamma^k \mathbf{D}_i^{k-1} \quad ; \quad \Gamma^k = \frac{\mathbf{G}_i^k \cdot \mathbf{G}_i^k}{\mathbf{G}_i^{k-1} \cdot \mathbf{G}_i^{k-1}} .$$

This preconditioning scheme can be immediately applied to compress the spectrum of the functional G . The case of a diagonal representation for the occupancies (as in the standard method discussed in the previous Chapter) will be discussed first, and then generalized to the rotation-invariant representation adopted for the functional G .

In the diagonal representation the total energy can be expanded around the minimum as a simple quadratic form $\sum_i f_i \epsilon_i c_i^2$ (the index i does not depend on \mathbf{G} in f_i and ϵ_i); if the scaled variables $\tilde{c}_i = \sqrt{f_i} c_i$ are introduced [44], the quadratic form becomes $\sum_i \epsilon_i \tilde{c}_i^2$, with the desired compression of the spectrum following from this new metric. From the prescription outlined before for the simplified preconditioning scheme, all that is needed now in order to construct the occupancy-preconditioned search directions \mathbf{G}_i is just a renormalization of the usual gradients with the inverse square of the scaling factor, thus arriving at the intuitive result:

$$\mathbf{G}_i = \frac{1}{f_i} \mathbf{g}_i = -\frac{1}{f_i} \frac{\delta A}{\delta \psi_i^\star} = -\hat{H} \psi_i \quad (3.8)$$

The preconditioning for the gradients in the rotation-invariant representation can now be easily obtained by calculating each gradient in a generic non-diagonal form, transforming then the result in the reference frame where the occupancies are diagonal, preconditioning it as it has been done for the diagonal scheme, and rotating finally back the resulting expression in the original representation. The gradients \mathbf{g}_i are given by

$$\mathbf{g}_i = -\frac{\delta G}{\delta \psi_i^\star} = -\sum_j f_{ji} \hat{H} |\psi_j\rangle , \quad (3.9)$$

or, in the primed representation in which the occupation matrix \mathbf{f} is diagonal ($\mathbf{f}' = f'_{ii} \delta_{ij} = \mathbf{U} \mathbf{f} \mathbf{U}^\dagger$), by

$$\mathbf{g}'_i = -\frac{\delta G}{\delta \psi_i'^*} = -\sum_j f'_{ji} \hat{H} |\psi'_j\rangle = -f'_{ii} \hat{H} |\psi'_i\rangle .$$

In this diagonal representation, the preconditioned gradient is straightforwardly

$$\mathbf{G}'_i = -\hat{H} |\psi'_i\rangle = -\hat{H} \left(\sum_m U_{im}^* |\psi_m\rangle \right) ,$$

leading to the desired result for the expression of the preconditioned gradient in a non-diagonal representation

$$\mathbf{G}_i = \sum_n U_{in}^{\dagger*} \mathbf{G}'_n = \sum_m \left(\sum_n U_{in}^{\dagger*} U_{nm}^* \right) \hat{H} |\psi_m\rangle = -\hat{H} |\psi_i\rangle . \quad (3.10)$$

The previous result is very useful from the computational point of view, since it achieves both the goal of greatly improving the rate of convergence, updating the higher bands with the same speed of the lower filled bands, and that of simplifying the expressions that are used to compute the gradients, going from (3.9) to the much simpler (3.10).

In addition to this occupancy preconditioning, a standard kinetic-energy preconditioning is also used [88] [50], in order to speed the convergence in the early phases of the minimization.

The outer loop of orbital minimization The operations that are performed during one iteration on the orbitals are summarized here:

- the preconditioned gradient $-\hat{H} |\psi_i\rangle$ is calculated, and it is mixed with the previous search direction, providing the new search direction;

- the new search direction is projected out of the subspace spanned by the orbitals, to assure first-order orthonormality of the orbitals along the search;
- the search direction defines a multidimensional (all-bands, all plane-waves, all \mathbf{k} -points) line; the derivative of the free energy along this line is calculated at the present position (the previous projection assures that this derivative is calculated exactly);
- a step along the search line is performed, based on the current value of the free energy, of its derivative, and of the expected decrease in energy
- the orbitals are reorthogonalized, and the new free energy is calculated;
- with these three constraints (initial free energy and free energy derivative, new free energy) a parabola is fitted, and the orbitals are updated accordingly.

This procedure is very stable, and even in the most difficult cases the parabolic search is quasi-ideal; this result is the clear outcome of the present formulation, and the simplification and stability that it is achieved by reprojecting the occupation matrix to its minimum value at every iteration. As an example of this stability, the results of the parabolic interpolation are shown in Fig. 3.1, for one of the long aluminium cells (a 1x1 Al(110) slab of 15 layers, 32 Å long, sampled at $(\frac{1}{4}, \frac{1}{4}, \frac{1}{4})$). The figure shows the ratio between the predicted (from the derivative at the initial point) and the calculated free energy (at the fitted minimum); in the ideal case of a perfectly quadratic behaviour this ratio would be always equal to $\frac{1}{2}$, and this is indeed the case to an excellent approximation. As a final remark, it should be noted that the

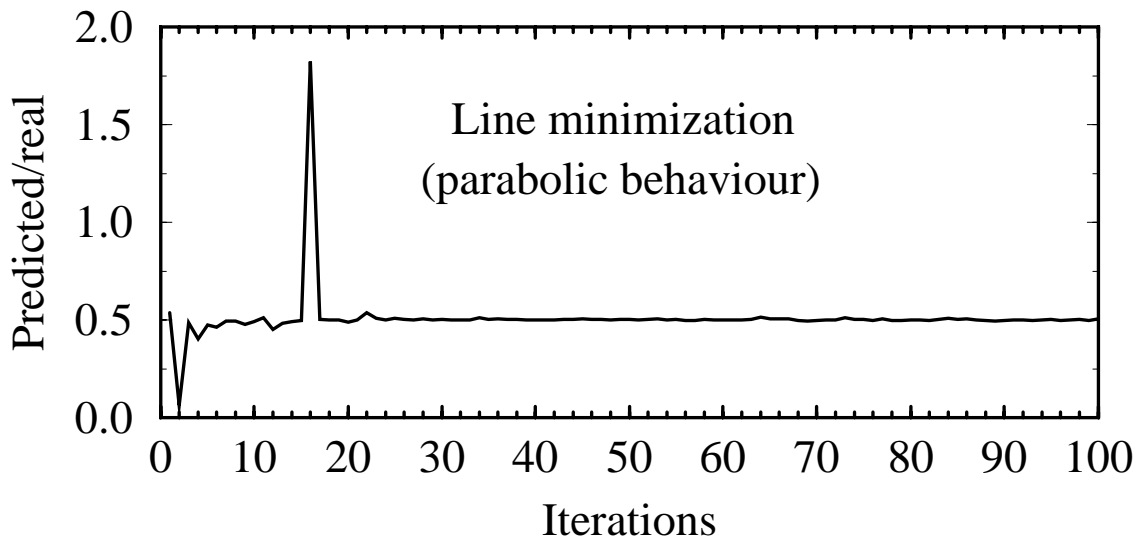


Figure 3.1: Ratio between the predicted and the calculated free energy differences in the parabolic fit for the orbital minimization, in the case of a 1x1 15-layer Al(110) slab, 32 Å long

parabolic fit is done with a free energy calculated in the trial step that has not been projected down (it is A , and not G). This is not at all serious, since it leads to a conservative choice for the minimum, and seems to induce only a negligible effect (this can also be tested, either by correctly performing the f_{ij} minimization also at the trial point, or by systematically overshooting by some percents the fitted minimum).

3.2.2 Occupation matrix: an iterative scheme

The inner loop for the update of the occupation matrix f_{ij} is done at fixed orthonormal $\{\psi_i\}$; this implies that there is no need to recalculate the different matrix elements for the kinetic energy or for the non-local pseudopotential, and there are no orthogonalization operations involved. The objective is to minimize the free energy at fixed orbitals, taking into account the changes in the charge density, and consequently in the Hartree and exchange-correlation terms, that occur whenever the occupation matrix is changed.

The choice that is adopted here has a very simple and appealing physical explanation: the rationale is that, if the problem was not self-consistent, the solution for the equilibrium f_{ij} would be found by straightforwardly diagonalizing the Hamiltonian matrix, calculating the thermal distribution, and eventually rotating that back to the orbital representation. Since the problem is self-consistent, and the Hamiltonian responds to the new occupation matrix by changing its Hartree and exchange-correlation term, the non-self-consistent solution will be used only as a search direction for the iterative updating of the matrix f_{ij} .

This choice displays an excellent fast convergence for the minimization process, it coincides with the directions of steepest descent close to self-consistency, and it provides an appealing physical approach to the solution of the problem, highlighting the role of the non-diagonal cross-terms in the self-consistent process. Finally, since it does not rely directly on derivatives for the choice of the descent direction, it allows naturally the extension of the self-consistency process to the exotic thermal distributions that will be introduced in Chapter 4.

The procedure is organized as follows: the matrix h_{ij} , with the kinetic-energy and non-local contributions, is determined once for all before entering the inner loop, and will not change inside it. Either in the case that the loop is entered after an orbital update, or as a second or subsequent iteration in the loop that is being performed, the first quantity to evaluate is the new input charge density, due to the new $\{\psi_i\}$ or the new f_{ij} . For clarity, it will be assumed that the m^{th} iteration of the inner loop is taking place. The new charge density is calculated according to

$$n^{(m)}(\mathbf{r}) = \sum_{ij} f_{ji}^{(m)} \psi_i^*(\mathbf{r}) \psi_j(\mathbf{r}); \quad (3.11)$$

this is actually the most intensive calculation that has to be performed in this loop, and the bottleneck that keeps it from being completely inexpensive from the computational point of view. As it is written, the calculation is based on the non-diagonal real-space representation; The strategy that we have adopted is to resort, for the only purpose of calculating the charge density, to a diagonal representation. The occupation matrix is diagonalized, the orbitals are rotated in reciprocal space, and then the charge density is calculated as in a traditional scheme, summing on the diagonal elements. This change of representation is done for the only purpose of dealing with the bands in reciprocal space, but it still obviously requires a rotation of all the orbitals, whose cost scales as in the orthonormalization process of the outer loop (although for all the systems studied but the very large ones the orthonormalization costs have not reached the asymptotic limit). If at all possible, it would be very useful to adopt some quasi approximate scheme that could perform this operation with a better efficiency, making thus the all inner loop negligibly expensive.

From the new charge density, the Hartree and exchange-correlation energies $E_{\text{Hxc}}^{(m)}$ and potentials $V_{\text{Hxc}}^{(m)}(\mathbf{r})$ are determined (and the eventual local contributions of the pseudopotential), together with their matrix elements

$$V_{ij}^{(m)} = \langle \psi_i | V_{\text{Hxc}}^{(m)} | \psi_j \rangle . \quad (3.12)$$

In addition, the current entropy $S^{(m)}$ is computed, diagonalizing \mathbf{f} ,

$$f_{ij}^{(m)} = \sum_l Y_{il}^{(m)\dagger} f_l^{(m)} Y_{lj}^{(m)} , \quad (3.13)$$

and so the current value of the total free energy is known. Now a search direction for the f_{ij} minimization is derived; with the new matrix elements for the Hartree/exchange-correlation term, the Hamiltonian matrix is constructed and diagonalized:

$$H_{ij}^{(m)} = h_{ij} + V_{\text{Hxc}}^{(m)} = \sum_l Z_{il}^{(m)\dagger} \epsilon_l^{(m)} Z_{lj}^{(m)} . \quad (3.14)$$

As discussed before, if the problem was not self-consistent the previous operation would give us the exact eigenvalues, and the relative occupancies would be determined via the Fermi function and with an appropriate chemical potential μ to guarantee charge conservation. In the orbital representation this solution of the non-self-consistent problem would thus be:

$$\tilde{f}_{ij}^{(m)} = \sum_l Z_{il}^{(m)\dagger} f(\epsilon_l^{(m)} - \mu) Z_{lj}^{(m)} . \quad (3.15)$$

Since the problem is self-consistent, the matrix $\tilde{f}_{ij}^{(m)}$ is chosen just as the search direction in the space of the f_{ij} , and a full line minimization is performed along the multidimensional segment connecting the current matrix \mathbf{f} and the search end-point $\tilde{\mathbf{f}}^{(m)}$:

$$\mathbf{f}^{(m+1)} = \mathbf{f}^{(m)} + \beta \Delta \mathbf{f}^{(m)} , \quad (3.16)$$

where $\Delta \mathbf{f}^{(m)} = \tilde{\mathbf{f}}^{(m)} - \mathbf{f}^{(m)}$. This choice for the search direction contributes to the success of the method: it parametrizes an unconstrained search (since the trace is equal to N both for the end-points and for every matrix linearly in between), that is determined by the eigenvalues of the non-self-consistent Hamiltonian, thus attracting all the occupations towards the representation in which they commute with the Hamiltonian and towards the thermal equilibrium values that they would assume (in the diagonal representation) at self-consistency.

Additionally, the free energy and its derivative along the search line can be easily calculated with its consistent charge density at the two end-points $\beta = 0$ and $\beta = 1$, providing the constraints to fit accurately the minimum along this line, taking into account the variations of the charge density that come from the f_{ij} . At $\beta = 0$ the free energy has already been calculated, and its derivative along the line search is (since Y diagonalizes the occupation matrix):

$$\begin{aligned} A'(\beta = 0) &= \sum_{ij} \Delta \mathbf{f}_{ji}^{(m)} \frac{\delta A}{\delta f_{ji}} = \\ &= \sum_{ij} \Delta \mathbf{f}_{ji}^{(m)} \left[h_{ij} + V_{ij}^{(m)} - T \sum_l Y_{il}^{(m)\dagger} s'(f_l^{(m)}) Y_{lj}^{(m)} \right] . \end{aligned} \quad (3.17)$$

The second point chosen for the fit is the other extreme $\beta = 1$, where the charge density is

$$\tilde{n}^{(m)}(\mathbf{r}) = \sum_{ij} \tilde{f}_{ji}^{(m)} \psi_i^*(\mathbf{r}) \psi_j(\mathbf{r}) \quad (3.18)$$

and the ‘local’ matrix elements are

$$\tilde{V}_{ij}^{(m)} = \langle \psi_i | V_{\text{Hxc}}[\tilde{n}^{(m)}] | \psi_j \rangle . \quad (3.19)$$

The free energy can now be calculated at $\beta = 1$ together with its derivative

along the search line:

$$A'(\beta = 1) = \sum_{ij} \Delta \mathbf{f}_{ji}^{(m)} \left[h_{ij} + \tilde{V}_{ij}^{(m)} - T \sum_l Z_{il}^{(m)\dagger} s'(\tilde{f}_l^{(m)}) Z_{lj}^{(m)} \right]. \quad (3.20)$$

With these four values, a cubic polynomial is interpolated; invariably, the minima located by a cubic interpolation and a parabolic one are very close, and for all practical purposes identical. This reflects the very smooth behaviour of the free energy along the search line, since the orbital terms (the kinetic energy and the non-local pseudopotential) vary only linearly, the Hartree energy is perfectly quadratic, and the remaining non-linear parts coming from the exchange-correlation and the entropy are very well-behaved. After the minimum is located, the occupation matrix gets updated, and either this loop starts over again, or the outer loop on the orbitals is entered.

3.3 Applications and comparisons

3.3.1 Self-consistency and molecular dynamics

The method has been implemented as described on the frame of the previously developed strictly variational all-bands electronic structure code, also part of this thesis work. In what follows a comparison is presented of the efficiency in the convergence of the total free energies and of the Hellmann-Feynman forces between the ensemble-DFT formulation and the standard method of updating via the occupation dynamics and the subspace rotations. The system chosen is consistently the thick slab of 15 layers of Al(110) (32 Å long, with 4 eV of Gaussian smearing, and sampled at $(\frac{1}{4}, \frac{1}{4}, \frac{1}{4})$); the choice of this system as a test case comes from its role in exemplifying all

the difficulties that arise in developing an efficient scheme, and in being very unforgiving against any possible non-variational step. In addition, it represents an excellent test case in view of the simulations that will be presented in Chapter 5, that deal with the dynamics of Al slabs in periodic boundary conditions, and that are performed in large unit cells.

In Fig. 3.2 the convergence of the free energy as a function of the number of iterations is shown, in a semi-logarithmic scale, for the system described. The label “ab” refers to the standard all-bands scheme, and “dm₂” and “dm₄” to the ensemble-DFT approach, with 2 or 4 iterations in the inner loop. The computational cost between the standard scheme and the ensemble-DFT with 2 iterations is roughly equal; in particular the standard scheme often has to reduce the mixing factor between the search in the orbitals and in the occupancies, due to the very complicated mixed-response that the system displays in that formulation. As it can be seen, the efficiency in the convergence of the free energy is distinctly better for the new methodology. For this specific case, due to the very specific geometry of the long and narrow cell, the performance keeps improving with the number of iterations in the inner loop, more or less saturating in around 8 iterations. In the current implementation, it is usually not convenient to perform more than 2 (or 3, 4) iterations, since their cost is not negligible, and it is more useful to dedicate also time towards improving the orbitals. It should be said that smaller cells (i.e. with a typical dimension less than 32 Å) show a much less pronounced improvement with the iterations in the inner loop, and two keeps being the optimal number of iterations for most practical purposes (for small systems there is little or no difference between one and two iterations). It can be

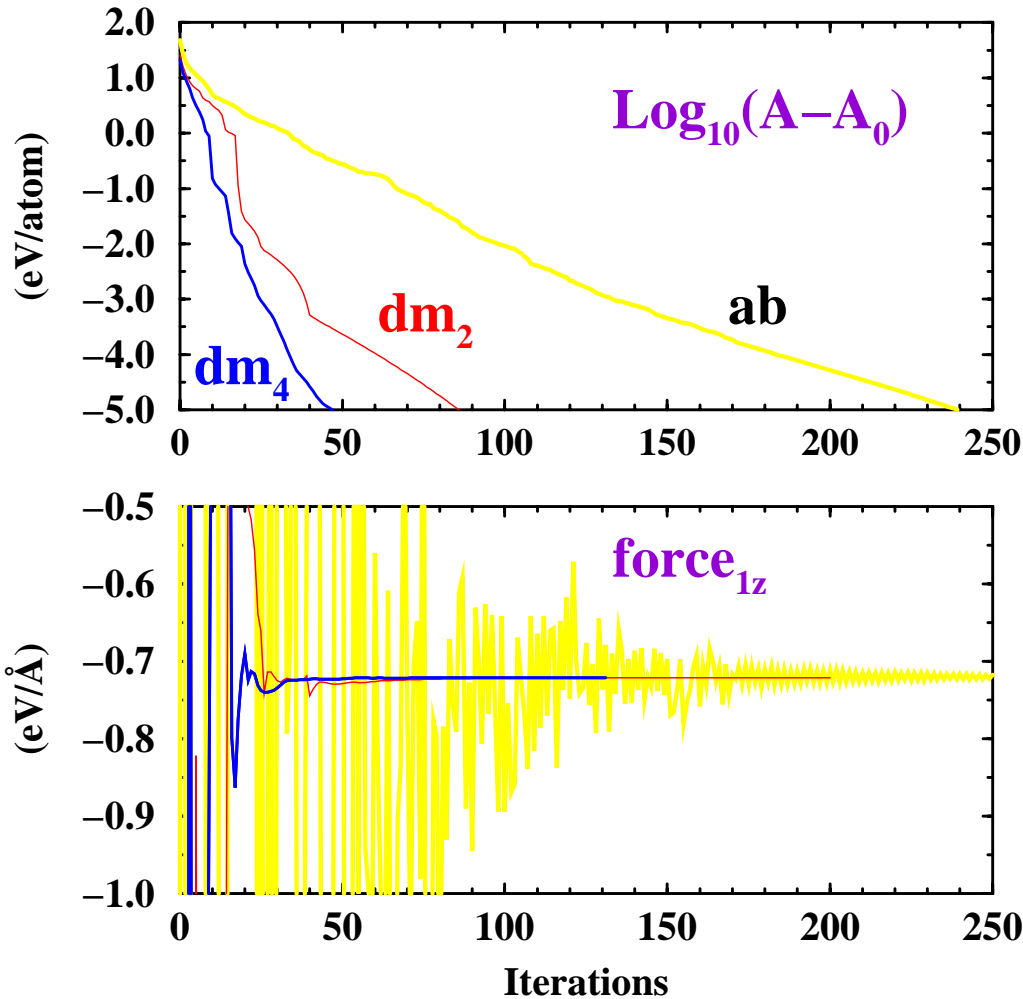


Figure 3.2: Convergence of the total free energy (in a semi-logarithmic scale) and of the Hellmann-Feynman forces (in the z -direction for the surface atom) in the 15-layer Al(110) slab, as a function of the number of all-bands iterations, for the standard method (ab) and for the case of ensemble-DFT with 2 or 4 iterations in the inner loop (dm_2 and dm_4 respectively)

suggested that, due to the very high-cost of calculating the non-local elements of the electron-ion interactions and to the small prefactor associated with the unfavourable scaling of the orthogonalization procedure or of the subspace rotations, in the case of very large systems the procedure outlined here would

become even more convenient, due to the great increase in performance that several inner loops can produce, without the overheads associated with the non-local pseudopotentials.

Even more dramatic is the improvement of the convergence rate for the Hellmann-Feynman forces (here the component in the z -direction for one of the two surface atoms is shown). This exemplifies all the potential that the projected formulation for G introduces, with its goal of reprojecting the occupation matrix at every iteration on the G surface. The typical poor convergence of the forces for the standard method is also clearly seen in the picture, and that is linked to the very non-local dynamics that derives from the update of the occupations and from the subspace rotations. It should be noted that these characteristic features would only be enhanced going towards larger systems.

Even if it wouldn't be practical, it is nevertheless interesting to observe the performance in the asymptotic limit of full convergence in the inner loop, for this difficult case, and that is shown in Fig. 3.3. Again, the total free energies and forces are plotted just for the first iterations (there is an expansion by a factor of 10 in the horizontal scale). It can be noticed how the convergence on the forces, in particular, is already acceptable (it would certainly be so for starting an ionic relaxation) at the end of the third iteration, where it differs by less than .1 eV/Å from the converged value. Obviously, in the limit of a very large number of bands in the calculation (comparable to the number of plane waves, which is certainly not the case here), the inner loop would perform the full minimization without the need of ever updating the orbitals, since the dimension of the orbital subspace would be equal to that

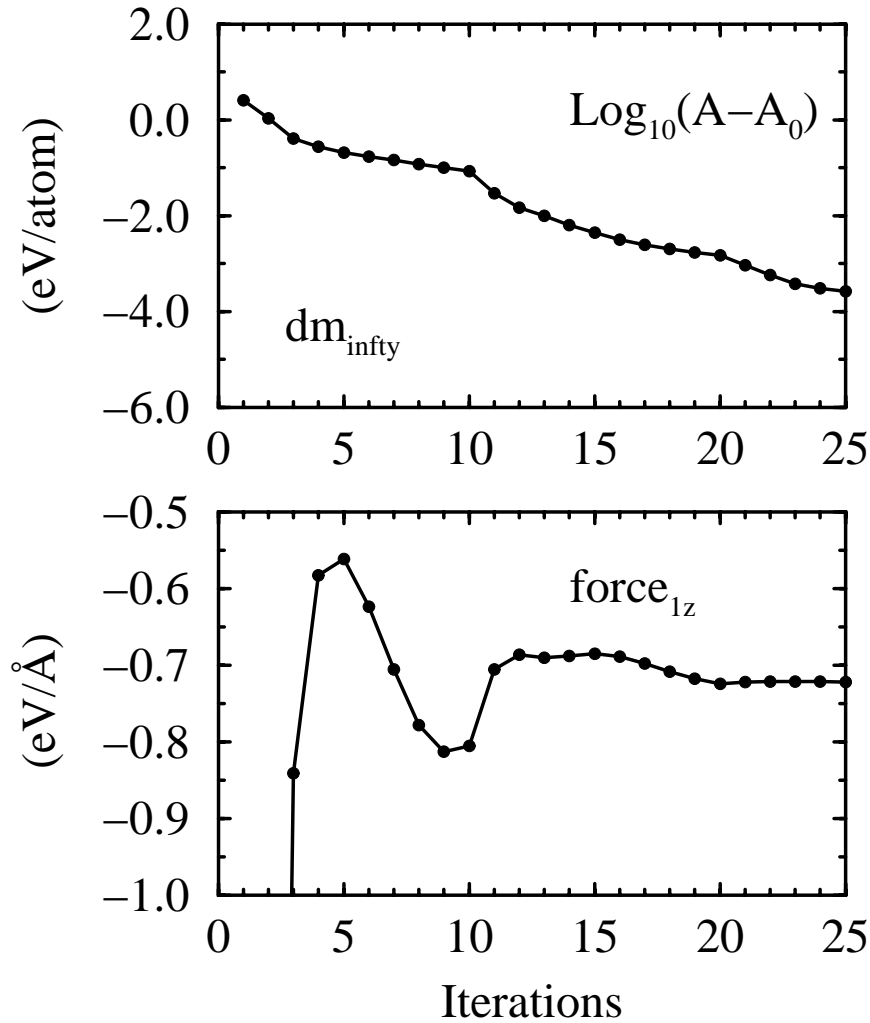


Figure 3.3: Convergence of the total free energy (in a semi-logarithmic scale) and of the Hellmann-Feynman forces (in the z -direction for the surface atom) for the 15-layer slab as a function of the number of iterations, for the case of ensemble-DFT fully converged in the inner loop.

of the variational basis, and so the procedure would optimize iteratively the problem (not to mention that the diagonalizing cost would become the key

issue).

As it can be expected from the excellent convergence of the ionic forces, the algorithm is very well suited for performing molecular dynamics simulations. A 1 ps simulation has been performed in the microcanonical ensemble for the 15-atoms cell, with a timestep of 2 fs and with a standard Verlet integration for the equations of motion, starting from the unrelaxed configuration. The comparison between the standard method and ensemble-DFT is shown in Fig. 3.4; it is immediately apparent the very rapid cooling and damping of the ions that takes place in the run done with the standard method. On the contrary, the conservation of the constant of motion is excellent with ensemble-DFT, to the point that the oscillations in the constant of motion can just be attributed to the timestep in the Verlet integration, and when a straight line is interpolated on the data, the resulting drift is just 1 meV/ps for this cell of 15 atoms. In the standard formulation the conservation is almost three orders of magnitude worse, and the conservation is satisfied with a drift of .8 eV/ps per 15 atoms. These simulations were performed with the constraints of reaching the same tolerance in the convergence of the free energy at every iteration; almost identical results in the conservation of the constant of motion are obtained if the convergence criterion is chosen to be a fixed number of iterations for every time-step. The latter method nevertheless misses the need to adjust the computational effort along the real dynamics of the system, and can introduce poorly converged steps along the simulation.

In conclusion, it has been shown here that we have now available a formulation for the electronic structure problem, and a practical algorithm for its

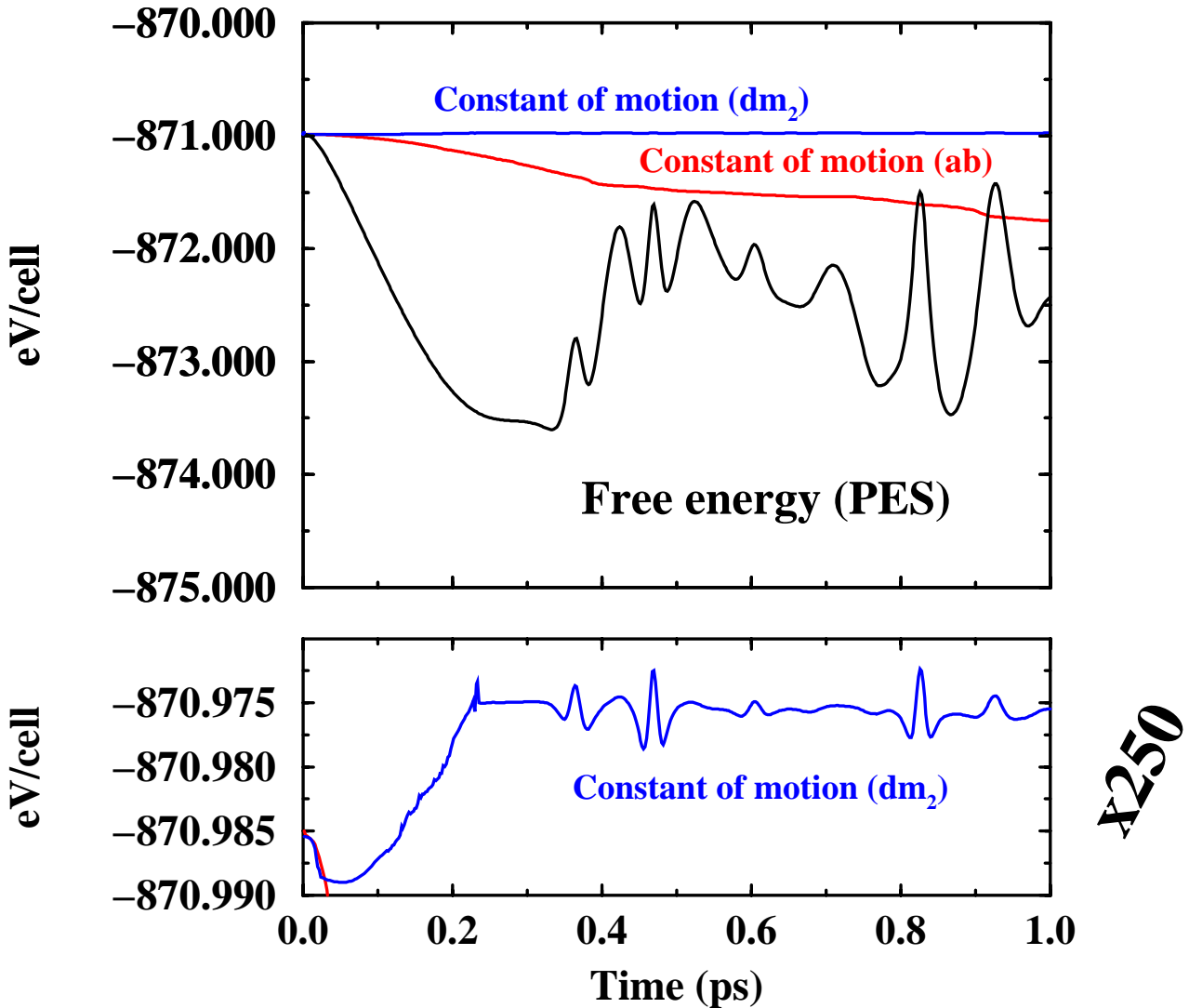


Figure 3.4: Conservation of the constant of motion in a 1 ps molecular dynamics run, for the 15-layer slab. The free energy is shown here together with the constant of motion for a run performed with the standard method and one done with ensemble-DFT. An enlargement for the latter case is also shown.

implementation, of exceptional stability and optimally suited for performing accurate and inexpensive molecular dynamics simulations in metallic sys-

tems. Some of these simulations on realistic physical cases (the first ever on a metallic surface) will be presented in Chapter 5.

3.3.2 Ionic relaxations

The requirements of efficiency and stability that have long been discussed for the case of the direct minimization of the electronic functionals can be applied also to the problem of structural relaxations, i.e. to the problem of finding the positions of local or global equilibrium for the ions. The problem of finding a global minimum is a very difficult one, and there are no simple strategies available. The concept of simulated annealing [82] is very powerful, but is too expensive to be adopted in its proper formulation in a first-principle calculation, although it can be well used for determining the nearest local minimum (tautologically the nearest minimum is that whose basin of attraction for the given algorithm contains the configuration of the system in its initial conditions).

There is no reason why the local minimum can not be located directly, by minimizing the potential energy surface $\mathcal{V}(\{\mathbf{R}_I\})$ as a function of the ionic coordinates. The usual justification that suggests for the development of alternative methods comes from the realization that, whenever the ions are moved, all the expensive and delicate work done for converging the electrons is lost, and so it is preferable to adopt strategies that try to reach a minimum for the electronic and the ionic variables at the same time. The best strategy depends strongly on the system that is investigated; for the case of metallic systems, and prompted by the excellent convergence of the ionic forces displayed in the previous Section, a direct minimization procedure has

been implemented.

This amounts to minimizing directly the functional $\mathcal{V}(\{\mathbf{R}_I\})$, using the Hellmann-Feynman forces as its derivatives with respect to the ionic positions. The set of ionic forces defines then a multidimensional line in the configurational space of the ions, and a parabolic minimization is implemented, in a spirit similar to the parabolic minimization for the orbital updating. The great advantage of this approach is that it is often very appropriate to adopt large (and in this case optimal) ionic steps at the beginning of a relaxation, since it would be quite useless maintaining electronic coherence along a region of space that is so far away from equilibrium. Additionally, the direct minimization is a method that can be made as robust as it is required, and so it is naturally suited as an all-purpose algorithm.

In addition to a steepest descent choice for defining the line of minimization, more sophisticated alternatives are available, in the form of, again, conjugate-gradient or variable-metric methods. For the present case, the former method has been adopted, relying on the relative insensitivity that atoms far apart would manifest to each other in a metal. The overall performance is again very good and very robust. An example is shown here in Fig. 3.5 and Fig. 3.6, where the structure to be minimized is a 72 atoms system, represented by a 8-layer thick 3x3 Al(110) slab. As can be seen, the convergence is exponential in the number of iterations up to a very good approximations, and 3-4 iterations give already a very satisfactory answer. In addition, the electronic problem at every ionic configuration does not need to be solved to full self-consistency, since the only requirement is having ionic forces roughly correct. This formulation is also currently being applied to the case of the

grain boundary sliding in aluminium, and the computational convergence is excellent for such a system with very small barriers [127]. Typical figures for a 60-atom cell show that $\sim 4 - 6$ iterations bring the largest forces down from few eV/ \AA to less than 0.01 eV/ \AA , similar to what has been observed in the relaxation shown in Fig. 3.5 (in both cases starting from the ideal unrelaxed structure).

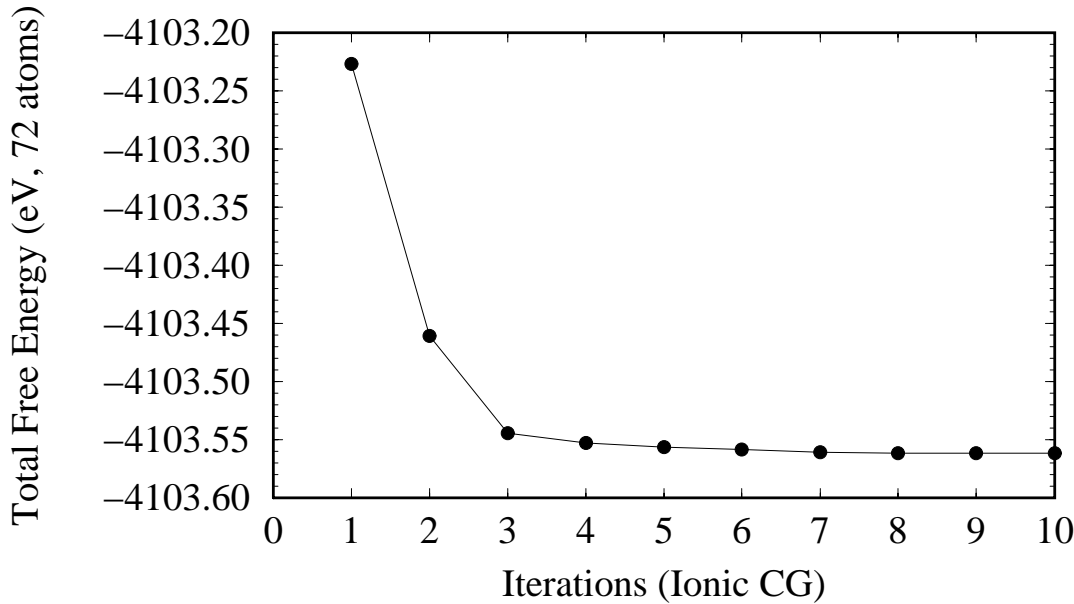


Figure 3.5: Total free energy as a function of the number of ionic iterations for the structural relaxations of a 3x3 Al(110) 8-layer slab.

3.4 Further developments

As a final note, it should be mentioned what are the possible developments of the approach presented here, in addition to its main goal of performing

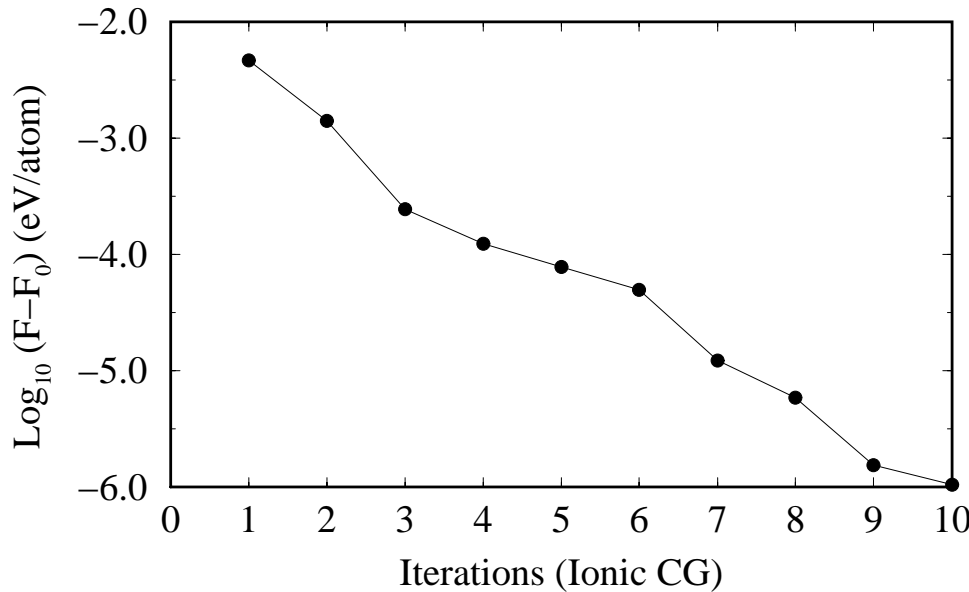


Figure 3.6: Same as the previous figure, in a semi-logarithmic scale.

efficient molecular dynamics and structural relaxations in metals.

The iterative minimization of the inner loop will be exploited in Chapter 4 to introduce exotic, non-monotonic thermal distributions in a variational fashion. Additionally, the present formulation can help clarifying if it is at all possible to define a density-functional theory for non-monotonic occupancies or can provide a general scheme for defining density-functional theories in the case of monotonic occupancies (for Fermi-Dirac statistics the proof has been given by Mermin [3]). In fact, if the iterative procedure is shown to converge to a unique result under these circumstances, it can lead via a constrained-search formulation to a meaningful definition (from the point of view of density-functional theory) of the functional $G[n(\mathbf{r})]$ under a variety

of conditions.

The connection with linear-response theory in metals would also be very interesting [119] [128], in particular towards the characterization of the subspaces that are spanned by the first-order and higher-orders derivatives of the wavefunctions in the presence of a smearing, in relation to the gauge chosen [128].

From a more computational-oriented point of view, there are some extensions that could be implemented, such as introducing an unconstrained minimization of the orbitals along the lines of [89], exploiting the control on internal rotations that has been shifted to the matrix f_{ij} . Another possibility would be trying to simulate the fine sampling of many \mathbf{k} -points with the introduction of several matrices $\mathbf{f}_{ij,\mathbf{k}}$, while keeping only one set of orbitals. Finally, this approach could benefit a Car-Parrinello implementation for systems with fractional occupancies and subspace rotations, by compressing to zero the slow frequencies of motion for these operations without having to perform them in the space of the orbitals.

Chapter 4

Generalized entropy and cold smearing

Introduction

The use of a finite-temperature formulation as a technical device to improve the sampling accuracy in the Brillouin Zone is discussed. The variational formulation in terms of a *generalized free energy* [117] is outlined, together with the insight that it provides in understanding the role of the temperature, or of the broadening, in total energy calculations. The relation between the smearing technique for the density of states of a metal and the introduction of an entropic term in the total energy functional is presented [119]. The methods proposed to correct for the systematic errors introduced by the temperature or by the broadening are discussed and evaluated [44] [118]. In particular it is shown that formulations where the occupation numbers can be negative lead to uncorrect results and *should not be used* in self-consistent

calculations. Finally, the novel formulation of *cold smearing* is presented, that overcomes the difficulties inherent in previous proposals.

4.1 Generalized free energy

It was argued in Section 2.3.3 that the deterioration of the sampling accuracy in calculating the total charge density and the kinetic/non-local terms in the total energy functional was directly related to the presence of a discontinuity in the functions to be integrated, since the occupation numbers $f(\epsilon_{i\mathbf{k}})$ in the integrands drop to zero whenever $\epsilon_{i\mathbf{k}}$ crosses the Fermi surface. On the other hand, this discontinuity is a feature that is characteristic only for the electron gas at zero temperature; the sharp discontinuity at the Fermi energy in the Fermi-Dirac distribution becomes smoother with increasing electronic temperature, and the precision of a given sampling mesh increases. This can be also observed in actual calculations: if a finite-temperature picture is introduced, the complete convergence with respect to the \mathbf{k} -point sampling in the Brillouin Zone is reached with coarser meshes at higher electronic temperatures.

It is thus natural to focus attention on a possibly general mechanism to introduce and gauge different schemes that achieve the goal of smoothing the Fermi discontinuity. In this framework De Vita and Gillan introduced the concept of a generalized free energy [117]: an additional term is heuristically added to Janak's functional, in order to make it variational with respect to the occupation numbers¹ (see also Ref. [112]). The generalized free energy is

¹In all that follows a picture in the diagonal representation for the occupation numbers will be assumed, for the sole reason of notation. The extension to a rotation-invariant

thus formulated as in (1.36):

$$\begin{aligned} A [\sigma; \{\psi_i\}, \{f_i\}] &= \sum_i f_i \langle \psi_i | \hat{T}_e + \hat{V}_{nl} | \psi_i \rangle + E_{\text{Hxc}}[n] - \sigma S[\{f_i\}] + \\ &+ \mu (N - \sum_i f_i) + \sum_i f_i \epsilon_i (\langle \psi_i | \psi_i \rangle - 1) \end{aligned} \quad (4.1)$$

$$n(\mathbf{r}) = \sum_i f_i \psi_i^*(\mathbf{r}) \psi_i(\mathbf{r}) , \quad (4.2)$$

where the additional term $S[\{f_i\}]$, a function of the occupancies only, has been added in order to allow for the variational requirement, and μ and $\lambda_i = f_i \epsilon_i$ are the Lagrange multipliers used to impose the charge conservation and the normalization of the orbitals. The parameter σ is also introduced, to complete the analogy with a finite-temperature formulation. Now, the idea is to first impose the stationarity requirements on this functional, and then to derive the relations that this stationarity propagates to the dependence of $S[\{f_i\}]$ on the occupation numbers. The equilibrium conditions are:

$$\frac{\delta A}{\delta \psi_i^*} = 0 \Rightarrow f_i \hat{H} \psi_i = f_i \epsilon_i \psi_i \quad (4.3)$$

$$\frac{\partial A}{\partial \lambda_i} = 0 \Rightarrow \langle \psi_i | \psi_i \rangle = 1 \quad (4.4)$$

$$\frac{\partial A}{\partial f_i} = 0 \Rightarrow \langle \psi_i | H | \psi_i \rangle - \mu = T \frac{\partial S}{\partial f_i} \quad (4.5)$$

$$\frac{\partial A}{\partial \mu} = 0 \Rightarrow \sum_i f_i = N \quad (4.6)$$

The first relation is in the form of the Janak-Kohn-Sham equations; it should be noted that orthogonality follows from this diagonal equation itself, and need not be explicitly imposed. Eq. 4.5 provides the fundamental link between the functional form of the entropy with respect to the occupation numbers and the equilibrium dependence of the occupation numbers on the formalism is straightforward.

expectation values of the Hamiltonian. An inverse approach will be pursued: instead of starting from a counting relation (the Pauli principle) and determining an equilibrium distribution (the Fermi-Dirac) from the requirement of maximizing the entropy (as in statistical mechanics), with the entropy itself a measure of the number of states available, the equilibrium distribution is arbitrarily chosen, and the form of the entropy that follows from the minimization requirement is derived.

The choice is made for the (fictitious) thermal distribution to be written as

$$f(x) = \int_{-\infty}^x g(t) dt , \quad (4.7)$$

where $g(t)$ is a broadening function normalized to 1 (or 2, in the case of spin degeneracy). This relation provides an operative definition of the fictitious temperature as an *integrated broadening*, with the full freedom to choose the function g , as long as the usual physical constraints on the occupancies are satisfied. This relation can be propagated to the entropy; in the non-interacting picture the entropy is a linear combination of single-particle terms

$$S[\{f_i\}] = \sum_i S_i = \sum_i S(f_i) , \quad (4.8)$$

and so a functional form for the entropy can be determined by integrating

$$\frac{dS}{df} = \frac{\epsilon - \mu}{\sigma} = -x \Rightarrow \frac{dS}{dx} = -x \frac{df}{dx} \quad (4.9)$$

$$f(x) = \int_{-\infty}^x g(t) dt \Rightarrow S_i = \int_{-\infty}^{x_i} -t g(t) dt . \quad (4.10)$$

The previous relation provides an operative connection between the choice of a broadening function and the actual form of the entropy; as an example, if the following form for $g(t)$ is chosen (assuming spin-degeneracy),

$$g(t) = \frac{2}{(e^{\frac{t}{2}} + e^{-\frac{t}{2}})^2} , \quad (4.11)$$

the entropy that is derived according to the procedure above is:

$$S = -2 \sum_i [y_i \log y_i + (1 - y_i) \log(1 - y_i)] , \text{ with} \quad (4.12)$$

$$y_i = \frac{f_i}{2} = \frac{1}{e^{\frac{\epsilon_i - \mu}{\sigma}} + 1} = \frac{1}{e^{-x} + 1}. \quad (4.13)$$

In addition to recovering this well-known result, the freedom in choosing the broadening function can be exploited to identify arbitrary generalized free energies as a function of the thermal distributions. As an example, it is often convenient to employ in practical calculations [129] a Gaussian entropy,

$$S = \frac{1}{\sqrt{\pi}} \sum_i e^{-\left(\frac{\epsilon_i - \mu}{\sigma}\right)^2} \quad (4.14)$$

as obtained from the broadening

$$g(t) = \frac{2}{\sqrt{\pi}} e^{-t^2} . \quad (4.15)$$

One problem of generalizing beyond the Fermi-Dirac distribution is that, in all the other generalized schemes, an important result is lost: the entropy is not any more expressible as a function of the occupation numbers f_i , but only as a function of their inverse under the equilibrium thermal distribution, namely the ϵ_i . It should be noted that (4.5) implies

$$\frac{dS}{df_i} = -x_i, \quad (4.16)$$

i.e. the derivative of the entropy is equal to the opposite of the normalized distance between the Fermi energy and the inverse of the occupation; this relation is useful if the steepest-descent directions on the occupancies are needed.

4.2 Smeared functionals

In their initial formulation [103] [104] broadening schemes were exploited to improve the accuracy in the sampling and to stabilize the iterative convergence in the presence of level crossings. In particular, the authors of Ref. [103], who originally introduced the technique, relied on the idea of broadening the exact density of states in order to partially extend the sampling to neighbouring regions around the necessarily limited set of \mathbf{k} -points used for the self-consistency process. Starting from an ideal, unsmeared density of states,

$$n(\epsilon) = \sum_{i\mathbf{k}} \delta(\epsilon - \epsilon_{i\mathbf{k}}), \quad (4.17)$$

the smeared density $\tilde{n}(\epsilon)$ is introduced via a convolution with a function $\tilde{\delta}$,

$$\tilde{n}(\epsilon) = \int_{-\infty}^{\infty} d\epsilon' \frac{1}{\sigma} \tilde{\delta}\left(\frac{\epsilon - \epsilon'}{\sigma}\right) n(\epsilon'), \quad (4.18)$$

that is some smoother approximation of the original Dirac's delta. In the limit $\tilde{\delta} \rightarrow \delta$, the unsmeared density of states is recovered, since it is

$$\tilde{n}(\epsilon) = \sum_{i\mathbf{k}} \frac{1}{\sigma} \tilde{\delta}\left(\frac{\epsilon - \epsilon_{i\mathbf{k}}}{\sigma}\right). \quad (4.19)$$

The new smeared density of states is used to calculate the smeared band-energy term, defined as

$$\tilde{E}_{band} = \int_{-\infty}^{\mu} d\epsilon \epsilon \tilde{n}(\epsilon), \quad (4.20)$$

in alternative to the usual formulation

$$E_{band} = \sum_i f_i \epsilon_i. \quad (4.21)$$

It has been demonstrated by de Gironcoli [119] that this approach is completely equivalent to the one discussed before, i.e. the smeared total energy

functional is equivalent to a generalized free energy whose form depends on the choice of the broadening. In the smeared band-energy term one can exactly isolate the additional generalized entropic term dependent on the occupation numbers only. The derivation of this result is useful for the later discussion, and so it is worked out here in detail. Starting from the original [103] form for the smeared band-energy term, and then summing and subtracting $\frac{\epsilon'}{\sigma}$ and inverting the order of the integration, these equalities are obtained:

$$\begin{aligned}
\tilde{E}_{band} &= \int_{-\infty}^{\mu} d\epsilon \epsilon \tilde{n}(\epsilon) \\
&= \int_{-\infty}^{\mu} d\epsilon \epsilon \int_{-\infty}^{\infty} d\epsilon' \frac{1}{\sigma} \tilde{\delta}\left(\frac{\epsilon - \epsilon'}{\sigma}\right) n(\epsilon') \\
&= \int_{-\infty}^{\infty} d\epsilon' n(\epsilon') \int_{-\infty}^{\mu} d\epsilon \epsilon \frac{1}{\sigma} \tilde{\delta}\left(\frac{\epsilon - \epsilon'}{\sigma}\right) \\
&= \int_{-\infty}^{\infty} d\epsilon' n(\epsilon') \int_{-\infty}^{\mu} d\epsilon \sigma \left(\frac{\epsilon - \epsilon' + \epsilon'}{\sigma}\right) \frac{1}{\sigma} \tilde{\delta}\left(\frac{\epsilon - \epsilon'}{\sigma}\right) \\
&= \int_{-\infty}^{\infty} d\epsilon' \epsilon' n(\epsilon') \int_{-\infty}^{\mu} d\epsilon \frac{1}{\sigma} \tilde{\delta}\left(\frac{\epsilon - \epsilon'}{\sigma}\right) + \\
&\quad + \sigma \int_{-\infty}^{\infty} d\epsilon' n(\epsilon') \int_{-\infty}^{\mu} d\epsilon \left(\frac{\epsilon - \epsilon'}{\sigma}\right) \frac{1}{\sigma} \tilde{\delta}\left(\frac{\epsilon - \epsilon'}{\sigma}\right) \\
&= \int_{-\infty}^{\infty} d\epsilon' \epsilon' n(\epsilon') \int_{-\infty}^{\frac{\mu - \epsilon'}{\sigma}} dx \tilde{\delta}(x) + \\
&\quad + \sigma \int_{-\infty}^{\infty} d\epsilon' n(\epsilon') \int_{-\infty}^{\frac{\mu - \epsilon'}{\sigma}} dx x \tilde{\delta}(x) . \tag{4.22}
\end{aligned}$$

The previous expression can be simplified by introducing the “occupation” function f , defined as

$$f\left(\frac{\mu - \epsilon'}{\sigma}\right) = \int_{-\infty}^{\frac{\mu - \epsilon'}{\sigma}} dx \tilde{\delta}(x) \tag{4.23}$$

and the “entropy” function S , defined as

$$S\left(\frac{\mu - \epsilon'}{\sigma}\right) = - \int_{-\infty}^{\frac{\mu - \epsilon'}{\sigma}} dx x \tilde{\delta}(x) ; \quad (4.24)$$

with these definitions the band-energy term can be rewritten as

$$\begin{aligned} \tilde{E}_{band} &= \int_{-\infty}^{\infty} d\epsilon' \epsilon' n(\epsilon') f\left(\frac{\mu - \epsilon'}{\sigma}\right) + \\ &- \sigma \int_{-\infty}^{\infty} d\epsilon' n(\epsilon') S\left(\frac{\mu - \epsilon'}{\sigma}\right) \\ &= \sum_{i\mathbf{k}} \epsilon_{i\mathbf{k}} f\left(\frac{\mu - \epsilon_{i\mathbf{k}}}{\sigma}\right) - \sigma \sum_{i\mathbf{k}} S\left(\frac{\mu - \epsilon_{i\mathbf{k}}}{\sigma}\right) \end{aligned} \quad (4.25)$$

finally establishing the link with the previous formulation. In particular, the entropic term can be analyzed further, in order to highlight its relation with the broadening function $\tilde{\delta}$. If we assume that the unsmeared density of states can be expanded in powers of ϵ ,

$$n(\epsilon') = \frac{1}{k!} \sum_{k=0}^{\infty} \frac{d^k n}{d\epsilon^k} (\epsilon' - \epsilon)^k = \frac{1}{k!} \sum_{k=0}^{\infty} n^{(k)}(\epsilon) (\epsilon' - \epsilon)^k \quad (4.26)$$

the entropy can now be written as:

$$\begin{aligned} S &= - \int_{-\infty}^{\infty} d\epsilon' \int_{-\infty}^{\mu} d\epsilon n(\epsilon') \left(\frac{\epsilon - \epsilon'}{\sigma}\right) \frac{1}{\sigma} \tilde{\delta}\left(\frac{\epsilon - \epsilon'}{\sigma}\right) \\ &= - \int_{-\infty}^{\mu} d\epsilon \int_{-\infty}^{\infty} d\epsilon' \frac{1}{k!} \sum_{k=0}^{\infty} n^{(k)}(\epsilon) (\epsilon' - \epsilon)^k \left(\frac{\epsilon - \epsilon'}{\sigma}\right) \frac{1}{\sigma} \tilde{\delta}\left(\frac{\epsilon - \epsilon'}{\sigma}\right) \\ &= - \int_{-\infty}^{\mu} d\epsilon \int_{-\infty}^{\infty} d\epsilon' \frac{1}{k!} \sum_{k=0}^{\infty} n^{(k)}(\epsilon) (-1)^k \sigma^k \left(\frac{\epsilon - \epsilon'}{\sigma}\right)^{k+1} \tilde{\delta}\left(\frac{\epsilon - \epsilon'}{\sigma}\right) \\ &= \sum_{k=0}^{\infty} \sigma^k \int_{-\infty}^{\mu} d\epsilon n^{(k)}(\epsilon) (-1)^{k+1} \frac{1}{k!} \int_{-\infty}^{\infty} x^{k+1} \tilde{\delta}(x) dx \\ &= \sum_{k=0}^{\infty} c_k n^{(k-1)}(\mu) \sigma^k , \end{aligned} \quad (4.27)$$

where the coefficients c_k have been introduced:

$$c_k = (-1)^{k+1} \frac{1}{k!} \int_{-\infty}^{\infty} x^{k+1} \tilde{\delta}(x) dx , \quad (4.28)$$

and with the straightforward generalization $n^{(-1)}(\mu) = N$. In particular, it is seen that the entropy has no zero-order term in the smearing/temperature, as it should be, if the broadening function $\tilde{\delta}$ is even; the first term in the series is then

$$S = c_1 n(\mu) \sigma ; \quad c_1 = \int_{-\infty}^{\infty} dx x^2 \tilde{\delta}(x). \quad (4.29)$$

4.3 Entropy corrections

It has been argued that the introduction of a finite-temperature picture can greatly improve the accuracy towards the statistical errors in the sampling, allowing for the use of coarse special-points meshes that would otherwise be inadequate in a zero-temperature formulation.

The temperature, or the broadening, introduces also a systematical error; in order to obtain a significant smearing of the Fermi discontinuity, temperatures are introduced that range from few tenths of an eV to 1-2 eV. It should be pointed out that these broadenings are for the electronic degrees of freedom, and their effect is often small or negligible, especially in simple metals; as an example, the density of states for bulk aluminium, as calculated consistently with the different smearings used, and using fine integration meshes, is shown in Fig. 4.1. The white and grey areas are respectively the total and the occupied density of states for the (Gaussian) broadening indicated, and calculated consistently at that broadening. As can be observed, there is little difference even in the fine features of the density profiles; this behaviour is typical of bulk simple metals, that display a quasi-ideal parabolic density of states, as in the non-interacting electron gas.

The formulations that have been presented here elucidate that there are

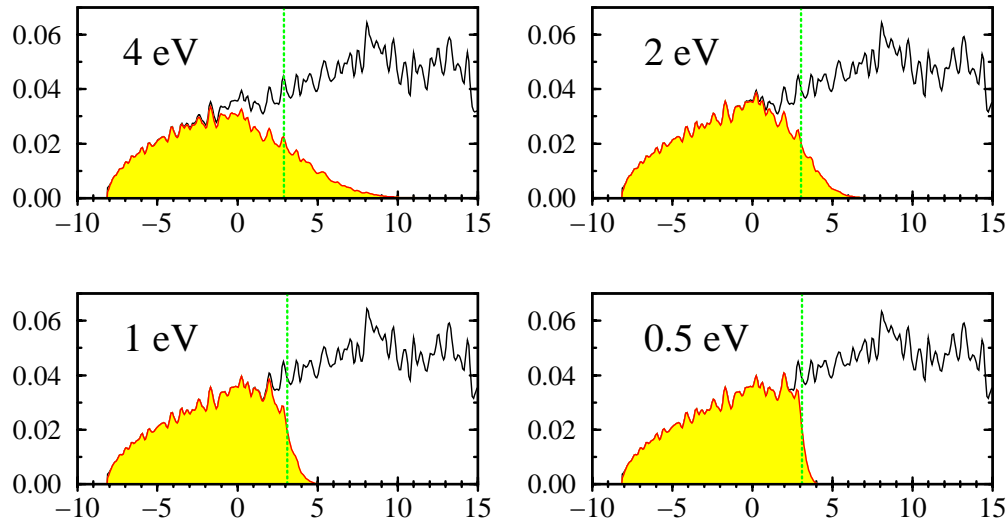


Figure 4.1: Density of states for bulk aluminium calculated self-consistently at different (Gaussian) broadenings (the horizontal axes are in eV, the vertical axes in arbitrary units). The total and the occupied (shaded) densities of states are shown.

simple ways to correct for some systematic errors associated with the temperature. This will lead to a development in which these corrections are used to full advantage, and comparatively large smearing widths, with the many advantages that they bring in, are used, while some of the associated errors are corrected for, at least to the most significant order in the smearing.

4.3.1 Energy

It is possible to combine two of the previous results to determine the behaviour of the total free energy as a function of the fictitious temperature [117]. The minimization procedure for the functional (4.1) implies that, when the minimum is reached, the following relation must hold:

$$\frac{\partial A}{\partial \sigma} = \frac{dA}{d\sigma} . \quad (4.30)$$

This follows straightforwardly from the minimization on the $\{\psi_i\}$ and on the $\{f_i\}$; at the self-consistent minimum all the partial derivatives of the free energy with respect to the orbitals and the occupancies are zero, and so the dependence on σ is all that is left. But the partial derivative of the free energy with respect to σ is $-S$, and so the fundamental relation

$$\frac{dA}{d\sigma} = -S(\sigma) \quad (4.31)$$

is proved. Additionally, the behaviour of S with the temperature has been outlined in the previous discussion on the smeared functionals, and it is

$$S = c_1 n(\mu) \sigma + \mathcal{O}(\sigma^2) = \gamma \sigma + \mathcal{O}(\sigma^2). \quad (4.32)$$

These two relations can be joined to determine the Taylor expansion of the total free energy as a function of σ around $\sigma = 0$:

$$A(\sigma) = A(0) + \sigma (-S)|_{\sigma=0} + \frac{1}{2} \sigma^2 \frac{d}{d\sigma} (-S)|_{\sigma=0} + \mathcal{O}(\sigma^3) \quad (4.33)$$

$$A(\sigma) = E(0) - \frac{1}{2} \gamma \sigma^2 + \mathcal{O}(\sigma^3) \quad (4.34)$$

(at zero temperature the total energy $E(0)$ and the free energy $A(0)$ obviously coincide). Now, since $A = E - \sigma S$, the dependence of E on σ is

also determined if the S correct up to the second order is introduced in the previous relation,

$$E(\sigma) = E(0) + \frac{1}{2} \gamma \sigma^2 + \mathcal{O}(\sigma^3). \quad (4.35)$$

From these two relations it can be seen that an estimate for the limit at zero temperature of the total and free energies can be obtained from their finite-temperature values. The *entropy-corrected* functional is thus defined as

$$E_0(\sigma) = \frac{E(\sigma) + A(\sigma)}{2} = E(0) + \mathcal{O}(\sigma^3). \quad (4.36)$$

This relation is shown in all its accuracy in Fig. 4.2, where the total, free and entropy-corrected energies are plotted for the case of a bulk Al system. Two main issues should be noted: the dependence of the corrected energy on the temperature is clearly eliminated to the quadratic order, to the point that in this system (somewhat ideal) the error on the estimate of the zero-temperature total energy that is obtained with a calculation at 3 eV of smearing is less than 3 meV/atom (this is a fully converged number; energy differences are, as always, much better). In addition, while a calculation with little smearing does require fine meshes of special points to converge accurately, calculations at larger smearing require less and less \mathbf{k} -points, and at 2-3 eV the (8 8 8) mesh for the FCC cell guarantees excellent convergence, with a sampling effort perfectly comparable to the case of semiconductors, even adequate for determining notorious delicate quantities as, say, the shear modulus for Al². The results for the structural parameters of the pseudopotential(s) used in this work are shown in Fig. 4.3; these have been tested

²Without resorting to a corrected smearing scheme, even thousands of \mathbf{k} -points would give unsatisfactory convergence; the case is discussed in Ref. [117]

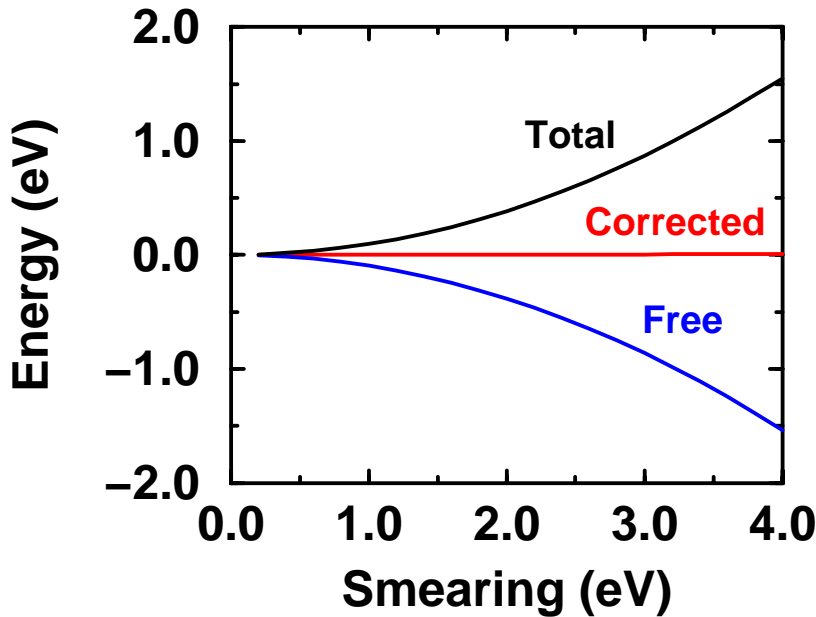


Figure 4.2: Total, free and corrected energies for bulk Al as a function of the (Gaussian) broadening. Full sampling convergence even at low temperatures is obtained using a fine (12,12,12) mesh of Monkhorst-Pack points for the 4-atom cubic unit cell.

for convergence down to more typical smearings (0.5 eV-1 eV), even though for this system the differences are negligible. It should be stressed that all the structural parameters have been determined as entropy-corrected energy differences; if the total free energy or the total energy would have been used, a lattice parameter around 3% larger or smaller, respectively, would have been determined; this effect is clearly due to the electron-gas pressure due to the occupation of the higher, isotropic bands.

	a_0 (Å)	B (Kbar)	B (from C)	C_{11} (Kbar)	C_{12} (Kbar)	C_{44} (Kbar)
al013a	4.02	768	751	1038	608	285
al013b	4.06	773				272
expt.	4.05	783	794	1143	619	316

Figure 4.3: Structural parameters calculated at 3 eV of smearing and 10 special points in the irreducible wedge of the FCC cell. Al013a converges with 200 eV of cutoff, al013b with 80 eV.

4.3.2 Forces and other derivatives

Although the possibility to perform calculations at high smearings and few \mathbf{k} -points is very attractive, and it does provide accurate estimates of the total energy at zero temperature—that is often the quantity of interest—it should be stressed that the correction procedure is a non-variational a-posteriori treatment, and as such is not straightforwardly suitable for performing molecular dynamics, where forces consistent with the chosen potential energy must be adopted.

The ionic forces calculated from the ground state are the Hellmann-Feynman derivatives of the variational functional, and thus are the derivatives of the free energy; this point can be exemplified by actually calculating the work done by displacing an atom, and comparing it to the total and free energy difference. The results are in Fig. 4.4; the discrepancy between the Hellmann-Feynman forces and the derivatives of the total energy is ca. 5%, as is typical in bulk solids and liquids. For the case of a slab calculation the difference would be greater, since the pressure that the thermal excitations exert on the electron gas forces an expansion of the system whenever

\mathbf{d}	ΔE (eV)	ΔA (eV)	Work $\mathbf{d} \cdot \mathbf{f}_{HF}$ (eV)
$4.02 \cdot 10^{-2}$	$8.658 \cdot 10^{-2}$	$9.549 \cdot 10^{-2}$	$13.205 \cdot 10^{-2}$
$4.02 \cdot 10^{-3}$	$12.180 \cdot 10^{-3}$	$12.844 \cdot 10^{-3}$	$13.205 \cdot 10^{-3}$
$4.02 \cdot 10^{-4}$	$12.534 \cdot 10^{-4}$	$13.173 \cdot 10^{-4}$	$13.205 \cdot 10^{-4}$
$4.02 \cdot 10^{-5}$	$12.601 \cdot 10^{-5}$	$13.206 \cdot 10^{-5}$	$13.205 \cdot 10^{-5}$

Figure 4.4: Change in the energy and in the free energy in a displacement \mathbf{d} of one atom in a bulk 4-atom cell, together with the work done in the displacement

there is some available vacuum that can be easily filled in. For this reason, one should be very careful in performing straightforward molecular-dynamics simulations in a slab employing forces that are not consistent with the potential energy surface chosen (i.e. the free energy); it might be argued that even in a bulk system this care should be taken into account, especially when dealing with the dynamic correlations around vacancies and impurities.

One possibility would be to devise a scheme able to calculate the true derivatives of the introduced entropy-corrected potential energy surface. This is actually possible, and the relation between the Hellmann-Feynman forces and the entropy-corrected forces can be obtained by resorting once again to the fundamental relation that holds at the self-consistent minimum, namely

$$\frac{dA}{d\sigma} = -S(\sigma) . \quad (4.37)$$

The goal here is to obtain the corrected forces

$$-\frac{dE_0}{d\mathbf{R}} = -\frac{dA}{d\mathbf{R}} - \frac{\sigma}{2} \frac{dS}{d\mathbf{R}} ; \quad (4.38)$$

where the derivative $-\frac{dA}{d\mathbf{R}}$ is just the Hellmann-Feynman force. The term $\frac{dS}{d\mathbf{R}}$

can be calculated by substituting S with $-\frac{dA}{d\sigma}$, thus obtaining

$$-\frac{dE_0}{d\mathbf{R}} = \mathbf{f}_0 = \mathbf{f}_{HF} + \frac{\sigma}{2} \frac{d^2 A}{d\mathbf{R} d\sigma} . \quad (4.39)$$

Exchanging the order of the derivation in the latter term the final result is obtained:

$$\mathbf{f}_0 = \mathbf{f}_{HF} - \frac{\sigma}{2} \frac{d\mathbf{f}_{HF}}{d\sigma} . \quad (4.40)$$

This result is of a general nature, and can be applied also to the other derivatives of the corrected-energy. At variance with the case of the energy, the correction on the forces is no longer a straightforward post-hoc contribution, but requires the evaluation of the derivative of the Hellmann-Feynman forces with respect to the ionic temperature. This derivative can be either calculated with some perturbative scheme, or straightforwardly determined by direct differentiation (in this case there would be no advantage in going to the linear-response formulation, given the simplicity of the perturbation)

It must be said that, given the difficulties in converging the ionic forces in a metal, especially with traditional electronic-structure schemes, this approach does not constitute a practical way to perform a realistic calculation in a large system, since the accuracy needed in order to properly extrapolate the zero-temperature limit of the force would require the calculations of the derivatives $\frac{d\mathbf{f}_{HF}}{d\sigma}$ to an extremely high degree of tolerance.

The formulation is nevertheless conceptually appealing, and it gives a more complete framework to the approach of the entropy-correction. As a final case, some actual results for this algorithm of force correction are presented in Fig. 4.5, for the case of a 3-layer 1x1 Al(110) slab. The symbols represent the Hellmann-Feynman forces for a given smearing and a given mesh, while the lines refer to the equivalent corrected force. The typical

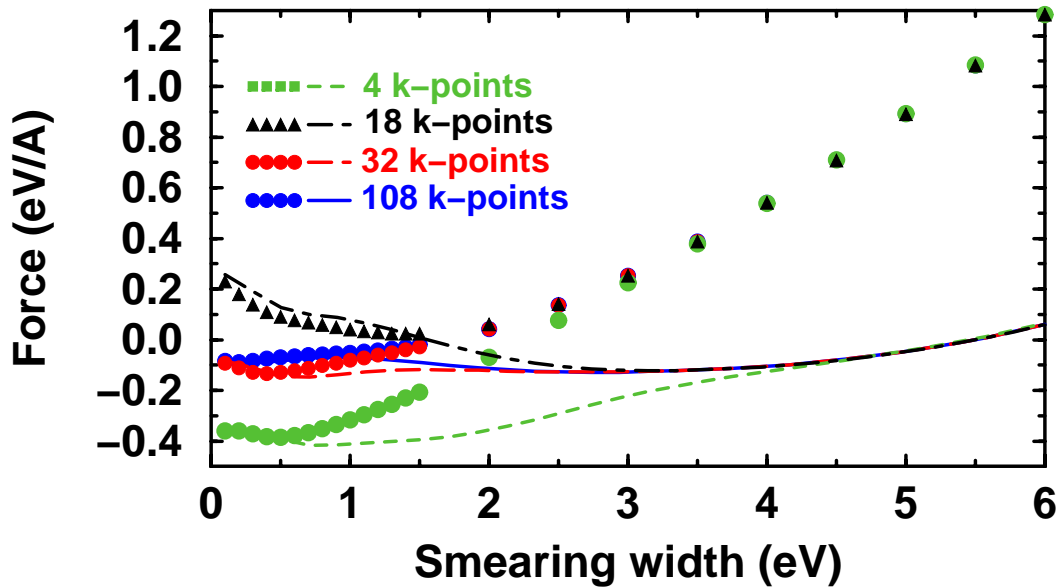


Figure 4.5: Force in the z direction for the surface atom of a 3-layer 1x1 Al(110) slab, as a function of the (Gaussian) broadening and for different meshes of special points in the irreducible wedge of the Brillouin zone.

features described up to now are clearly exemplified: it can be seen that at very high temperature the convergence is much faster with respect to the sampling, and very few \mathbf{k} -points can provide full convergence. Going towards regions of moderate smearing a plateau is encountered, where the smearing is still sufficiently high to allow for a significant economy on the number of \mathbf{k} -points, but the higher-order terms in the energy have become negligible. At lower temperatures, the sampling instability takes in, and the results obtained with various meshes start to differ, although the more accurate meshes converge to a value that is very similar to what all the meshes gave in

the mid-range of temperatures for the corrected forces. Needless to say, when performing any smeared/finite-temperature metallic calculation the typical plateaus should be roughly identified in advance, in order to optimize the number of \mathbf{k} -points that are necessary, without entering either the region of higher-order coupling with the temperature, or the region of sampling instability.

4.4 Cold smearing

Methfessel-Paxton broadening A different strategy to correct for the systematic errors introduced by the temperature formulation takes the approach of choosing a suitable smearing function in order to minimize from the beginning the coupling with the temperature. This is the strategy that has been proposed by Methfessel and Paxton [118], and applied first to tight-binding models. It is also gaining popularity among the first-principles community, and several calculations have been performed adopting this scheme. The idea is simply explained recalling the expression for the entropy as a power series in σ :

$$S = \sum_{k=0}^{\infty} c_k n^{(k-1)}(\mu) \sigma^k$$

where the coefficients c_k have been introduced:

$$c_k = (-1)^{k+1} \frac{1}{k!} \int_{-\infty}^{\infty} x^{k+1} \tilde{\delta}(x) dx .$$

Now it is natural to take $\tilde{\delta}(x)$ as an even function (otherwise the entropy at zero temperature would be different from zero); Methfessel and Paxton propose to choose for $\tilde{\delta}(x)$ the first N terms of the expansion of the Dirac's

delta in Hermite polynomials (in the Gaussian metric). That is

$$\delta(x) = \sum_{n=0}^{\infty} A_n H_{2n}(x) e^{-x^2} \quad (4.41)$$

$$\tilde{\delta}_N(x) = \sum_{n=0}^N A_n H_{2n}(x) e^{-x^2} \quad (4.42)$$

with the additional definitions for the coefficients A_n and the polynomials H_n :

$$A_n = \frac{(-1)^n}{n! 4^n \sqrt{\pi}}$$

$$H_0(x) = 1, \quad H_1(x) = 2x$$

$$H_{n+1}(x) = 2x H_n(x) - 2n H_{n-1}(x).$$

It follows from the way $\tilde{\delta}_N(x)$ is constructed that all the coefficients c_k up to the order $2N + 1$ in the power series for the entropy will be zero. For the present purpose of electronic-structure calculations we are interested in eliminating just the main contribution that comes from the quadratic term in the free energy, i.e. from the linear order in the entropy. For this purpose is sufficient to consider $\tilde{\delta}_1(x)$ as the smearing function to be used for the integrations; the effectiveness of higher order approximations would be wiped away (at least in simple metals) by the necessity of increasing the \mathbf{k} -point sampling necessary to achieve convergence (in the limit of $N \rightarrow \infty$ $\tilde{\delta}_N(x)$ becomes the Dirac's delta and recovers all the problems that the smearing scheme is trying to solve). The discussion that follows does anyhow apply to the higher order corrections as well. Explicitly, the zero-th order and the first order functions are, respectively, the well-known Gaussian broadening

$$\tilde{\delta}_0(x) = \frac{1}{\sqrt{\pi}} e^{-x^2} \quad (4.43)$$

and the first-order Hermite-Gaussian

$$\tilde{\delta}_1(x) = \frac{1}{\sqrt{\pi}} \left(\frac{3}{2} - x^2 \right) e^{-x^2}. \quad (4.44)$$

It can be seen immediately that this $\tilde{\delta}_1(x)$ sets to zero c_1 and c_2 , thus leading to a dependence of the free energy on the temperature that is of quartic order only. The attractive feature of this approach is that all the ionic forces and the other derivatives of the free energy are consistently calculated, and there is no need for some expensive a-posteriori corrections. Although appealing, this formulation introduces two very serious problems:

- the thermal distribution is now no longer monotonic
- the occupation numbers are not positive definite

Both problems originate from the same constraint, namely the need to integrate to zero $c_1 \sim \int x^2 \tilde{\delta}(x) dx$, and both are serious problems if the goal is to perform self-consistent large-scale calculations.

In fact, since the non-monotonic occupation numbers do not define uniquely their inverse element on the energy axis, it becomes impossible to write an explicit form for the generalized entropy for a set of occupation numbers, since the generalized entropy needs to be expressed in terms of the energies, and not in terms of the occupation numbers. When the distribution is monotonic, it is sufficient to invert the values for the occupancies and to use the relative energies in the generalized free energy; but this is no longer the case here. In addition to this, it is now also impossible to determine an explicit expression for the steepest descent directions for the occupations (or to take into account the dependencies in the chemical potential, if a formulation in terms of pseudo-energies is used [40]). All of this implies that

a direct minimization with the occupation numbers treated as dynamical variables becomes increasingly problematic in the limit of large systems.

On the other hand, the occupation numbers can be treated as dependent variables, e.g. taken to be determined by the (diagonal) expectation values of the Hamiltonian. This approach can be successfully applied to small cells; nonetheless, whenever the dimensions of the cell increase, all the implicit nonlinear constraints that are attached to an updating of the wavefunctions, and that can not be taken into consideration explicitly, make the problem ill-conditioned, and the directions of steepest descent are not guaranteed to actually decrease the free energy (for the very good reason that in each direction for a ψ_k all the terms of the form $\sum_i \frac{\delta A}{\delta f_i} \frac{\delta f_i}{\psi_k}$ should also be added).

Finally, the introduction of negative occupation numbers has severe consequences from both the theoretical and the practical point of view, as it will be shown. In particular, the electron charge density is not any more guaranteed to be positive definite, and additionally all the theorems of representability for the density matrices break down. In principle also the chemical potential is not uniquely defined, although this shouldn't be a problem for all ordinary systems with a smooth density of states along the energy axis.

Reformulating the problem In what follows several issues will be addressed:

- it will be shown that it is possible to constrain the occupation numbers to be positive while still satisfying the constraint of killing the linear term c_1 in the entropy (and thus the quadratic term in the free energy).

- some strategies will be presented that could bring in the feature of a strictly variational evolution for the self-consistent minimization, even in the presence of non-monotonic occupation numbers
- an example will be shown that highlights the dangers of employing negative occupation numbers

It hasn't been realized that some algebraic manipulation can actually solve the most serious problem of the Methfessel-Paxton scheme, namely the existence of negative occupation numbers. In brief, the idea is to focus the search on a broadening function e^{-x^2} times a polynomial, and then trying to satisfy the whole set of constraints, which in this case are:

$$\begin{aligned} \int_{-\infty}^{\infty} \tilde{\delta}(x) dx &= 1 && \text{normalization} \\ \int_{-\infty}^{\infty} x \tilde{\delta}(x) dx &= 0 && S(0) = 0 \\ \int_{-\infty}^{\infty} x^2 \tilde{\delta}(x) dx &= 0 && \text{cold smearing} \\ \int_{-\infty}^t \tilde{\delta}(x) dx &\geq 0 && \text{positive occupancies} \end{aligned}$$

Since the Gaussian is an even function, the even terms in the polynomial will take care of the normalization and cold smearing constraints, while the odd terms will be used to impose the constraint of having a physical entropy (that is, going to zero at zero temperature) and finally to take care of the positive occupancies constraint. The simplest form that is needed is a third order polynomial, and some algebra brings all the constraints to be satisfied by the following smearing function, that we call the

Cold Smearing

$$\tilde{\delta} = \frac{1}{\sqrt{\pi}} \left(a x^3 - x^2 - \frac{3}{2} a x + \frac{3}{2} \right) e^{-x^2} \quad (4.45)$$

where the parameter a has still some degree of freedom in its role of constraining the occupancies to be positive definite. The choice that has been made in this work, and the one to be suggested, is

$$a \sim -0.5634.$$

Alternatively, $a = -\sqrt{2/3}$ can be used. The first choice minimizes the inevitable bump on the region where the occupancies are close to 2, while the second choice imposes to the thermal distribution to be strictly monotonical in the region of zero occupancies (see Fig. 4.7 for a detail). The cold smearing broadening defined above is shown in Fig. 4.6, together with the case of a simple Gaussian broadening and a first-order Methfessel-Paxton.

The efficiency of the cold smearing in eliminating the quadratic coupling between the energy and the temperature is shown in Fig. 4.8, for a model that is often used in this connection. A rigid band-structure (from the Empirical Pseudopotential scheme [65]) filled with an arbitrary number of electrons (12 for this case of α -tin) is integrated using a very fine Brillouin Zone mesh (32 32 32) and the results are plotted as a function of the smearing. It is clearly seen that there is a negligible difference with the case of the entropy-correction approach, both schemes killing at least one order in the coupling with the temperature.

A relevant issue that should be addressed when these non-monotonic, exotic thermal distributions are introduced is the implementation of a proper minimization strategy. As has been pointed out before, the problem is subtle, since an updating of the occupancies needs a direction to be established, unless the occupancies are considered as dependent variables. For these reasons, the method of ensemble-DFT seems the most promising framework for

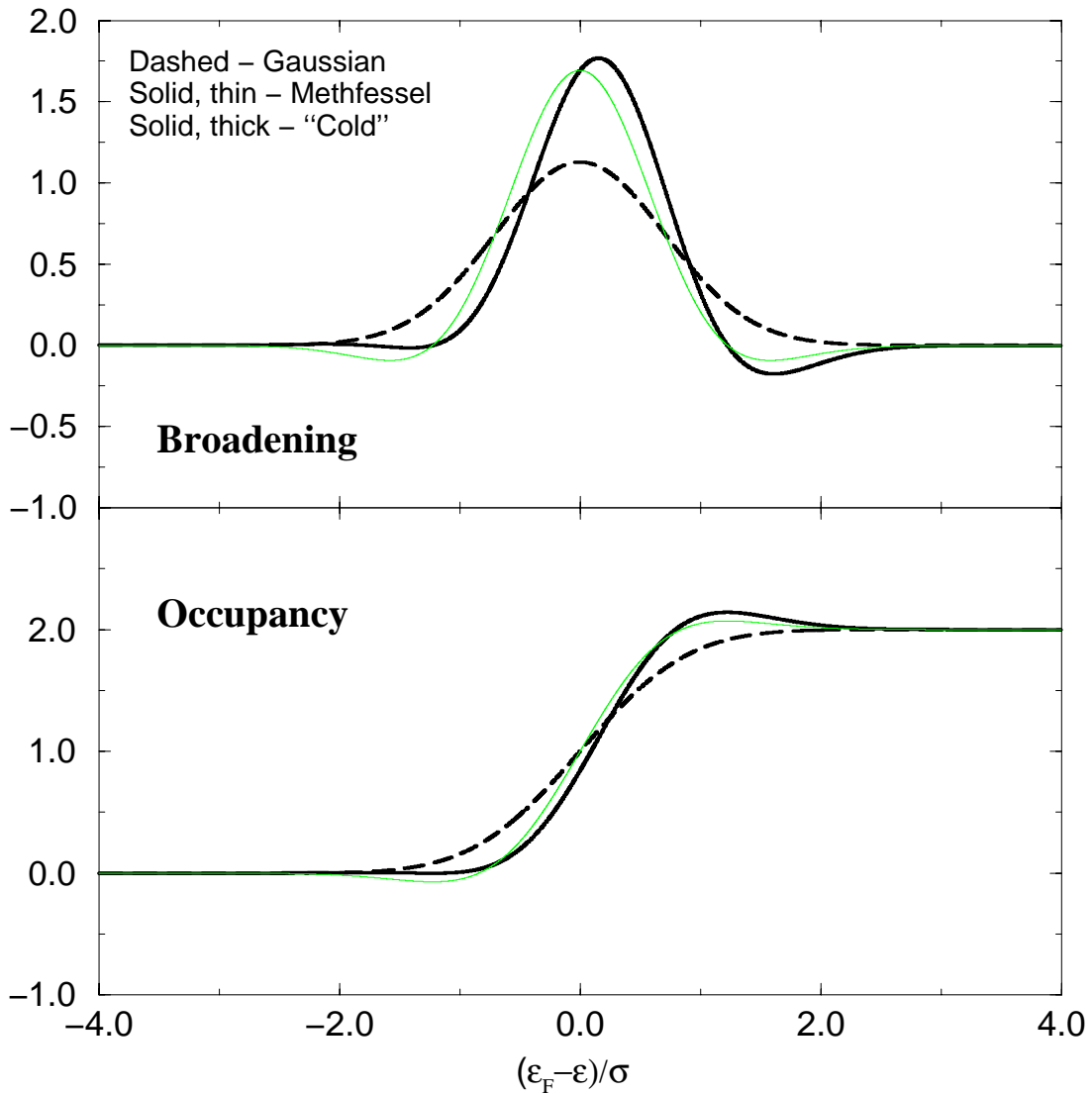


Figure 4.6: Broadening function and integrated thermal occupancy for the case of the Gaussian smearing, the first-order Methfessel-Paxton and for the cold smearing introduced here. The occupancies in the latter case are always greater than zero.

developing (if at all possible) a strictly variational formulation. The search direction that is chosen in the inner loop does not pose any requirements

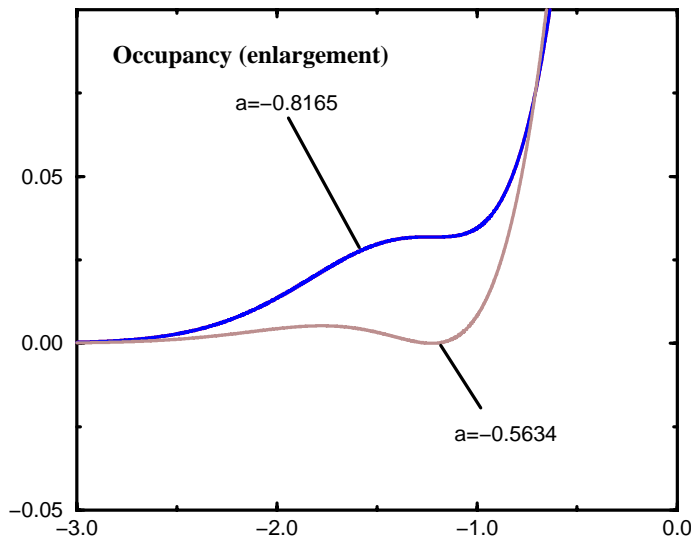


Figure 4.7: Detail of the thermal distributions in correspondence of the two values proposed for a in the broadening function.

on the occupation distribution; actually, the driving force for the motion is given by the eigenvalues of the Hamiltonian and by the rotation that brings the occupancy matrix to commute more with the Hamiltonian. The problem arises when the free energy and not just the search direction needs to be calculated, since it is not possible to derive from an occupation matrix (even in the diagonal form) the corresponding value for the generalized entropy. More accurately, there is actually a single very relevant occurrence in which this is possible: in the inner loop for the ensemble-DFT, at $\beta=1$ a set of eigenvalues is given, and the occupancies are determined from those eigenvalues; thus, at $\beta=1$, it is always perfectly feasible to calculate the entropy, the free energy, and the derivatives along the search directions. The problem

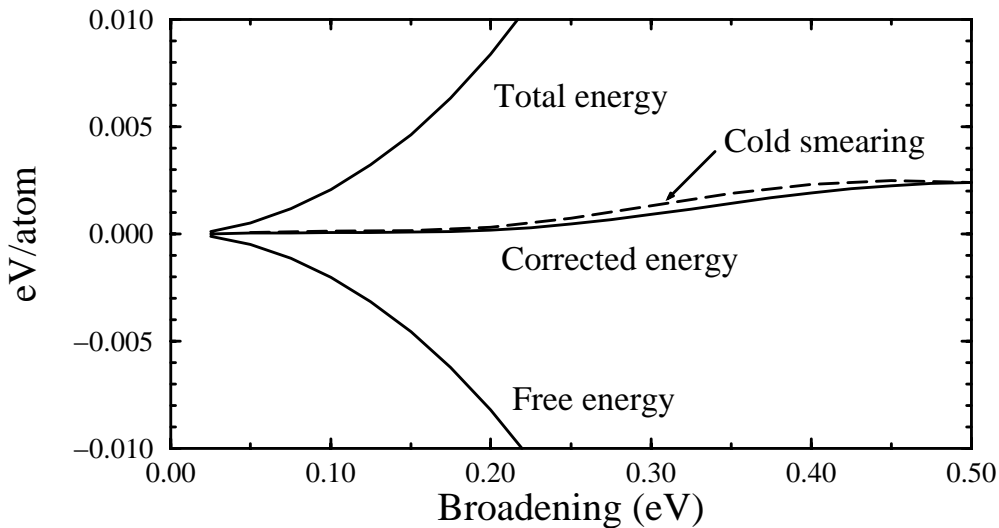


Figure 4.8: Comparison between the cold smearing and the corrected energy, in the model case of α -tin with 12 electrons, as discussed in the text.

occurs whenever one is away from the occupation representation in terms of eigenvalues, that happens only at $\beta=1$.

This is a point that needs further investigation; for the time being, the technique of cold smearing has been implemented with a constant step dynamics in the inner loop. Since the inner loop is always able to choose the optimal directions, the only problem is calculating the proper step along the search line. This does not seem a simple task, since it would require the

knowledge for a generic set of occupancies of the entropy, and so we resort to taking a fixed step at every iteration. The step is conservatively small, and every now and then (whenever the total energy at $\beta=1$ is lower than the value it has at the current position) a full step to $\beta=1$ is taken. This approach is practically very satisfactory in molecular dynamics runs. If a self-consistent minimization needs to be performed from scratch, the efficiency is somewhat reduced.

Other possibilities are being investigated: the entropy could be redefined to be a function of the density, and not of the occupation matrix. The prescription to calculate the entropy for a given set of f_{ij} would be now to calculate the charge density with those f_{ij} , and then from the charge density the relative Hamiltonian and its set of eigenvalues, that would be used to calculate the generalized entropy. Alternatively, the second derivative along the search line could be calculated exactly in the inner loop for $\beta = 1$, and that would provide the fitting of a parabola along the search. Finally, an approximate scheme could be introduced, that would predict a step based on some isomorphism with a monotonic distribution.

In any case, the present implementation with a fixed step in the inner loop seems very stable. In addition, since all the quantities of interest can be calculated exactly at $\beta = 1$, a firm control of the convergence is available. It is thus very interesting to compare the results (see Fig. 4.9) of some test calculations that have been performed on the 15-layer 1x1 Al(110) slab, for the case of the Gaussian smearing, the cold smearing and the Methfessel-Paxton first-order broadening. All these three calculations have been performed with the same fixed step strategy (although that was not necessary in the case of

the Gaussian). The convergence of the force on the top layer (greatly expanding the system, because of the very large broadening chosen) and of the opposite of the force on the bottom layer has been monitored. The convergence, although not as fast as in the case of the proper Gaussian smearing with the optimal step, is very good. The striking result is the convergence of the Methfessel-Paxton calculation to an unphysical solution in which the forces in the unit cell are not symmetric, as they should be. In addition, the calculation appears to be fully converged, and the derivatives along the search directions for the Hamiltonian, or those at $\beta = 1$ in the inner loop, have all safely converged to zero almost to machine precision. The case needs further investigation, but it suggests strongly that the utmost care should be taken before using schemes that allow for the case of negative occupations.

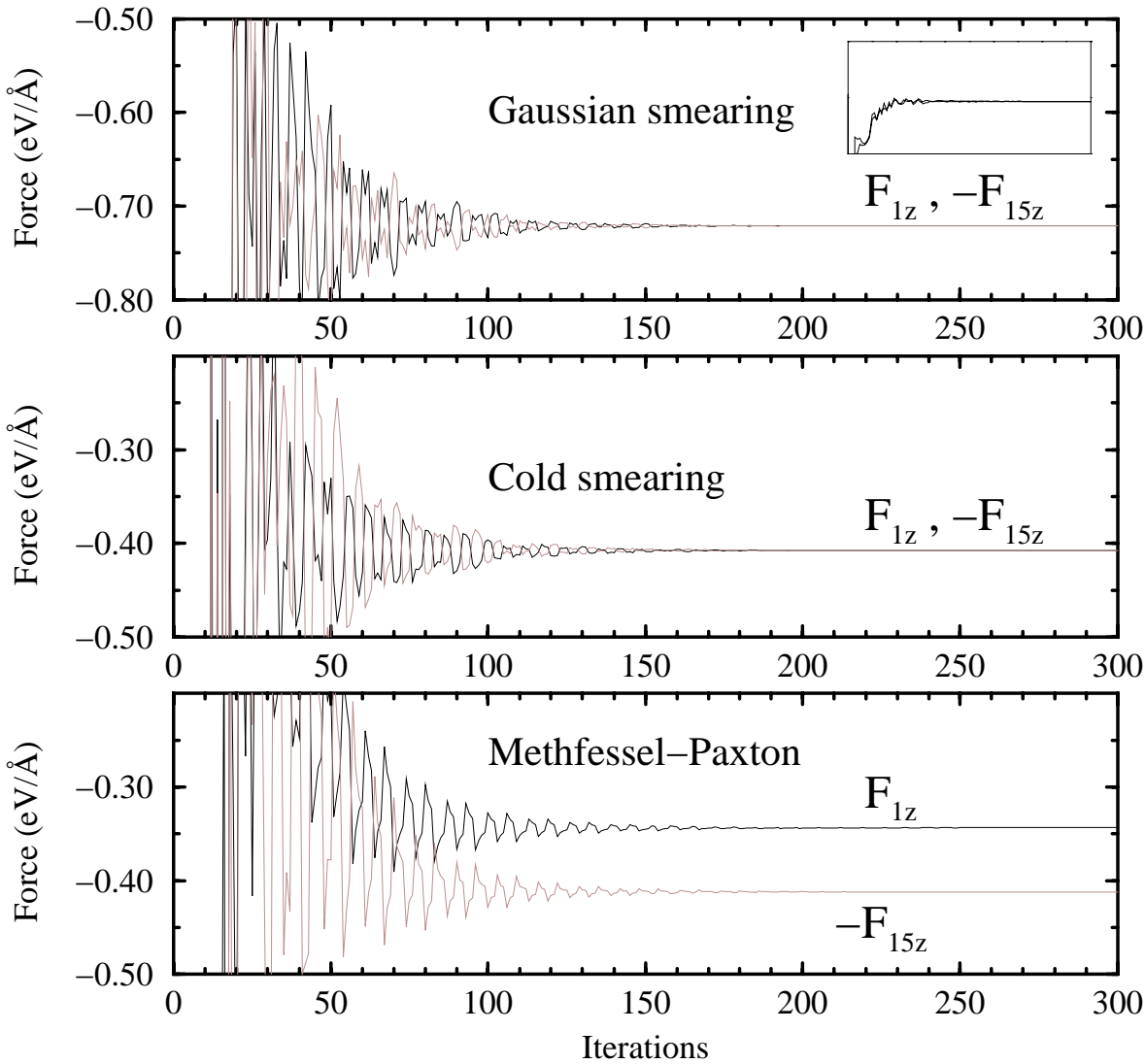


Figure 4.9: Convergence of the z -component of the force in the top layer, and of the opposite of the force in the bottom layer, for the 15-atom slab, with these three choices for the smearing function. The inset shows the first 100 iterations for the Gaussian case, with a vertical scale 20 eV/Å wide.

Chapter 5

Ensemble-DFT molecular dynamics

Introduction

The method of Ensemble Density Functional Theory, in conjunction with the technique of cold smearing, is applied here to the study of the finite-temperature properties of the low-index Al(110) and Al(111) surfaces. Fully quantum-mechanical first-principles simulations are applied for the first time to the study of the surface of a metal; these simulations have become affordable as a consequence of the methodological advances discussed in this work. The canonical-ensemble molecular dynamics averages reproduce to a good accuracy the experimental data, when these are available; in addition, novel predictions are made on the microscopic processes that characterize the onset of the disordering and the melting transition. In this respect, the most useful scope for first-principles molecular dynamics shifts from being a strategy to perform configurational averages to becoming a tool to sample the

most relevant features of the complex configuration space around the onset of concerted phenomena, as is the case for disordering or diffusion events. Once the more likely dynamical events have been identified, accurate free-energy estimates could be obtained with procedures of thermodynamic integration.

5.1 Molecular dynamics simulations

The connection between the Schrödinger equation for the electrons in the field of fixed ions that has been considered up to now, and a dynamical picture in which the ions themselves are allowed to move, is made with the help of the Born-Oppenheimer separation [130]. The intuitive picture is that, since the typical ionic frequencies are much smaller than the electronic ones, the problem can be simplified by decoupling these two degrees of freedom, considering the ions as moving in a potential energy surface that is determined at every instant by the electronic ground state. This idea can be formally justified taking the limit for the ratio of the electronic and ionic masses going to zero in the full Schrödinger equation for the electronic and ionic coordinates, and keeping the lower order terms. This results in a coupled Schrödinger equation for the electronic wavefunction in the parametric field of the ionic coordinates, and in a Schrödinger equation for the ionic coordinates in the potential energy surface determined, for every ionic configuration, from the Born-Oppenheimer electronic ground state (see Chap. 12, Ref. [13]). The Schrödinger equation for the ionic wavefunction will be taken in its classical limit, i.e. the second law of dynamics, leading to an additional simplification that is an excellent approximation for all but the lightest nuclei at low temperatures.

It should be mentioned that the Born-Oppenheimer picture ceases to be verified in a metal [131], since the available electronic excitations overlap in energy with the ionic frequencies. Nevertheless it can be shown that, for most practical purposes, the relevant vertex corrections are negligible (*Migdal's theorem* [132]), and a pseudo-Born-Oppenheimer separation can be assumed. The rationale behind Migdal's theorem is that the phonons do influence only the states around the Fermi energy, while the whole of the electron gas, of which the states around the Fermi energy are a tiny fraction, does influence the phonon dispersions. So, a Born-Oppenheimer separation is justified to first approximation in terms of the limited phase-space available for electron-phonon processes. The validity of this approximation breaks down when a significant portion of the phase space becomes available for the transitions, e.g. in the case of Fermi surface nesting. It should be added that for the case of aluminium, the typical plasmon frequencies are in a region that goes from 10 eV (surface) to 15 eV (bulk).

5.1.1 Technical details

All the calculations presented here have been based on the LDA approximation for the exchange-correlation. The pseudopotential used, extensively tested, is an optimized projector-reduced s-non-local pseudopotential, generated according to [69] [70] [71] (M.-H. Lee, al013b; the structural parameters are in Fig. 4.3); convergence with respect to a basis of plane waves is reached at a cutoff of 80 eV.

The unit cell used for the simulations of the (110) surface in periodic boundary conditions contains a 3x3 (110) slab, with 8 layers of atoms sepa-

expt., th.	d ₁₂	d ₂₃	d ₃₄	d ₄₅	d ₅₆	d ₆₇	d ₇₈
100 K, LEED [133]	-8.6 %	+5.0 %	-1.6 %				
297 K, LEED [134]	-8.5 %	+5.5 %	+2.2 %	+1.6			
70 K, LEED [135]	-6.9 %	+4.1 %	-3.7 %				
316 K, LEED [135]	-7.6 %	+5.0 %	-3.2 %				
15 layers, 288 k	-10.9 %	+5.6 %	-4.0 %	+3.0 %	-0.5 %	+ 0.8 %	-0.7%
8 layers, 288 k	-9.6 %	+6.6 %	-2.9 %	+7.5 %			
8 layers, 9 k	-9.2 %	+6.8 %	-4.2 %	+3.2 %			

Figure 5.1: Multilayer relaxations for the Al(110) surface, at 0.5 eV of cold smearing. The slab is 1x1 in the plane parallel to the surface.

rated by 5 layers of vacuum, containing thus 72 atoms and with approximate dimensions of 12 Å x 9 Å x 19 Å. The bulk system studied is realized with the same geometry but without the vacuum layers. The sampling of the Brillouin Zone is performed with the $(\frac{1}{4}, \frac{1}{4}, \frac{1}{4})$ Baldereschi point [99], at 0.5 eV of cold smearing. The \mathbf{k} -point convergence has been tested on the 1x1 surface, and the results are presented in Fig. 5.1, where the zero-temperature multilayer relaxations have been determined, either at full convergence (using a (12,12,2) Monkhorst-Pack mesh) or using the Baldereschi point for the 3x3 cell, folded out to the 9 \mathbf{k} -points in the 1x1 cell. The results for a longer cell are also shown, together with the available experimental data. It should be stressed that this choice for the sampling is far superior to the choice of the Γ point; additionally, the system studied is a periodic cell, and not a disordered liquid.

The lattice parameter in the xy -plane at a given temperature has been determined using the experimental bulk thermal expansion, renormalized in

the form of an expansion coefficient, that was applied to the LDA zero-temperature lattice parameter.

The molecular dynamics simulations are performed integrating the ionic equations of motions with a leap-frog Verlet algorithm coupled to a Gaussian constraint thermostat (see Sec. 7.4.3 of Ref. [136]), that gives a proper canonical distribution for the positions (and an almost canonical one for the momenta, ref. cit.). Due to the efficiency in the convergence of the electronic problem, very large, *classical timesteps* can be afforded. The choice here is of 4 fs at each step. After every position updating, the system is converged back to a tolerance of 5 meV/cell; the tolerance is defined as the dispersion width of the last 5 total energies (the algorithm is variational on the free energy and not on the total energy, obviously).

The average number of iterations to converge back to tolerance depends on the temperature (at the given timestep), and goes from roughly 10 iterations at 300 K to 15 iterations at 600 K. This tolerance produces in a microcanonical simulation a conservation of the constant of motion that is perfectly satisfactory (.1 eV/cell/ps), given also the infinite heat bath that is available in the canonical coupling. More relevant is the fact that the fluctuations of the constant of motion are comparable and smaller than the temporal oscillations in the temperature that are seen in the microcanonical evolution of a previously equilibrated system (for a 300 K slab, the oscillations are ∓ 30 K, as expected).

A linear extrapolation of the wavefunctions has been performed from one timestep to the other; this procedure should have still room for improvements, especially as a consequence of the subspace coherence that is conserved in

ensemble-DFT. Preliminary tests show that quadratic extrapolations initially improve significantly the conservation of the constant of motion, but they tend to deteriorate faster, if a constant number of iterations per timestep is chosen in order to make a meaningful comparison.

With these parameters, the average performance is 0.8 ps of simulation per CPUday on a vector supercomputer, or 0.12 ps per CPUday on a DEC Alpha; these numbers roughly double in the case of the bulk system, because less iterations are needed to converge to tolerance and the system is smaller (the calculations are still FFT-bound—70% of the CPU time—given also that orthogonalizations, or non-local elements for the pseudopotential, are not needed in the inner loop). In addition, the tolerance chosen can be easily relaxed in the case of the bulk, where the Hellmann-Feynman forces converge much faster.

A tolerance-based convergence criterion seemed more appropriate than a fixed-iterations strategy, for the very reason that efficiency in the former case is always optimized, and the freedom to adapt to instantaneous configurations difficult to converge is preserved. In Fig. 5.2 the 15-layer slab of Al is examined again under these two conditions (2 fs timestep, microcanonical evolution with an ionic temperature up to 1500 K; the 1x1 cell obviously can not melt). It can be observed that in the worst scenario possible (a fixed number of iterations at each timestep, and a cold smearing with fixed steps in the inner loop) there are some discontinuities due to single timesteps that have been very poorly converged. It should be added that the average number of iterations for the fixed-tolerance case is lower than the choice made for the fixed-iterations strategy, and that explains the differences in the con-

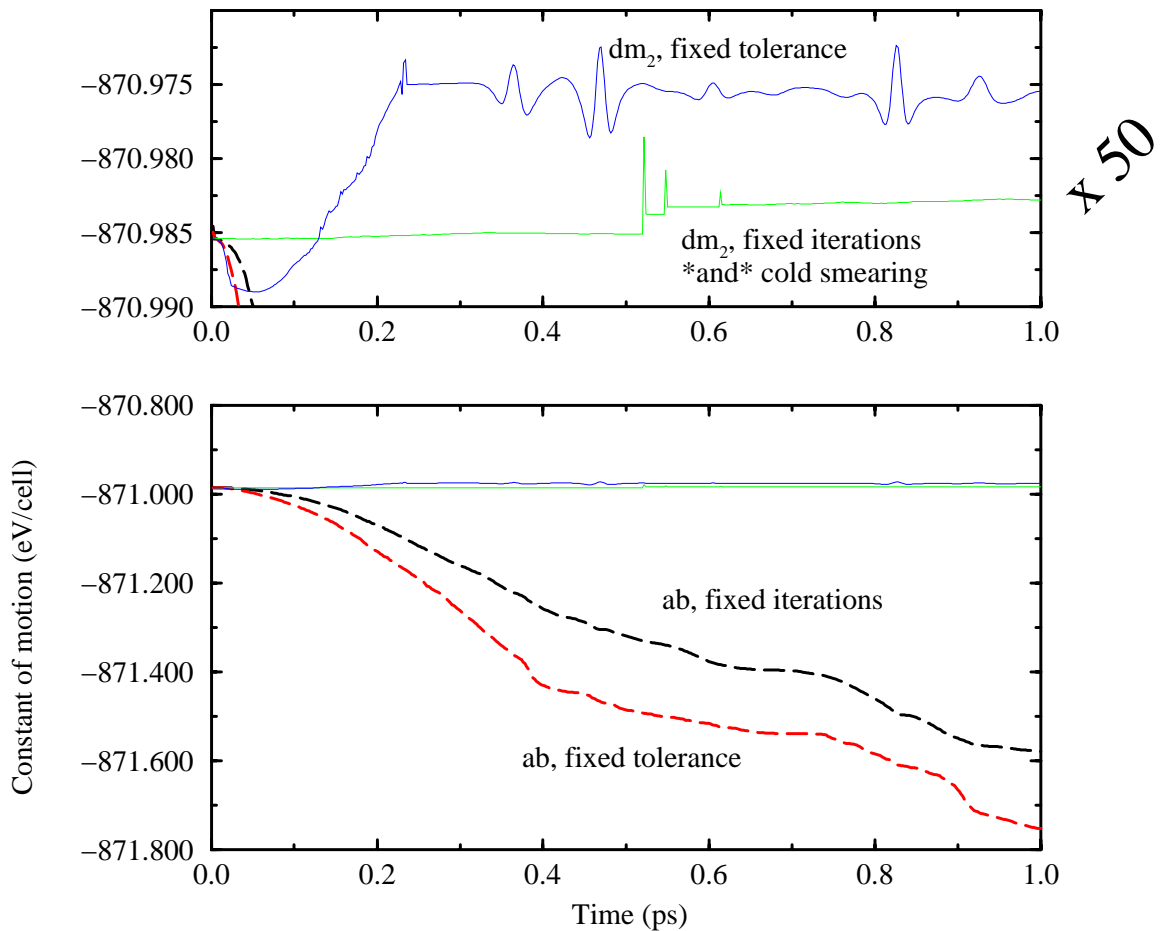


Figure 5.2: Constant of motion for the 15-layer Al(110) supercell, using the standard method (dashed lines) or ensemble-DFT, either with a set tolerance at every timestep or with a fixed number of iterations. Gaussian smearing is used, except for ensemble-DFT at fixed iterations, where the cold smearing and the inner loop fixed step is used; this constant of motion has been rigidly translated for comparison. The number of iterations in the fixed-number strategy is larger than the average for the fixed-tolerance strategy. The drift for ensemble-DFT is roughly three orders of magnitude smaller.

servation of the constant of motion. This example shows again the striking difference in performance between the two approaches, particularly in the case in which the same fixed number of iterations for ensemble-DFT and for the standard method is used (additionally, ensemble-DFT is used here with the cold smearing, that doesn't allow optimal steps in the inner loop).

5.2 Metal surfaces at finite temperature

The thermodynamic stability of metal surfaces presents a very rich phenomenology [137] [138]: whereas the exotic reconstructions of semiconductors surfaces, driven by the strong covalent dangling bonds, are missing, the interplay of subtle energetic and entropic effects leads to a variety of different behaviours in dependence of the temperature. At lower temperatures surfaces can be either *relaxed* with respect to the ideal bulk geometry, or *reconstructed* in some simple way (e.g. in the *missing row* transition). The zero-temperature relaxation can often be understood in terms of simple models [139] based on charge-density considerations, as in the case of the *contraction* for the inter-layer distance of the surface atoms found in the less packed, open surfaces, and that can be understood as a mechanism to increase the density surrounding the surface atoms, that “dive” towards the bulk.

Higher temperatures enhance the unbalance between the different anharmonic contributions, and lead to a pattern of relaxations or derelaxations for the inter-layer spacings [140] [141] [142] [143] [144]. In addition, entropic effects can lead to a *deconstruction* of the eventual reconstructed phase. At increasing temperature the more open surfaces can start to develop defects

(e.g. the formation of adatoms and vacancies), while to more closed-packed surfaces, with a more costly defect formation energy, can keep the ordered coherence up to the melting point. This different behaviour with temperature can be expected to influence strongly the free energy barriers and the mechanisms of diffusion for the adatoms present on the surface. In addition, some peculiar phase transitions of the surface do happen, whenever the free energy for the formation of overlayer structures vanishes. Notably, a *roughening* transition [145] can take place, characterized by a diverging height-height correlation along the surface, that takes the form of a terraced landscape. This could be preceded by a *pre-roughening* transition [146] [147] in which the disordering is confined to the surface overlayer and the long range stability is preserved, in what is a *disordered flat* phase.

Before reaching the melting temperature of the bulk system, it is possible that a self-wetting initiates on the surface already at a lower temperature, as a consequence of the half-balanced periodic potential that the surface ions experience, and of the increased anharmonicity around the equilibrium positions [148]. The phenomenology of the surface melting and premelting is quite complex [138]: different surfaces, or different orientations of the same system, can exhibit a complete melting, where the thickness increases while the bulk transition temperature is approached, or just a limited, blocked melting of the upper layers. The characterization of these process is a current area of research, with focused experimental [149] [150] and theoretical research [151] [141] [142].

5.3 Computational LEED

The results of the simulations performed on the aluminium surfaces will be presented here, with the goal of showing the efficiency, precision, and microscopic understanding that characterize this first-principle approach. Several experimental studies of the finite temperature properties have appeared recently [152] [153] [154] [155] [156]; the theoretical works are based on semi-empirical methods [151] [157] or limited to zero-temperature total energy calculations [158] (in themselves a fundamental source of understanding).

5.3.1 Bulk Al

As a first application, and as a test of all the methodology and of the molecular dynamics algorithm, two simulations have been performed for the bulk system at 300 K and 600 K. The cell is in the same geometry of the subsequent slab calculations, i.e. it is a 3x3 (110) cell 8-layer thick. Sampling is performed with the Baldereschi point, 0.5 eV of cold smearing. The results are shown in Fig. 5.3, where the bulk mean square displacements (their z -component, precisely, that is what we compare the slab case with) are plotted, averaging over a window 1 ps wide along the $\sim 2.5 - 3$ ps runs. The results are in excellent agreement with the theoretical and experimental data [159], giving us confidence on the validity of all the implementation.

5.3.2 Al(110): thermal relaxations

The understanding of the anharmonicities at the surface is of fundamental interest to elucidate the microscopic mechanisms related to the relaxation,

roughening and premelting. Additionally, it is a case that escapes accurate characterization with pseudo-empirical methods. In Fig. 5.4 the results for the temperature dependence of the interlayer relaxations are shown, highlighting both a very strong surface anharmonicity at temperatures higher than 300 K, and, contrary to expectations [140], an enhancement of the top layer contraction with increasing temperature [135].

5.3.3 Al(110): layer-resolved displacements

The analysis of the mean square displacements is repeated here for the case of the slab and shown in Fig. 5.5; the data are now resolved layer by layer. The mean square displacements for the inner layers (the two central ones) are now slightly higher than the data for the bulk, as a result of the finite thickness of the cell. The most striking and unexpected result is the large increase of the displacements for the *second layer*, while the results for the surface are not much higher than the bulk.

The results for the mean square displacements along the z axis (perpendicular to the surface) are summarized in Fig. 5.6, as a function of the temperature. It is clearly apparent that a very large increase for the 2^{nd} layer is taking place. This result can be rationalized thinking at the vacuum as a hard wall, that inhibits the spilling of the oscillations for the atoms in the first layer, that are thus somewhat confined in their motion perpendicular to the surface. On the contrary, the atoms in the second layer are almost as loosely bound as the atoms in the first layer by the breakdown of the potential periodicity, but they do not need to change much their coordination and the surrounding charge density in the motion perpendicular to the surface,

and, due to the very open structure of the (110) surface, have some channels of oscillation in the middle of the 1x1 surface cell.

The increasing contraction of the distance between the first and the second layer can now be also understood in terms of this enhanced displacement of the 2nd layer toward the vacuum; a similar feature with the second layer compressing itself toward the first will be apparent when the liquid is observed. The large enhancement of the displacements for the second layer has never been observed in an experiment on a surface, including the one of Ref. [135] on Al(110). It should be noted that the mean square displacements are not direct observables in a experiment, but are reverse-engineered from the LEED data. Some marginal increase in the second-layer displacements was noticed in the molecular-dynamics simulations of Ref. [142].

The results are all converged (some exception made for the case of 500 K) with respect to the statistical averages. These are shown in Fig. 5.7 at the different temperatures, as a function of a time parameter t . The value plotted at a time t represents the average done from t to the end of the run for the square of the displacement around an average position consistently calculated as the average from the time t to the end of the run. Ideally, the curves would have some initial oscillations (decreasing in amplitude for longer runs) while the system thermalizes, then would become flat, and then, with more and more statistical errors, would converge to zero.

A stringent test has been performed by increasing the Brillouin Zone sampling (and doubling the convergence tolerance, just in case). The results are shown in Fig. 5.8, for the temperature of 500 K, and for the displacements in the first and the second layer. Averages are again shown as described

before, and represent at a time t the average from there to the end of the run, after having discarding the initial configurations of the run going from 0 to t . Three sets of results are shown: with the original Baldereschi sampling of $(\frac{1}{4}, \frac{1}{4}, \frac{1}{4})$, with $(\frac{1}{4}, \frac{1}{4}, 0)$, and with an accurate sampling coming from a submesh of the (4,4,4) Monkhorst-Pack mesh for the 3x3 orthorombic cell. These latter points are $(\frac{1}{8}, \frac{1}{8}, \frac{1}{4})$, $(-\frac{3}{8}, -\frac{3}{8}, \frac{1}{4})$, $(-\frac{1}{8}, \frac{3}{8}, -\frac{1}{4})$, and $(\frac{3}{8}, -\frac{1}{8}, -\frac{1}{4})$, that have shown very accurate convergence for cells smaller than this [127]. Although the simulation with 4 \mathbf{k} -points is not complete, it shows a clear trend in the direction discussed.

At a temperature of 600 K, the system starts to disorder, and, given the finite size of the slab, each disordering event breaks seriously the coherence of the potential, inducing more disordering. The result is that at this temperature the slab melts, although a thicker slab would have conserved the regular ionic arrangement in the inner layers.

5.3.4 Al(111)

The behaviour of the Al(110) surface can be contrasted with that of the more packed Al(111) surface. In this case the slab considered is in a orthorombic cell, with 3x4 atoms in the surface and 6-layer thick, thus still composed of 72 atoms. The surface area is now smaller, and the sampling with only one special point is at the limit of accuracy. There are no 2 special points that show better performance than the single Baldereschi point, and so we resort to a simulation with 4 \mathbf{k} -points, the same as those used in the Al(110) test. The results for the first 1 ps run are shown in Fig. 5.9; those that were obtained previously with only one special point are very similar to

these. It can be immediately noticed that there is no tendency to disorder, as it is expected (the surface does not melt experimentally); in addition, the behaviour of the second layer is as usually predicted, and the displacements are smaller than in the first layer.

5.4 Sampling the phase space

The systems studied in the previous Section have been analyzed in their thermodynamical properties; first-principles molecular dynamics can also be used for an equally challenging, and interesting, problem. In complex processes, it is impossible to determine from few total-energy calculations the amount of configuration space that would be available at a certain temperature for the system. Molecular dynamics becomes thus a very valuable technique to sample the most relevant features in the phase space. Few examples will be given in the following; the rationale is that, once a working idea of the system studied is obtained, more accurate calculations can be done to test some hypothesis, and free-energy differences can be evaluated via thermodynamical integration, whose accuracy relies on choosing the most appropriate paths.

5.4.1 Preroughening, diffusion and liquid layering

For temperatures close to 600 K it was noted that the slab considered for the (110) calculations was starting to disorder, with the side effect that all the system was melting. To avoid this the same system is studied, where now the bottom 3 layers are coupled to a thermostat at 300 K while the upper 5 layers are coupled to a thermostat at 600 K. In this way, the system keeps

indefinitely the coherence for the lattice underlying the disordering surface. The temperature is now less well defined on the surface, since the system at 600 K has only 45 atoms, and in addition there is a gradient of temperature imposed from the confining 300 K system. For this reason, and in general for the considerations related to the finite size of the slab, the temperature chosen for a simulation should be considered as an approximation to the corresponding real temperature (although the structure of the phase space is correctly identified).

When a simulation is performed under these conditions, the formation of vacancies occurs spontaneously, signaling that the free energy of formation of the adatom/vacancy pair is close to zero. One of these events is shown in Fig. 5.10, occurring in the first picosecond of the simulation. The diffusing surface atom moves from its initial position to the center of the rectangle that is the (110) surface cell, and then moves on top of the long bridge barrier, where it remains for several ionic frequencies, oscillating in coordination with the other atoms, but with no signs of being attracted back to its empty site, or to exchange with a surface atom. A similar behaviour takes place for the subsequent adatom/vacancy formation events. Additionally, the atoms in the second layer have excursions that reach the top of the first layer, although the coordination of these events suggests that it is not a tunneling of the atom in the second layer across the surface, but a local deformation that quickly brings the atom back to its level.

It is interesting to compare these results with a long run done with two isolated adatoms on the top and the bottom of the (110) surface, in a smaller slab 6-layer thick. The trajectories are shown in Fig. 5.11; the adatoms do

not attempt any diffusion process, neither exchange nor over-barrier jump. When the temperature is raised from the 450 K of the first 4 ps of simulation to 500 K, a diffusion event takes suddenly place in the bulk, in the third layer while an atom in the second layer is performing an excursion towards the surface. From then on, the system starts to disorder and will eventually melt.

These two observations are consistent with a picture in which, at around 600 K, there is a proliferation of adatoms and vacancies, due to the low or null free energy of formation, while at the same time the adatoms do not diffuse away, probably because the free energy barrier for the diffusion is still high¹. Such a picture would be consistent with the existence of a disordered flat phase, originated by the vacancy/adatom pair formation, and stabilized by the comparatively high diffusion barriers. In order to proceed further, it is necessary to calculate directly via thermodynamic integration the free energy barriers for the processes involved, and it should be stressed how the finite-temperature picture can be significantly different from what can be understood in terms of potential energy surfaces [160].

Finally, the simulation of the original slab at 600 K is shown in Fig. 5.12. In addition to the already mentioned disordering and melting process, it is very interesting to notice that the contraction between the first and second layer, that was observed at lower temperatures, has taken distinctly the form of a density build-up at the interface between the vacuum and the inner liquid aluminium, where the atoms that were belonging to the second layer are

¹Especially if the exchange mechanism, that has a zero-temperature barrier of 0.33 eV [158], half of the over-barrier jump on the long bridge (0.60 eV, [158]), is unfavoured by entropic effects, due to fewer configurations in phase space available for the process.

now essentially confined in a common layer with the surface atoms. This phenomena point at the recently discovered layering oscillations at an interface between a liquid metal and the vapour; the present formulation would allow for a determination of the structure of this layer, as well as the structure of the disordered/liquid layer wetting the solid at lower temperature, in order to understand if the behaviour is of a liquid-like coordination, or it is more a solid-like system with a greatly enhanced diffusion via concerted exchanges.

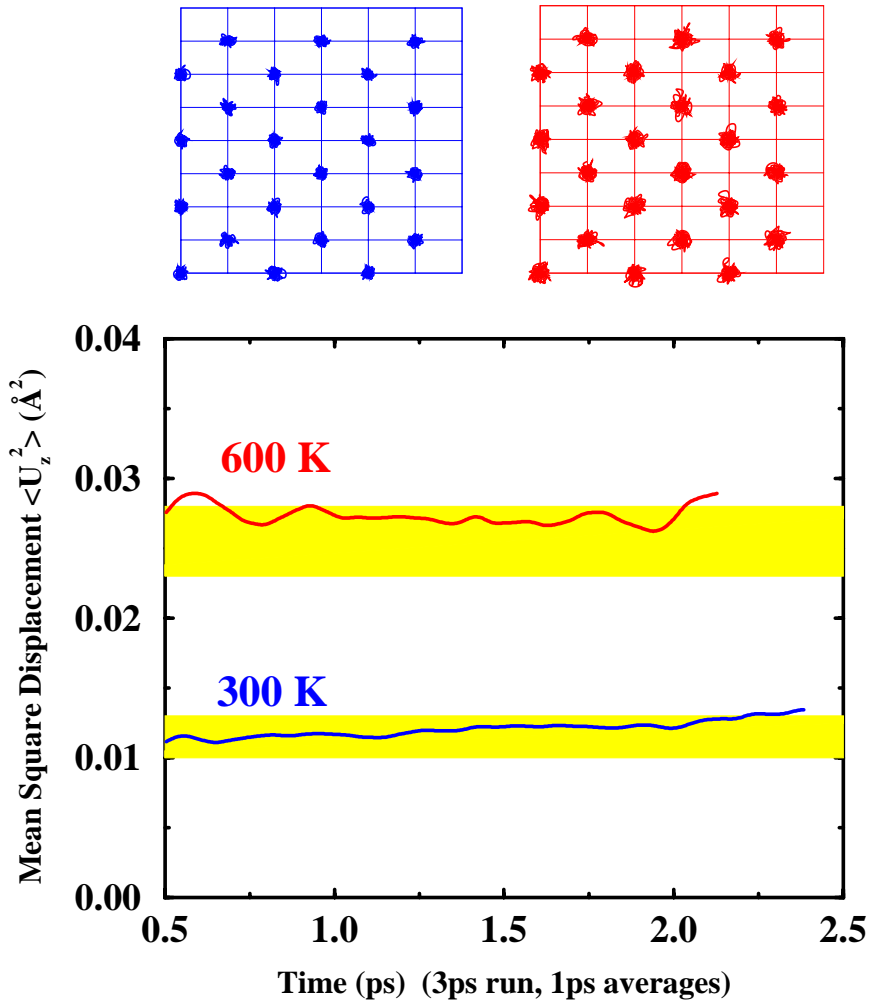


Figure 5.3: Mean square displacements along the z axis for bulk Al at 300 K and 600 K. Experimental data [159] are represented by the two grey bands; the theoretical data have been obtained averaging the run with a window 1 ps wide. Top left and right are the projections on the xz plane of the orbits in the 8 layers, at 300 K and 600 K respectively. Each orbit is the superposition of 3 atoms along the y axis.

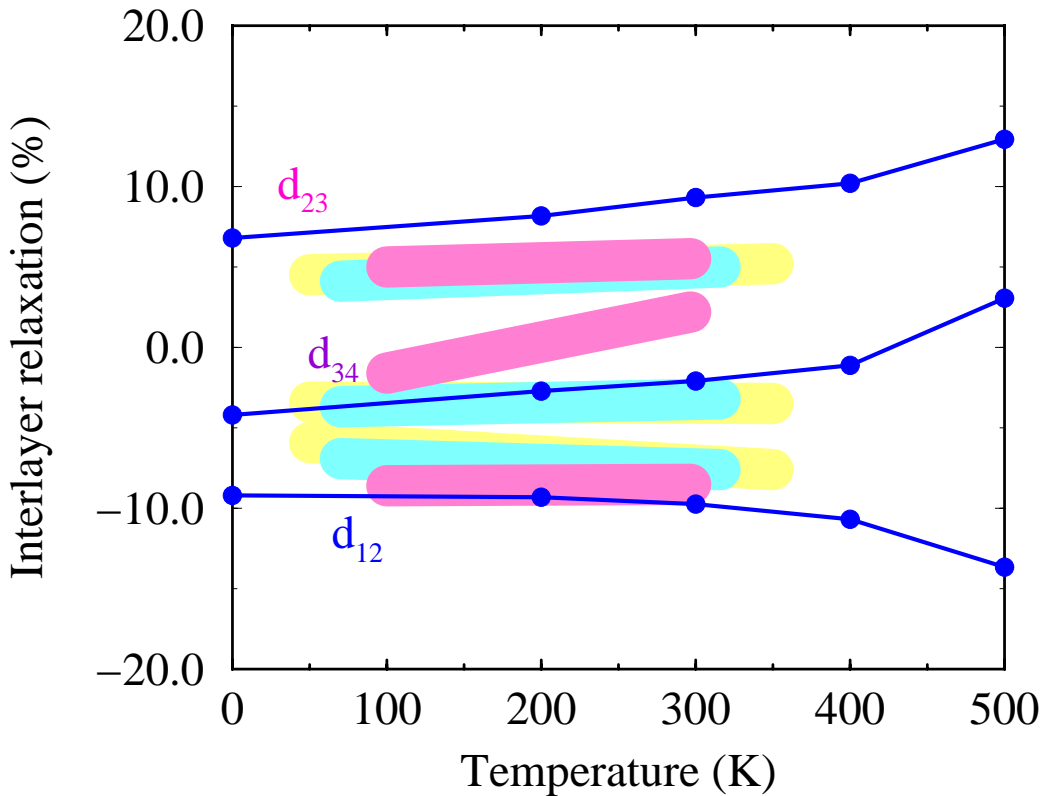


Figure 5.4: Multilayer relaxations in Al(110) as a function of the temperature. The percentile relaxations are calculated with respect to the lattice parameter appropriate to each temperature. Each run is ~ 3 ps long. Experimental data (3 different shades of grey for each interlayer relaxation) are from Ref. [135] and references therein.

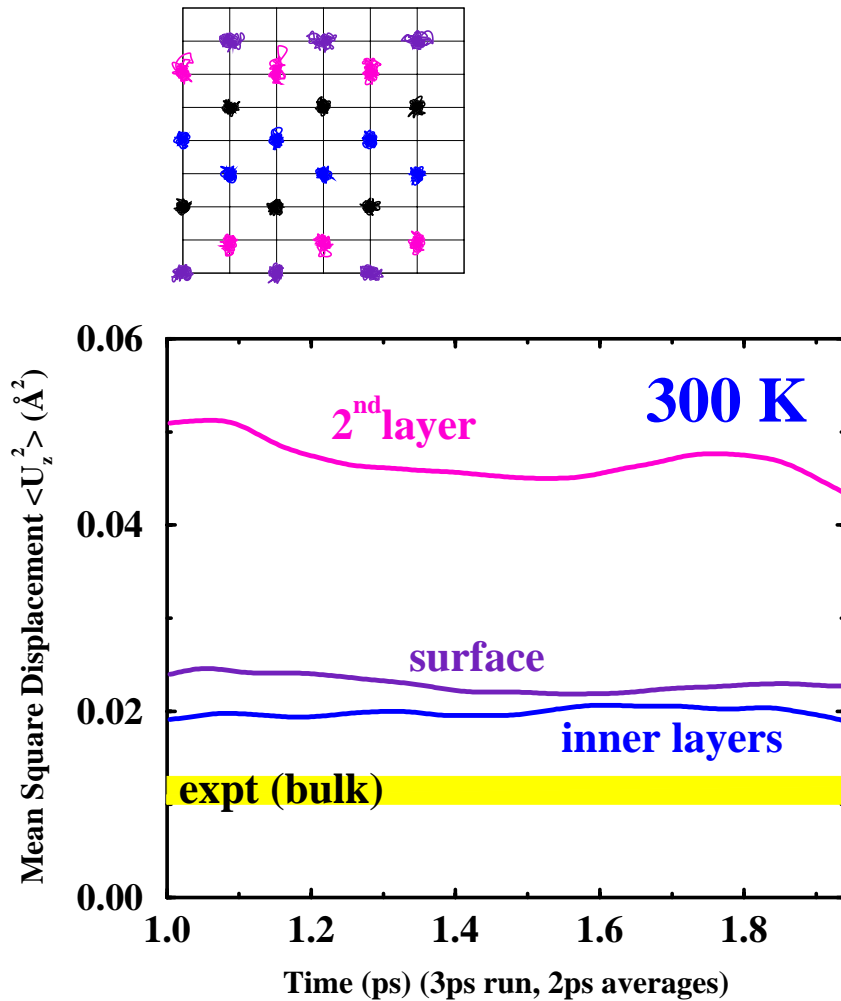


Figure 5.5: Mean square displacements along the z axis for an Al(110) slab at 300 K. Experimental data for the bulk are shown as a grey band [159]; the theoretical data have been obtained averaging the run with a window 2 ps wide. Top left are the projections on the xz plane of the orbits in the 8 layers of the slab.

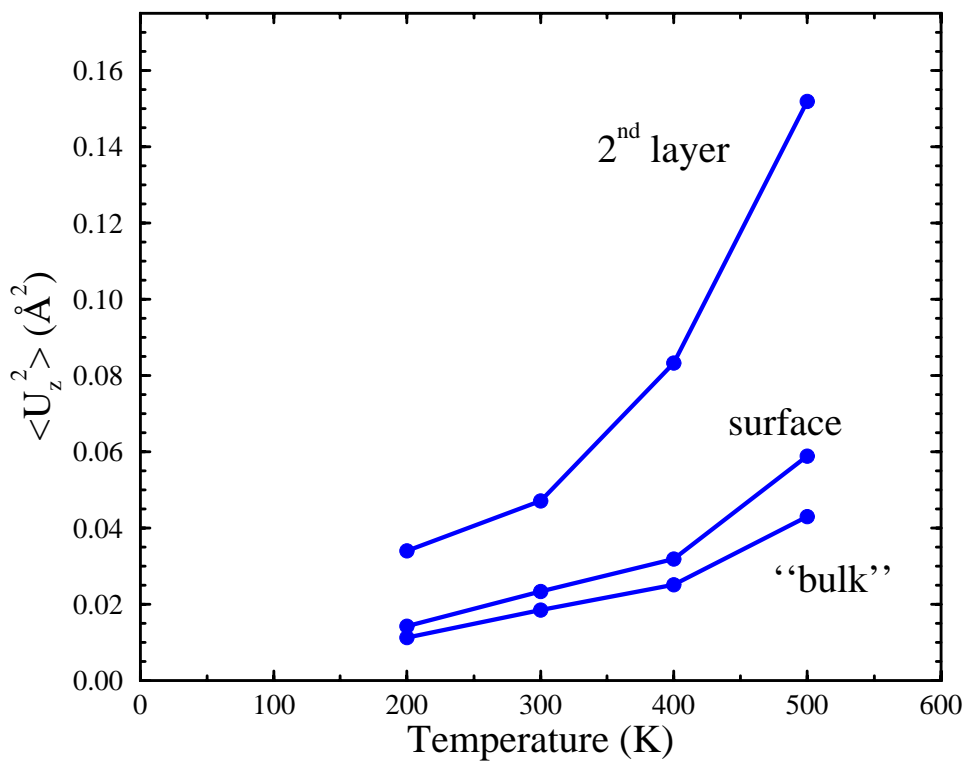


Figure 5.6: Mean square displacements along the z axis for the different layers, as a function of the temperature. “Bulk” refers to the two central layers. Averages are done on the full runs, each $\sim 3\text{ps}$ long.

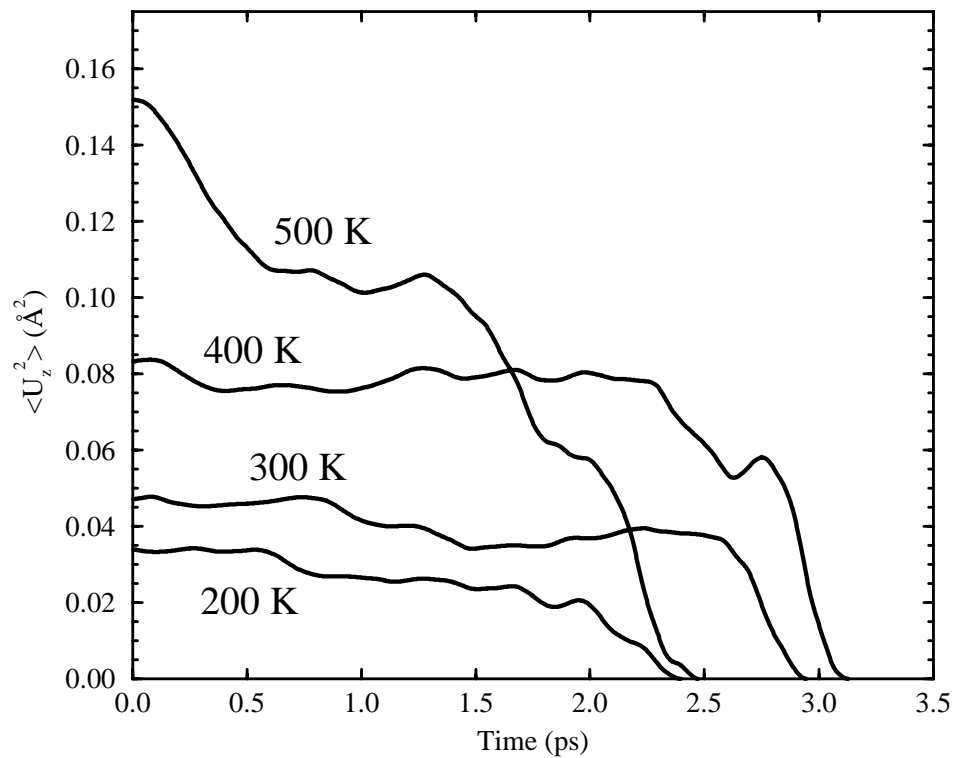


Figure 5.7: Mean square displacements for the second layer at different temperatures. The value at a time t represents the average done from t to the end of the run for the square of the displacement around an average position consistently calculated as the average from the time t to the end of the run.

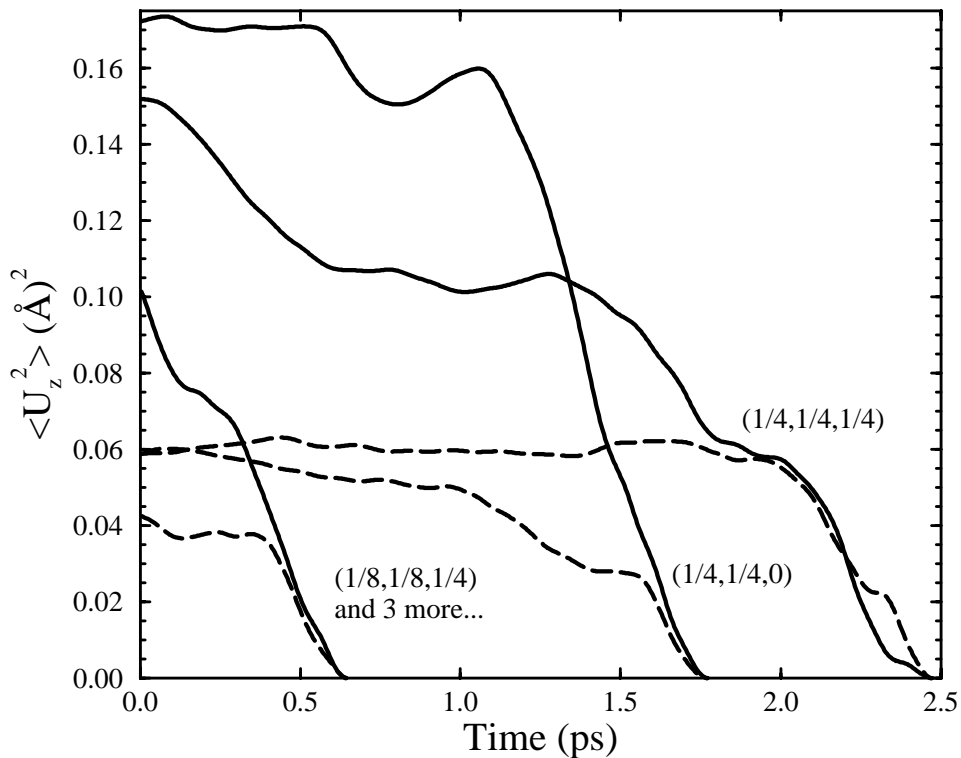


Figure 5.8: Mean square displacements for the first (dashed) and second layer (solid) at 500 K and with different Brillouin Zone samplings. The value at a time t represents the average done from t to the end of the run for the square of the displacement around an average position consistently calculated as the average from the time t to the end of the run.

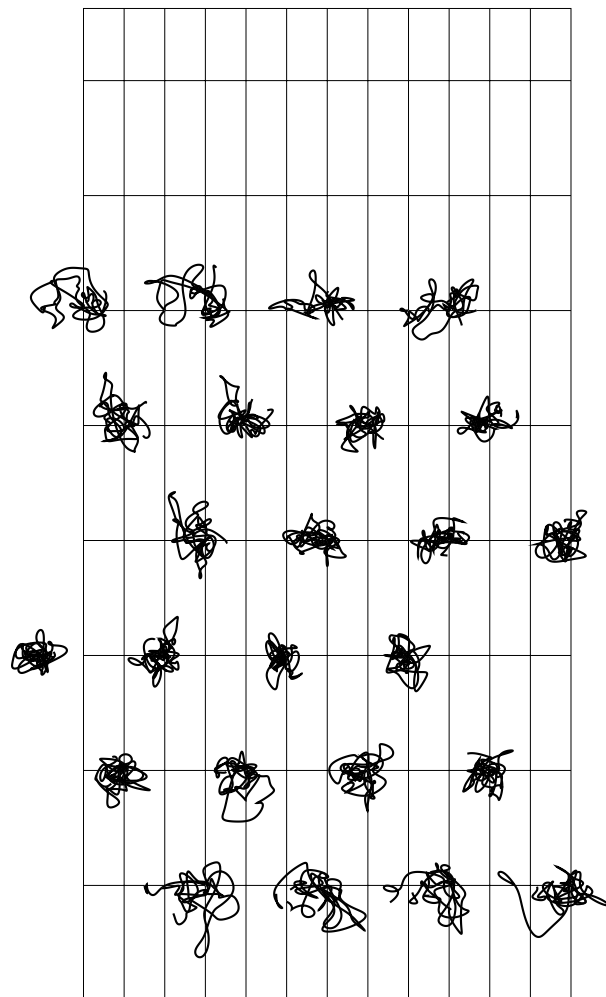


Figure 5.9: Dynamic trajectories for the ions in the Al(111) slab, at 600 K
(1 ps of simulation).

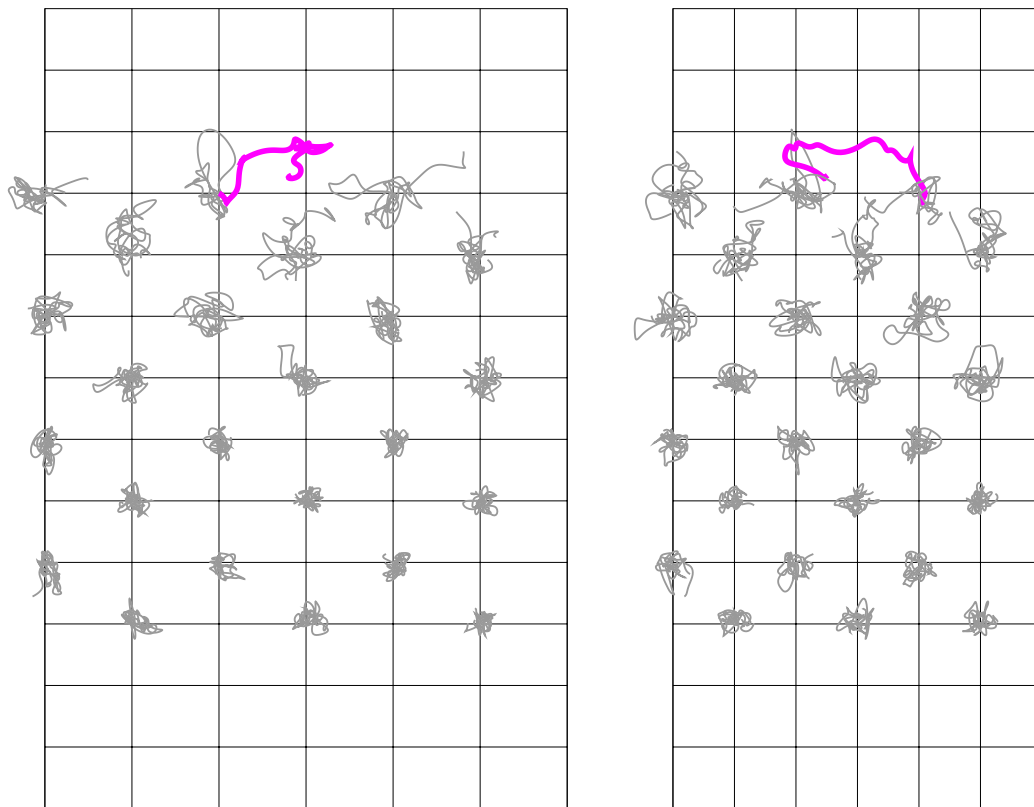


Figure 5.10: Dynamic trajectories for the ions in the Al(110) slab, with the top 5 layers at 600 K and the bottom 3 layers at 300 K; the first adatom/vacancy formation process is highlighted (1 ps of simulation). The xz and the yz projections are shown.

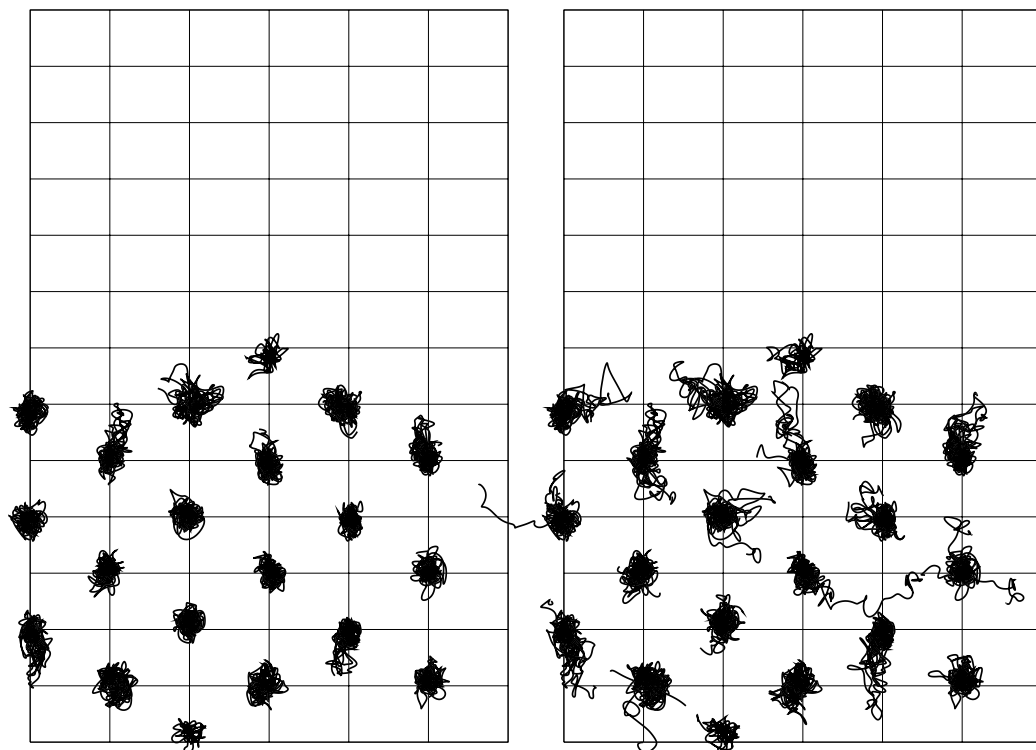


Figure 5.11: Dynamic trajectories for the ions in the 6 layers + 2 adatoms Al(110) slab; on the right are the first 4 ps at 450 K, on the left all the run with its additional 1 ps at 500 K.

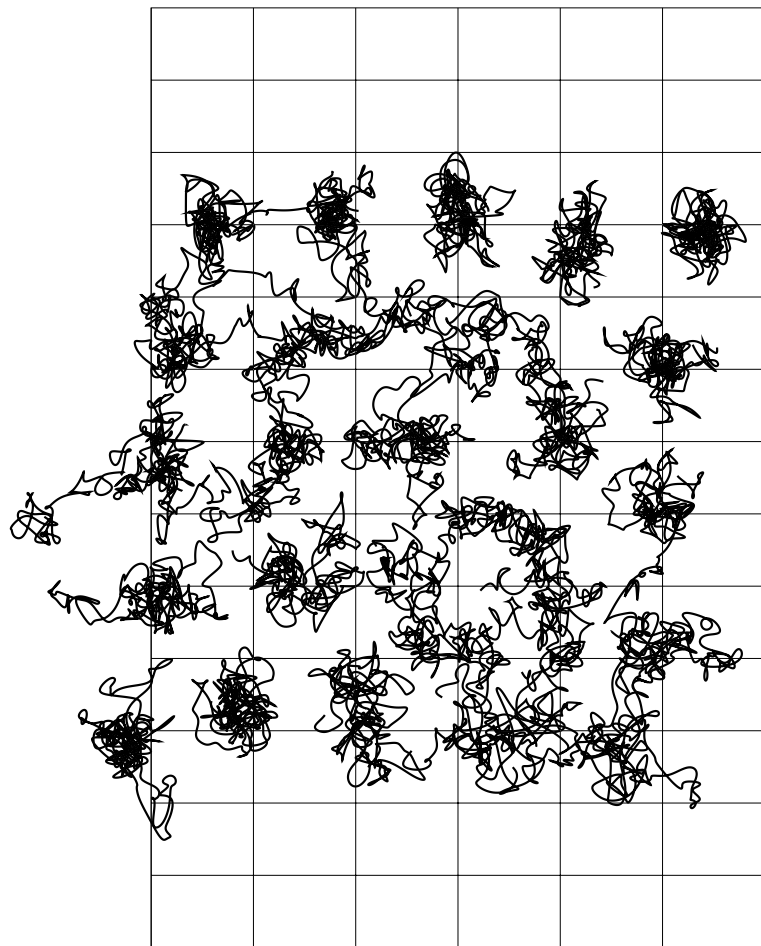


Figure 5.12: Dynamic trajectories for the ions in the Al(110) slab at 600 K, for a 3 ps simulation. An increased, layered density is clearly noted in proximity of the surfaces.

Conclusions

The present work has focused on the issues that arise in electronic structure calculations when the systems studied are metallic. The role of a proper variational formulation has been highlighted in its role of assuring a stable and robust convergence to the ground state; the finite-temperature picture for the electronic degrees of freedom has been shown to greatly improve the accuracy in the sampling of the Brillouin Zone, with a little cost in the systematic errors that are introduced by it.

A general reformulation of the problem has been provided, using the language of Ensemble Density Functional Theory, and a very efficient procedure for its implementation has been described. This approach treats consistently the fractional occupancies and the subspace rotations, typical features of a metallic system at finite temperature, as part of the same underlying problem, namely to solve the Liouville equation for the self-consistent Hamiltonian and the single-particle effective statistical operator. In addition to greatly improving the convergence for the free energies and the Hellmann-Feynman forces to the ground-state expectation values, this formulation allows for a consistent treatment of exotic fractional statistics. A realization of these statistics has been argued (the cold smearing), that provides a correction to a higher order in the temperature for the systematic errors introduced

by the finite-temperature treatment.

The whole methodology has been applied to the study of the thermal properties of some low-index aluminium surfaces, showing all the potentiality that first-principle calculations can bring to the field, with their accurate and detailed treatment of the microscopic time-scales and dimensions. In particular, some novel microscopic features that were beyond the level of accuracy of semi-empirical methods, and not directly available from experiments, have been identified and rationalized.

Much of the unsung work of this thesis has also gone into extensive testing and verification of the different issues presented, and to the full redevelopment of an electronic structure code, including the atomic-relaxation and molecular-dynamics algorithms.

Acknowledgments

I wish to express my deep gratitude to Mike Payne, for all the support and the confidence that he has given me at every stage of this work.

It is a great pleasure to acknowledge the collaboration with David Vanderbilt on the ensemble-DFT, and to look forward to the work to come.

I would like to thank Alessandro De Vita, that has given the momentum and background to start this project, and Jim White, for all his lucid and patient comments. Mike Gillan and Janusz Holender provided an early version of their all-bands implementation of CASTEP, and a warm hospitality at the University of Keele. Pembroke College and the University of Cambridge have offered an opportunity that I will always treasure, and the Commission of the European Communities has supported it with a 2-year doctoral fellowship of the “Human Capital and Mobility” program.

Hitachi Europe Ltd. has granted access to their SR3600 machine at the Maid-enhead headquarters, England, where some of the calculations of this thesis have been performed.

It is my joy and blessing to be able to dedicate this work to Trina, and to gratefully thank all our friends, that have shared so much with us.

Bibliography

- [1] E. Schrödinger, *Ann. Physik* **79**, 361, 489 (1926); *ibid.* **81** 109 (1926).
- [2] P. Hohenberg and W. Kohn, *Phys. Rev.* **136**, B864 (1964).
- [3] N. D. Mermin, *Phys. Rev.* **137**, A1441 (1965).
- [4] W. Kohn and L. J. Sham, *Phys. Rev.* **140**, A1133 (1965).
- [5] J. S. Bell, *Speakable and Unspeakable in Quantum Mechanics: Collected Papers on Quantum Philosophy*, Cambridge University Press, Cambridge (1987).
- [6] J. C. Phillips, *Phys. Rev.* **112**, 685 (1958); J. C. Phillips and L. Kleinman, *ibid.* **116**, 287 (1959).
- [7] M. L. Cohen and V. Heine, in *Solid State Physics* **24**, eds. H. Ehrenreich, F. Seitz and D. Turnbull, Academic Press, New York (1970).
- [8] M. Born and V. Fock, *Z. Phys.* **51**, 165 (1928).
- [9] F. J. Dyson, *J. Math. Phys.* **8**, 1538 (1967); F. J. Dyson and A. Lenard, *ibid.* **8**, 423 (1967).
- [10] E. H. Lieb, *Rev. Mod. Phys.* **48**, 553 (1976).

- [11] R. Courant and D. Hilbert, *Methods of Mathematical Physics*, p. 424, Interscience Publishers, New York (1953).
- [12] P. A. M. Dirac, *The Principles of Quantum Mechanics*, p. 45, Oxford University Press, Oxford (1958).
- [13] L. I. Schiff, *Quantum Mechanics*, McGraw-Hill, Singapore (1968).
- [14] D. R. Hartree, *Proc. Cambridge Phil. Soc.* **27**, 89 (1927); *ibid.* 111, **27** (1927); *ibid.* **27**, 426 (1928).
- [15] V. Fock, *Z. Phys.* **61**, 126 (1930); *ibid.* **62**, 795 (1930); J. C. Slater, *Phys. Rev.* **35**, 210 (1930).
- [16] H. Hellmann, *Einführung in die Quantenchemie*, Deuticke, Leipzig (1937); R. P. Feynman, *Phys. Rev.* **56**, 340 (1939).
- [17] P. Ehrenfest, *Z. Phys.* **45**, 455 (1927).
- [18] L. H. Thomas, *Proc. Cambridge Phil. Soc.* **23**, 542 (1927).
- [19] E. Fermi, *Rend. Accad. Lincei* **6**, 602 (1927); *ibid.* **7**, 342 (1928); *Z. Phys.* **48**, 73 (1928).
- [20] E. Teller, *Rev. Mod. Phys.* **34**, 627 (1962).
- [21] E. Smargiassi and P. A. Madden, *Phys. Rev. B* **49**, 5220 (1994).
- [22] B. Farid, private communication.
- [23] M. Levy, *Proc. Natl. Acad. Sci. USA* **76**, 6062 (1979).
- [24] M. Levy, *Phys. Rev. A* **26**, 1200 (1982).

- [25] E. H. Lieb, *Int. J. Quantum Chem.* **24**, 243 (1983).
- [26] W. Kohn, *Phys. Rev. Lett.* **51**, 1596 (1983).
- [27] H. Englisch and R. Englisch, *Phys. Stat. Sol. (b)* **123**, 711 (1984); *ibid.* **124**, 373 (1984).
- [28] T. L. Gilbert, *Phys. Rev. B* **12**, 2111 (1975).
- [29] L. D. Landau and E. M. Lifshitz, *Statistical Physics* Par. 5, Pergamon Press, Oxford (1980).
- [30] R. G. Parr and W. Yang, *Density Functional Theory of Atoms and Molecules*, Oxford University Press, Oxford (1988).
- [31] S. M. Valone, *J. Chem. Phys.* **73**, 1344 (1980); *ibid.* **73**, 4653 (1980).
- [32] J. Coleman, *Rev. Mod. Phys.* **35**, 668 (1963).
- [33] R. P. Feynman, *Statistical Mechanics*, Addison-Wesley, Reading Massachusetts (1972).
- [34] M. M. Valiev and G. W. Fernando, *Phys. Rev. B* **52**, 10697 (1995).
- [35] M. Levy and J. P. Perdew, in *Density Functional Methods in Physics*, R. M. Dreizler and J. da Providencia eds., Plenum, New York (1985); J. P. Perdew and M. Levy, *Phys. Rev. B* **31**, 6264 (1985).
- [36] E. H. Lieb, in *Density Functional Methods in Physics*, R. M. Dreizler and J. da Providencia eds., Plenum, New York (1985).
- [37] E. H. Lieb, *Rev. Mod. Phys.* **53**, 603 (1981).

- [38] J. F. Janak, *Phys. Rev. B* **18**, 7165 (1978).
- [39] J. Perdew and A. Zunger, *Phys. Rev. B* **23**, 5048 (1981).
- [40] M. Weinert and J. W. Davenport, *Phys. Rev. B* **45**, 13709 (1992).
- [41] J. Callaway and N. H. March, in *Solid State Physics* **38**, p. 235, eds. F. Seitz and D. Turnbull, Academic Press, New York (1984).
- [42] K. Huang, *Statistical Mechanics*, John Wiley & Sons, New York (1987).
- [43] W. Kohn and P. Vashista, in *Theory of the Inhomogeneous Electron Gas*, S. Lundqvist and N. H. March eds., Plenum, New York (1983).
- [44] M. J. Gillan, *J. Phys.: Condens. Matter* **1**, 689 (1989).
- [45] A. Alavi, J. Kohanoff, M. Parrinello, and D. Frenkel, *Phys. Rev. Lett.* **73**, 2599 (1994).
- [46] W. Yang, *Phys. Rev. A* **38**, 5504 (1988).
- [47] D. M. Ceperley and B. J. Alder, *Phys. Rev. Lett.* **45**, 566 (1980).
- [48] J. P. Perdew, J. A. Chevary, S. H. Vosko, K. A. Jackson, M. R. Pederson, D. J. Singh, and C. Fiolhais, *Phys. Rev. B* **46**, 6671 (1992).
- [49] R. Car and M. Parrinello, *Phys. Rev. Lett.* **55**, 2471 (1985).
- [50] M. C. Payne, M. P. Teter, D. C. Allan, T. A. Arias, and J. D. Joannopoulos, *Rev. Mod. Phys.* **64**, 1045 (1992).
- [51] P. A. M. Dirac, *Proc. Cambridge Phil. Soc.* **26**, 376 (1930).
- [52] S. H. Vosko, L. Wilk, and M. Nusair, *Can. J. Phys.* **58**, 1200 (1980).

- [53] N. H. March, in *Theory of the Inhomogeneous Electron Gas*, S. Lundqvist and N. H. March eds., Plenum Press, New York (1983).
- [54] J. Harris and R. O. Jones, *I. Phys. F* **4**, 1170 (1974); O. Gunnarsson and B. I. Lundqvist, *Phys. Rev. B* **13**, 4274 (1976); D. C. Langreth and J. P. Perdew, *Phys. Rev. B* **15**, 2884 (1977).
- [55] O. Gunnarsson, M. Jonson, and B. I. Lundqvist, *Phys. Rev. B* **20**, 3136 (1979).
- [56] W. Pickett, *Comp. Phys. Rep.* **9**, 115 (1989).
- [57] J. Ihm, *Rep. Prog. Phys.* **51**, 105 (1988).
- [58] J. R. Chelikowsky, N. Troullier, and Y. Saad, *Phys. Rev. Lett.* **72**, 1240 (1994).
- [59] F. Gygi, *Europhys. Lett.* **19**, 617 (1992); F. Gygi and G. Galli, *Phys. Rev. B* **52**, R2229 (1995).
- [60] E. L. Briggs, D. J. Sullivan, and J. Bernholc, *Phys. Rev. B* **52**, R5471 (1995).
- [61] G. Makov and M. C. Payne, *Phys. Rev. B* **51**, 4014 (1995).
- [62] N. W. Ashcroft and N. D. Mermin, *Solid State Physics*, Holt Saunders, Philadelphia (1976).
- [63] W. H. Press, S. A. Teukolsky, W. T. Vetterling, and B. P. Flannery, *Numerical Recipes*, Cambridge University Press, Cambridge (1992).
- [64] N. W. Ashcroft and D. C. Langreth, *Phys. Rev.* **155**, 682 (1967).

- [65] M. L. Cohen and T. K. Bergstresser, *Phys. Rev.* **141**, 789 (1966).
- [66] D. R. Hamann, M. Schlüter, and C. Chiang, *Phys. Rev. Lett.* **43**, 1494 (1979).
- [67] G. B. Bachelet, D. R. Hamann, and M. Schlüter, *Phys. Rev. B* **26**, 4199 (1982).
- [68] G. P. Kerker, *J. Phys. C* **13**, L189 (1980).
- [69] A. M. Rappe, K. M. Rabe, E. Kaxiras, and J. D. Joannopoulos, *Phys. Rev. B* **41**, 1227 (1990).
- [70] J. S. Lin, A. Qteish, M. C. Payne, and V. Heine, *Phys. Rev. B* **47**, 4174 (1993).
- [71] M.-H. Lee, *Advanced Pseudopotentials for Large Scale Electronic Structure Calculations*, Ph.D. Thesis, University of Cambridge (1995).
- [72] D. Vanderbilt, *Phys. Rev. B* **32**, 8412 (1985).
- [73] D. Vanderbilt, *Phys. Rev. B* **41**, 7892 (1990).
- [74] L. Kleinman and D. M. Bylander, *Phys. Rev. Lett.* **48**, 1425 (1982).
- [75] R. D. King-Smith, M. C. Payne, and J. S. Lin, *Phys. Rev. B* **44**, 13063 (1991).
- [76] A. Rahman, *Phys. Rev.* **136A**, 405 (1964).
- [77] G. Galli and A. Pasquarello, in *Computer Simulations in Chemical Physics*, M. P. Allen and D. J. Tildesley eds., Kluwer Academic Publishers, Dordrecht (1990).

- [78] D. K. Remler and P. A. Madden, *Mol. Phys.* **70**, 921 (1990).
- [79] F. Tassone, F. Mauri, and R. Car, *Phys. Rev. B* **50**, 10561 (1994).
- [80] H. C. Andersen, *J. Chem. Phys.* **72**, 2384 (1980).
- [81] M. Parrinello and A. Rahman, *Phys. Rev. Lett.* **45**, 1196 (1980).
- [82] S. Kirkpatrick, C. Gelatt, Jr. and M. Vecchi, *Science* **220**, 671 (1983).
- [83] R. Car and M. Parrinello, in *Simple Molecular Systems at Very High Density*, A. Polian, P. Loubeyre, and N. Boccara eds., Plenum Press, New York (1988).
- [84] G. Pastore, E. Smargiassi, and F. Buda, *Phys. Rev. B* **44**, 6334 (1991).
- [85] Q. M. Zhang, G. Chiarotti, A. Selloni, R. Car, and M. Parrinello, *Phys. Rev. B* **42**, 5071 (1990).
- [86] P. E. Gill, W. Murray, and M. H. Wright, *Practical Optimization*, Academic, London (1981).
- [87] I. Stich, R. Car, M. Parrinello, and S. Baroni, *Phys. Rev. B* **39**, 4997 (1989).
- [88] M. P. Teter, M. C. Payne, and D. C. Allan, *Phys. Rev. B* **40**, 12255 (1989).
- [89] T. A. Arias, M. C. Payne, and J. D. Joannopoulos, *Phys. Rev. Lett.* **69**, 1077 (1992).
- [90] T. A. Arias, M. C. Payne, and J. D. Joannopoulos, *Phys. Rev. B* **45**, 1538 (1992).

- [91] I. Stich, M. C. Payne, R. D. King-Smith, J. S. Lin, and L. J. Clarke, *Phys. Rev. Lett.* **68**, 1351 (1992).
- [92] A. De Vita, M. J. Gillan, J. S. Lin, M. C. Payne, I. Stich, and L. J. Clarke, *Phys. Rev. Lett.* **68**, 3319 (1992).
- [93] V. Milman, M. C. Payne, V. Heine, R. J. Needs, J. S. Lin, and M. H. Lee, *Phys. Rev. Lett.* **70**, 2928 (1993).
- [94] A. De Vita, I. Stich, M. J. Gillan, M. C. Payne, and L. J. Clarke, *Phys. Rev. Lett.* **71**, 1276 (1993).
- [95] J. A. White, D. M. Bird, M. C. Payne, and I. Stich, *Phys. Rev. Lett.* **73**, 1404 (1994).
- [96] R. Perez, M. C. Payne, and A. D. Simpson, *Phys. Rev. Lett.* **75**, 4748 (1995).
- [97] C. Molteni, G. P. Francis, M. C. Payne, and V. Heine, *Phys. Rev. Lett.* **76**, 1284 (1996).
- [98] G. H. Golub and C. F. Van Loan, *Matrix Computations*, Johns Hopkins University Press, Baltimore (1989).
- [99] A. Baldereschi, *Phys. Rev. B* **7**, 5212 (1973).
- [100] D. J. Chadi and M. L. Cohen, *Phys. Rev. B* **8**, 5747 (1973).
- [101] H. J. Monkhorst and J. D. Pack, *Phys. Rev. B* **13**, 5188 (1976).
- [102] J. Moreno and J. M. Soler, *Phys. Rev. B* **45**, 13891 (1992).
- [103] C.-L. Fu and K.-M. Ho, *Phys. Rev. B* **28**, 5480 (1983).

- [104] R. J. Needs, R. M. Martin and O. H. Nielsen, *Phys. Rev. B* **33**, 3778 (1986).
- [105] G. X. Quian, M. Weinert, G. W. Fernando, and J. W. Davenport, *Phys. Rev. Lett.* **64**, 1146 (1990).
- [106] M. P. Grumbach, D. Hohl, R. M. Martin, and R. Car, *J. Phys.: Condens. Matter* **6**, 1999 (1994).
- [107] G. Galli, R. M. Martin, R. Car, and M. Parrinello, *Phys. Rev. B* **42**, 7470 (1990).
- [108] S. Nosé, *Mol. Phys.* **52**, 255 (1984); S. Nosé, *J. Phys.: Condens. Matter* **2**, SA115 (1990).
- [109] P. E. Bloechl and M. Parrinello, *Phys. Rev. B* **45**, 9413 (1992).
- [110] E. S. Fois, J. I. Penman, and P. A. Madden, *J. Chem. Phys.* **98**, 6361 (1993).
- [111] G. W. Fernando, G.-X. Qian, M. Weinert, and J. W. Davenport, *Phys. Rev. B* **40**, 7985 (1989).
- [112] M. R. Pederson and K. A. Jackson *Phys. Rev. B* **43**, 7312 (1991).
- [113] Y. Yamamoto and T. Fujiwara, *Phys. Rev. B* **46**, 13596 (1992).
- [114] A. F. Wright and S. R. Atlas, *Phys. Rev. B* **50**, 15248 (1994).
- [115] N. Chetty, M. Weinert, T. S. Rahman, and J. W. Davenport, *Phys. Rev. B* **52**, 6313 (1995).

- [116] R. M. Wentzcovitch, J. L. Martins, and P. B. Allen, *Phys. Rev. B* **45**, 11372 (1992).
- [117] A. De Vita, *The Energetics of Defects and Impurities in Metals and Ionic Materials from First Principles*, Ph.D. Thesis, University of Keele (1992).
- [118] M. Methfessel and A. T. Paxton, *Phys. Rev. B* **40**, 3616 (1989).
- [119] S. de Gironcoli, *Phys. Rev. B* **51**, 6773 (1995).
- [120] P. E. Bloechl, O. Jepsen, and O. K. Andersen, *Phys. Rev. B* **49**, 16223 (1994).
- [121] J. A. White, D. M. Bird, and M. C. Payne, *Phys. Rev. B* **53**, 1667 (1996).
- [122] G. Kresse and J. Hafner, *Phys. Rev. B* **47**, 558 (1993).
- [123] G. Kresse and J. Hafner, *Phys. Rev. B* **49**, 14251 (1994).
- [124] J. M. Holender, M. J. Gillan, M. C. Payne, and A. D. Simpson, *Phys. Rev. B* **52**, 967 (1995).
- [125] J. M. Holender and M. J. Gillan, *Phys. Rev. B* **53**, 4399 (1996).
- [126] D. Vanderbilt and J. D. Joannopoulos, *Phys. Rev. B* **26**, 3203 (1982).
- [127] C. Molteni, private communication.
- [128] X. Gonze, *Phys. Rev. B* **52**, 1096 (1995).
- [129] C. Elsässer, M. Fähnle, C. T. Chan, and K. M. Ho, *Phys. Rev. B* **49**, 13975 (1994).

- [130] M. Born and J. R. Oppenheimer, *Ann. Physik* **84**, 457 (1927).
- [131] G. Chester, *Adv. Phys.* **10**, 357 (1961).
- [132] A. B. Migdal, *Sov. Phys. JETP* **7**, 996 (1958).
- [133] J. N. Andersen, H. B. Nielsen, L. Petersen, and D. L. Adams, *J. Phys. C* **17**, 173 (1984).
- [134] J. R. Noonan and H. L. Davis, *Phys. Rev. B* **29**, 4349 (1984).
- [135] H. Göbel and P. von Blankenhagen, *Phys. Rev. B* **47**, 2378 (1993).
- [136] M. P. Allen and D. J. Tildesley, in *Computer Simulation of Liquids*, Oxford University Press, Oxford (1987).
- [137] M. Bernasconi and E. Tosatti, *Surf. Sci. Rep.* **17**, 363 (1993).
- [138] F. Di Tolla, *Interplay of Melting, Wetting, Overheating and Faceting on Metal Surface: Theory and Simulations*, Ph.D. Thesis, Sissa/Isas (1995).
- [139] P. D. Ditlevsen and J. K. Norskov, *Surf. Sci.* **254**, 261 (1991).
- [140] C. S. Jayanthi, E. Tosatti, A. Fasolino, and L. Pietronero, *Surface Science* **152,153**, 155 (1985).
- [141] E. T. Chen, R. N. Barnett and U. Landman, *Phys. Rev. B* **41**, 439 (1990).
- [142] R. N. Barnett and U. Landman, *Phys. Rev. B* **44**, 3226 (1991).
- [143] L. Yang and T. S. Rahman, *Phys. Rev. Lett.* **67**, 2327 (1991).

- [144] P. D. Ditlevsen, P. Stoltze and J. K. Norskov, *Phys. Rev. B* **44**, 13002 (1991).
- [145] G. Mazzeo, *Interplay between surface in-plane ordering and roughening*, Ph.D. Thesis, Sissa/Isas (1992).
- [146] K. Rommelse and M. den Nijs, *Phys. Rev. Lett.* **59**, 2578 (1987).
- [147] G. Mazzeo, G. Jug, A. C. Levi, and E. Tosatti, *Phys. Rev. B* **49**, 7625 (1994).
- [148] J. W. M. Frenken and J. F. van der Veen, *Phys. Rev. Lett.* **54**, 134 (1985).
- [149] H. van Pinxteren, *Surfaces between melting and non-melting*, Ph.D. Thesis, FOM Amsterdam (1994).
- [150] A. Molenbroek, *Surface-melting instabilities at metal surfaces*, Ph.D. Thesis, FOM Amsterdam (1995).
- [151] P. Stoltze, J. K. Norskov, and U. Landman, *Phys. Rev. Lett.* **61**, 440 (1988).
- [152] A. W. Denier van der Gon, R. J. Smith, J. M. Gay, D. J. O'Connor, and J. F. van der Veen, *Surf. Sci.* **227**, 143 (1990).
- [153] A. W. Denier van der Gon, D. Frenkel, J. W. M. Frenken, R. J. Smith, and P. Stoltze, *Surf. Sci.* **256**, 385 (1991).
- [154] H. Dosch, T. Höfer, J. Peisl, and R. L. Johnson, *Europhysics Letters* **15**, 527 (1991).

- [155] A. Pavlovska, M. Tikhov, Y. Gun, and E. Bauer, *Surf. Sci.* **278**, 303 (1992).
- [156] M. Gester, D. Kleinhesslink, P. Ruggerone, and J. P. Toennies, *Phys. Rev. B* **49**, 5777 (1994).
- [157] A. M. Raphuthi, X. Q. Wang, F. Ercolessi, and J. B. Adams, *Phys. Rev. B* **52**, R5554 (1995).
- [158] R. Stumpf and M. Scheffler, *Phys. Rev. B* **53**, 4958 (1996).
- [159] E. V. Zarochentsev, S. P. Kravchuk, and T. M. Tarusina, *Sov. Phys. Solid State* **18**, 239 (1976).
- [160] D. E. Sanders and A. E. DePristo, *Surf. Sci. Lett.* **264**, L169 (1992).